DECONSTRUCTED HIGGSLESS MODELS OF ELECTROWEAK SYMMETRY BREAKING

By

Baradhwaj Panayancheri-Coleppa

A DISSERTATION

Submitted to
Michigan State University
in partial fulfillment of the requirements
for the degree of

DOCTOR OF PHILOSOPHY

Physics and Astronomy

2009

ABSTRACT

DECONSTRUCTED HIGGSLESS MODELS OF ELECTROWEAK SYMMETRY BREAKING

By

Baradhwaj Panayancheri-Coleppa

We study deconstructed Higgsless models of electroweak symmetry breaking. As the name implies, these models break electroweak symmetry without the presence of a scalar Higgs boson in the spectrum. These models are inspired by compactified extra dimensional models, where the $W_L W_L$ scattering amplitude is unitarized by a tower of new, heavy vector bosons in place of the Higgs. We study a simplified theory with only one set of extra vector bosons and derive the wavefunctions and couplings in this theory. We then extend this model to include a "top-Higgs" link, so as to separate the top quark mass generation from the rest of electroweak symmetry breaking, which still goes through via a Higgsless mechanism. This enables us to have new, heavy Dirac fermions that are light enough to be discovered at the LHC. We present the phenomenology of these heavy fermions, showing that they are discoverable at the 5σ level at the LHC for a wide range of masses. Finally, we move on to consider the question of unitarity and the heavy Dirac fermion mass generation by investigating the process $t\bar{t} \to W_L^+ W_L^-$ in a family of deconstructed Higgsless models, and show how the Appelquist-Chanowitz bound can be substantially weakened for sufficiently light Dirac fermions.

DEDICATION

I dedicate this thesis to my late grandmother, Ammani Paatti.

TABLE OF CONTENTS

LIST OF TABLES

LIST OF FIGURES

Images in this dissertation are presented in color

Chapter 1

Introduction

There are four basic kinds of forces in the world: the strong nuclear force, the weak nuclear force, electromagnetism, and gravity. These are distinguished from one another based on their strengths and range. For example, the gravitational force between two objects is proportional to the product of their masses and hence is relevant only when the objects involved are very massive. But gravity has an infinite range and hence plays the dominant role in determining the large scale structure of the universe. On the other hand, in the sub-atomic world, the strong, weak and electromagnetic forces dominate. The quantum theory that explains the nature of these sub-atomic forces is called the Standard Model of Particle Physics (SM for short), while the nature of gravity is so far explained by the classical theory of General Relativity.

The SM is a gauge theory and incorporates two different classes of particles - the matter content (fermions) and the force carriers (the gauge bosons). The force exterted by one particle on another is transmitted via the gauge bosons. The range of the force is dictated by the mass of the gauge boson involved - for example, electromagnetic forces that have infinite range are transmitted by massless photons while the short range weak nuclear force is transmitted by the heavy W and Z bosons. The beauty of the SM lies in the fact that it explains these two different kinds of forces

in one unified framework, i.e., as an electro-weak theory [1]. Of course, the strong nuclear forces are also built into the SM as a "color" gauge theory and the complete gauge group of the SM is $SU(3)_C \times SU(2)_W \times U(1)_Y$, where the subscripts C, W, and Y stand for color, weak, and hypercharge respectively. In this thesis, we will be largely concentrating on the electro-weak sector, i.e., the $SU(2)_W \times U(1)_Y$ part. To understand how the SM operates, let us begin by describing the simpler theory of Quantum Electrodynamics (QED).

1.1 Quantum Electrodynamics

Let us start by writing down the Dirac Lagrangian for a free electron of mass m:

$$\mathcal{L} = \overline{\Psi} i\gamma^\mu \partial_\mu \Psi - m\overline{\Psi}\Psi, \tag{1.1}$$

where Ψ is a four component Dirac spinor. This Lagrangian is invariant under a phase transformation:

$$\Psi \rightarrow \exp(ie\theta)\,\Psi, \tag{1.2}$$

where e is the electric charge. The parameter θ is independent of space-time and correspondingly, the transformation is termed "global". Moreover, since this is a one parameter group, the above Lagrangian is said be invariant under global $U(1)$ transformations, where U tells us that this is a unitary group. But suppose we insist that the parameter θ depend on space-time, i.e., $\theta \rightarrow \theta(x)$ (i.e., a *local* or *gauge* transformation). Then, of course, Eqn. (1.1) is no longer invariant.

$$\mathcal{L} \rightarrow \overline{\Psi} i\gamma^\mu \partial_\mu \Psi - m\overline{\Psi}\Psi - e\partial_\mu \theta \overline{\Psi}\gamma^\mu \Psi. \tag{1.3}$$

It is clear that the theory of a free electron cannot be invariant under local trnasformations. If we demand that this theory still be invariant, we are forced to add another ingredient whose $U(1)$ transformation would cancel the extra piece in Eqn. (1.3). From Maxwell's classical electromagnetic theory, we know that the photon field transforms inhomogenously under gauge transformations as follows:

$$A_\mu \rightarrow A_\mu - i\partial_\mu \theta(x). \tag{1.4}$$

This suggests that we add the photon field, A_μ, in such a fashion as to cancel the extra term in Eqn. (1.3). Thus, we write down the interaction term:

$$\mathcal{L}_{\text{int}} = e\overline{\Psi}\gamma^\mu \Psi A_\mu. \tag{1.5}$$

It can be verified that adding this term to the Dirac Lagrangian makes it invariant under local $U(1)$ transformations. The $U(1)$ gauge symmetry allows a kinetic energy term for the photon that takes the form:

$$\mathcal{L} = -\frac{1}{4} F_{\mu\nu} F^{\mu\nu}, \tag{1.6}$$

where $F_{\mu\nu} = \partial_\mu A_\nu - \partial_\nu A_\mu$. Note that a mass term for the photon of the form $m_A^2 A_\mu A^\mu$ is not allowed since this is not $U(1)$ invariant. Thus, the complete QED Lagrangian is given by (restricting ourselves to terms of dimension 4):

$$\mathcal{L}_{\text{QED}} = i\overline{\Psi}\gamma^\mu D_\mu \Psi - \frac{1}{4} F_{\mu\nu} F^{\mu\nu} - m\overline{\Psi}\Psi, \tag{1.7}$$

where

$$D_\mu = \partial_\mu - ieA_\mu, \tag{1.8}$$

is the covariant derivative. Promoting the ordinary derivative to a covariant derivative in the form of Eqn. (1.8) to make the Lagrangian gauge invariant is called the "Minimal coupling" prescription. Thus, we see that the principle of local gauge invariance determines the structure of the Lagrangian and also naturally introduces a vector boson into the theory. Next, we turn to the full Standard Model.

1.2 The Standard Model

The Standard Model Lagrangian can be constructed by extending the principles of the last section for the full group $SU(3)_C \times SU(2)_W \times U(1)_Y$. The matter content of the SM (quarks and leptons) come in three families (or generations). Both the quark and lepton families have electroweak interactions and hence transform under the $SU(2)_W \times U(1)_Y$ part of the SM gauge group. However, strong interactions (mediated by gluons) are only felt by the quarks, and thus only the quarks and gluons have $SU(3)$ charges (The non-Abelian nature of the gauge group permits self coupling of gluons, as opposed to electromagnetism). We give the quantum numbers of the quark and lepton fields under the SM gauge group below:

$$
\begin{aligned}
Q_L &= \begin{pmatrix} u_L \\ d_L \end{pmatrix} \sim (3, 2, +\tfrac{1}{6}), \quad d_R^C \sim (\bar{3}, 1, -\tfrac{1}{3}), \quad u_R^C \sim (\bar{3}, 1, +\tfrac{2}{3}), \\
L_L &= \begin{pmatrix} \nu_L \\ e_L \end{pmatrix} \sim (1, 2, -\frac{1}{2}), \quad e_R^C \sim (1, 1, 1),
\end{aligned}
\tag{1.9}
$$

The L and R stand for left and right handed helicity states, based on the Lorentz transformation properties of the fermion. The gauge interactions of the quarks can now be written down by extending the covariant derivative in Eqn. (1.8) to include the eight gluons (G_μ^A), the three weak gauge bosons (W_μ^A), and the hypercharge

gauge boson ($B\mu$).

$$\begin{aligned}\mathcal{L}^{\rm SM}_{\rm Gauge} = & i\overline{Q}_L\gamma^\mu\left[\partial_\mu - ig_3\frac{\lambda^A}{2}G^A_\mu - ig_1\frac{\sigma^A}{2}W^A_\mu - i\frac{1}{6}g_2B_\mu\right]Q_L \\ & + i\overline{u^c_R}\gamma^\mu\left[\partial_\mu - ig_3\frac{\lambda^A}{2}G^A_\mu + i\frac{2}{3}g_2B_\mu\right]u^c_R \\ & + i\overline{d^c_R}\gamma^\mu\left[\partial_\mu - ig_3\frac{\lambda^A}{2}G^A_\mu - i\frac{1}{3}g_2B_\mu\right]d^c_R \\ & + i\overline{L}_L\gamma^\mu\left[\partial_\mu - ig_1\frac{\sigma^A}{2}W^A_\mu + i\frac{1}{2}g_2B_\mu\right]L_L \\ & + i\overline{e^c_R}\gamma^\mu\left[\partial^\mu - ig_2B_\mu\right]e^c_R. \end{aligned} \tag{1.10}$$

Here, g_3, g_1 and g_2 are the $SU(3)_C$, $SU(2)_W$ and $U(1)_Y$ couplings respectively and the λ^A's and σ^A's are the GellMann and Pauli matrices for the $SU(3)$ and $SU(2)$ gauge groups.

As explained in the previous section, invariance under local gauge transformations demands that the associated gauge bosons be massless. But we know from their short range interactions that the weak gauge bosons do indeed have a mass. Thus, we conclude that in order to have massive gauge bosons, the symmetry must somehow be broken, i.e., the vacuum state must not respect the symmetries the Lagrangian does. This phenomenon, wherein the Lagrangian is symmetric under certain transformations while the ground state is not, is called "Spontaneous Symmetry Breaking" (SSB). In the SM, the breaking of the electroweak symmetry is engineered by introducing a scalar Higgs field [2], which has the following quantum numbers under $SU(2)_W$ and $U(1)_Y$:

$$\phi = \begin{pmatrix}\phi^+ \\ \phi^0\end{pmatrix} \sim (1, 2, +\tfrac{1}{2}). \tag{1.11}$$

The Lagrangian for the Higgs field can written as (restricting ourselves to terms of dimension four or less):

$$\mathcal{L}_{\text{Higgs}} = \frac{1}{2}\text{Tr}\left[D^\mu\phi^\dagger D_\mu\phi\right] - \frac{1}{2}m_H^2\text{Tr}(\phi^\dagger\phi) - \frac{\lambda}{4!}\text{Tr}(\phi^\dagger\phi)^2. \tag{1.12}$$

where the covariant derivative is given by:

$$D^\mu\phi = \left[\partial^\mu + ig_1\frac{\sigma^A}{2}W^A\mu - i\frac{1}{2}g_2B^\mu\right]\phi. \tag{1.13}$$

The Higgs also has Yukawa couplings to the matter fields as follows:

$$\mathcal{L}_{\text{Yukawa}} = \overline{Q}y_u\phi u_R + \overline{Q}y_d i\sigma_2\phi^* d_R + \overline{L}y_e\phi e_R + h.c. \tag{1.14}$$

where the y's are the Yukawa couplings. The quark and lepton fields should be written with a generational index (Q_L^i) to accomodate the three families - we are suppressing these indices here.

The potential for the Higgs field in Eqn. (1.12) takes the form of a "Mexican hat", as shown in Figure 1.1. The minimum of the potential does not lie at $\phi = 0$, but rather lies on a continuous $SU(2)$ manifold along the "trough" of the Mexican hat. One could do perturbation theory around any one of these minima. The choice of a particular vacuum breaks the gauge symmetry as it corresponds to choosing a particular direction in the $SU(2)$ space, so the vacuum is no longer invariant under $SU(2)$ rotations. Writing the Higgs doublet in a form that separates the Goldstone bosons (denoted $\pi(x)$) from the Higgs boson,

$$\phi(x) = e^{i\pi^i(x)\sigma^i/v}\begin{pmatrix} 0 \\ \frac{v+h(x)}{\sqrt{2}} \end{pmatrix}, \tag{1.15}$$

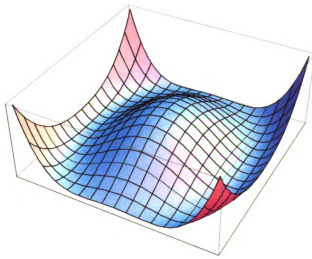

Figure 1.1: The potential for the Higgs field takes a "Mexican hat" form. The "trough" corresponds to continuous directions in which one can move expending zero energy - these correspond to the Goldstone boson modes.

we can write the vacuum expectation value (vev) of the Higgs as:

$$\langle 0|\phi|0\rangle = \begin{pmatrix} 0 \\ \frac{v}{\sqrt{2}} \end{pmatrix}, \tag{1.16}$$

where $v = \sqrt{-m_h^2/\lambda}$. The gauge interactions of the Higgs, Eqn. (1.12), now give rise to mass terms for the gauge bosons when we insert the vev of the Higgs. For the neutral gauge bosons, we find

$$\mathcal{L} = \begin{pmatrix} B_\mu & W_{3\mu} \end{pmatrix} \begin{pmatrix} \frac{1}{4}g_1^2v^2 & -\frac{1}{4}g_1g_2v^2 \\ -\frac{1}{4}g_1g_2v^2 & \frac{1}{4}g_2^2v^{,2} \end{pmatrix} \begin{pmatrix} B^\mu \\ W_3^\mu \end{pmatrix}. \tag{1.17}$$

We can diagonalize this matrix by unitary transformation using the matrix:

$$U = \begin{pmatrix} \cos\theta_w & \sin\theta_w \\ -\sin\theta_w & \cos\theta_{w,} \end{pmatrix} \tag{1.18}$$

where $\tan\theta_w = g_1/g_2$. We can identify the two mass eigenstates as:

$$\begin{aligned} A_\mu &= \cos\theta_w B_\mu + \sin\theta_w W_{3\mu}, \\ Z_\mu &= -\sin\theta_w B_\mu + \cos\theta_w W_{3\mu}, \end{aligned} \tag{1.19}$$

with masses

$$\begin{aligned} m_A^2 &= 0, \\ m_Z^2 &= \frac{1}{4}(g_1^2 + g_2^2)v^2. \end{aligned} \tag{1.20}$$

The charged gauge bosons also acquire a mass:

$$m_{W^\pm}^2 = \frac{1}{4}g_2^2 v^2, \tag{1.21}$$

where

$$W_\mu^\pm = \frac{1}{\sqrt{2}}\left(W_\mu^1 \mp iW_\mu^2\right). \tag{1.22}$$

We started with massless gauge bosons and a complex Higgs field with four real scalar degrees of freedom. We see that three of the four degrees of freedom of the Higgs have now become the longitudinal components of three gauge bosons, making them massive. However, there is one scalar physical degree of freedom that remains, which we identify as the Higgs boson, with mass:

$$m_h^2 = 2\lambda v^2. \tag{1.23}$$

Expressing the gauge eigenstates in Eqn. (1.10) in terms of the mass eigenstates, we

can write down the charged and neutral current interactions of the fermions.

$$\mathcal{L}_{CC} = \frac{e}{\sqrt{2}\sin\theta_w}\left(\bar{u}_L\gamma^\mu W_\mu^- d_L + \bar{e}_L\gamma^\mu W_\mu^- \nu_L\right) + hc. \tag{1.24}$$

$$\mathcal{L}_{NC} = \frac{e}{\sin\theta_w\cos\theta_w}\left\{T_3^f - Q_f\sin^2\theta_w\right\}\bar{f}\gamma^\mu Z_\mu f + eQ_f\bar{f}\gamma^\mu A_\mu f, \tag{1.25}$$

Here, $T_3^f = \pm 1/2$ is the third component of weak-isospin of the left-handed fermion f_L ($T_3^f = 0$ for f_R), and $Q^f = T_3^f + Y^f$. The electric charge, e, is defined as:

$$e = g_2\sin\theta_w = g_1\cos\theta_w = \frac{g_1 g_2}{\sqrt{g_1^2 + g_2^2}}. \tag{1.26}$$

The Yukawa interactions of the Higgs, Eqn. (1.14), now turn into mass terms for the fermions, and the Yukawa couplings are chosen so as to reproduce the correct fermion mass. Thus, we see that the phenomenon of SSB gives rise to mass terms for both the gauge and the fermionic sector of the SM.

1.2.1 Remarks on the Higgs sector

The SM is a phenomenologically successful theory whose predictions have been borne out by various experiments. But two facts still remain: the Higgs boson has not been found in collider experiments and, more importantly, the SM does not offer an explanation for why Electroweak Symmetry Breaking (EWSB) occurs in nature (the Higgs only *engineers* EWSB). These considerations motivate us to build models that go beyond the SM. Before we move on to present one such alternative, let us remark on one more purpose the Higgs serves in the SM. All calculations within the SM are performed as perturbative expansions in the small couplings. When one performs a computation for the cross-section of a particular process, it is important to check that the probability that the process occurs is less than one, so the results make

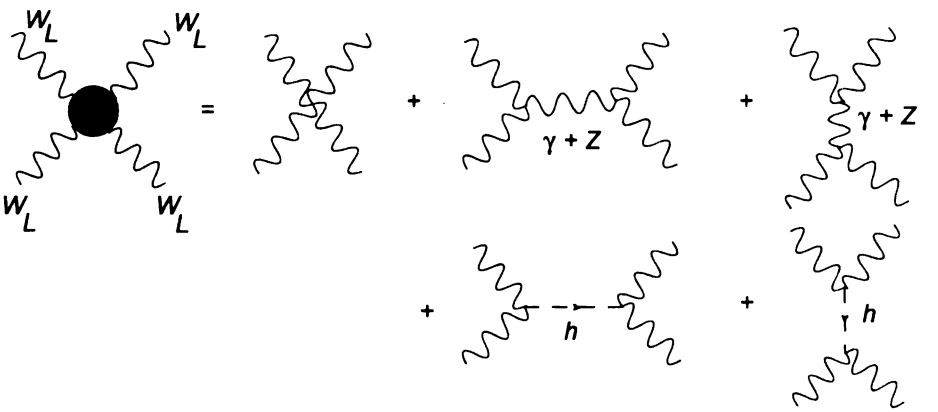

Figure 1.2: The Feynman diagrams for the longitudinal gauge boson scattering in the Standard Model. The E^4 contributions cancel due to gauge invariance. The E^2 contributions only vanish when we include the Higgs exchange diagrams.

physical sense. In other words, the theory has to be *unitary*. This is crucial because absence of unitarity indicates that the perturbation theory has broken down, and thus, self-consistency of perturbation theory requires the probability be bounded by one.

As an example, let us look at the longitudinal gauge boson scattering, i.e., the process $W_L W_L \to W_L W_L$ in the SM - the reason for the choice is that the longitudinal components are the ones acquired by the gauge bosons by eating the Goldstone fields, and hence are most closely asscociated with the Higgs mechanism. The Feynman diagrams that contribute to this process are shown in Figure 1.2. When we compute the amplitude for the entire process $W_L W_L \to W_L W_L$, and look at the large energy behavior, i.e., in the limit $E/m_W >> 1$, we find that the pieces of the amplitude that grows like E^4 cancel between the contact interaction and the photon and Z exchange diagrams. (This is due to gauge invariance which guarantees the relation $e = g_2 \sin\theta_W$). However, for the pieces that grows like E^2 to cancel, we have to include the Higgs exchange diagrams. Thus, we find that the Higgs not only serves to give masses to the gauge bosons and the fermions, but also serves to regulate the

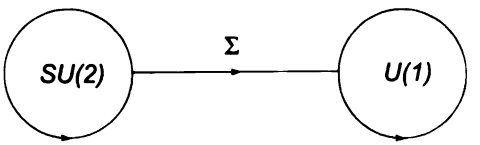

Figure 1.3: The Standard Model without the scalar Higgs boson. The result is an $SU(2)_L \times SU(2)_R$ non-linear sigma model with the $SU(2) \times U(1)$ part gauged.

bad high energy behavior of the theory. If we are to formulate a theory that goes beyond the SM *and* does not have a Higgs, we have to make sure the theory does not violate unitarity.

1.3 A Higgsless Standard Model

Though we established in the last section that the SM without the Higgs would not be unitary, it is still instructive to ask what the theory would look like if we do not include $h(x)$ in the theory. Let us start by reproducing Eqn. (1.15).

$$\phi = e^{i\pi^a\sigma^a/v}\begin{pmatrix} 0 \\ \frac{v+h(x)}{\sqrt{2}} \end{pmatrix}. \tag{1.27}$$

The above form clearly separates out the three Goldstone bosons (π^a) that become the longitudinal components of the gauge bosons from the physical Higgs boson. When the Higgs boson is eliminated, what remains is a non-linear $SU(2)_L \times SU(2)_R$ sigma model of which the $SU(2) \times U(1)$ part is gauged. We show this in pictorial notation in Figure 1.3. To derive the Lagrangian for this low energy effective theory, we plug in Eqn. (1.15) in the Higgs Lagrangian, Eqn. (1.12).

$$\mathcal{L} = \frac{1}{4}(v+h)^2\mathrm{Tr}\left[\left(D_\mu\Sigma^\dagger\right)\left(D_\mu\Sigma\right)\right] + \frac{1}{2}(\partial_\mu h)(\partial^\mu h) - \frac{1}{2}m_h^2(v+h)^2 - \frac{\lambda}{4!}(v+h)^4. \tag{1.28}$$

In the limit $m_h \to \infty$, we can read off the effective Lagrangian from the above equation by simply disregarding the Higgs field and it is given by:

$$\mathcal{L}_{\text{Goldstone}} = \frac{v^2}{4}\text{Tr}\left[\left(D_\mu\Sigma^\dagger\right)\left(D_\mu\Sigma\right)\right]. \tag{1.29}$$

and contains only the eaten pions. This picture is called a "non-linear sigma model".

The Goldstone boson equivalence theorem [3, 4] tells us that at high energies, the amplitude for absorption or emission of longitudinal gauge bosons is the same as the one for the corresponding eaten pion. We can determine the Feynman rules for $\pi - \pi$ scattering in this model by plugging in $\Sigma = e^{i\pi^a\sigma^a/v}$ in Eqn. (1.29) and expanding in powers of π/v. At tree level, there is only a contact interaction term and the amplitude for this is given by:

$$M(\pi^+\pi^- \to \pi^+\pi^-) = g^2\left(\frac{1+\cos\theta}{2}\right)\left(\frac{E}{m_W}\right)^2, \tag{1.30}$$

where θ is the scattering angle. It is hardly surprising that the E^2 growth does not cancel, as there is no physical Higgs boson in the spectrum. But the question we would like to address is whether it is possible to extend a theory of this kind by including additional particles to retain unitarity, in place of a Higgs.

How would one construct an electroweak symmetry breaking sector without a scalar particle? A glimpse to an answer to this question is provided by QCD. Consider QCD with two flavors - the up and down quarks. Let us, for the moment, assume that these are massless - the u and d quarks are light compared to the QCD scale, Λ_{QCD}= 300 MeV, and hence this is a good approximation. Then, the Lagrangian of QCD can be written down (with $\Psi = (u, d)$) as:

$$\mathcal{L}_{\text{QCD}} = i\bar{\Psi}_L\gamma^\mu D_\mu\Psi_L + i\bar{\Psi}_R\gamma^\mu D_\mu\Psi_R. \tag{1.31}$$

and is seen to possess a global $SU(2)_L \times SU(2)_R$ symmetry, the *chiral* symmetry. When the running QCD coupling constant becomes large at the scale of QCD ($\Lambda_{\rm QCD}$), the strong interactions bind quark anti-quark pairs into a composite spin-0 object: $\langle 0|\bar{\Psi}\Psi|0\rangle$ - this is analogous to the formation of Cooper pairs in the theory of superconductivity. This, like the Higgs in the SM, develops a vacuum expectation value $\langle\bar{\Psi}\Psi\rangle = \Lambda^3_{\rm QCD}$, thus spontaneously breaking the $SU(2)_L \times SU(2)_R$ chiral symmetry down to the diagonal subgroup, $SU(2)_V$. Each fermion field has a mass dimension 3/2, and thus the condensate has a mass dimension 3. Typically, spontaneously breaking a continuous symmetry generates massless Goldstone bosons. But the three QCD pions will *not* be massless, as we started with an *approximate* symmetry (i.e., valid only in the limit $m_{u,d} \to 0$). For this reason, the QCD pions are really *pseudo Goldtone bosons*. Now, if we were to describe EWSB using this picture, we would let these three pions be eaten by the $W^\pm$ and the Z, thus making the gauge bosons massive. Unfortunately, the scale characterizing the gauge boson masses would be wrong - the pion decay constant that sets the scale in this model is $f_\pi = 93$MeV, but we know that the electroweak scale that sets the scale of the W and Z bosons is $v = 246$ GeV. Thus, QCD, though successful in achieving the correct symmetry breaking pattern, cannot reproduce the correct gauge boson masses. However, one could construct a "scaled up" version of QCD, called Technicolor [5, 6, 7], wherein technicolor interactions (assumed to be confining, like QCD) bind techni-quark techni-antiquark pairs into a $\langle\bar{\Psi}_{\rm TC}\Psi_{\rm TC}\rangle$ condensate. The scale of technicolor interactions (i.e., the scale at which technicolor interactions become strong and form condensates) can be tuned to reproduce the correct gauge boson masses. To get fermion masses, this picture has to be extended, and the resulting theory, called "Extended Technicolor" (ETC) is described in [7, 8, 9, 10, 11].

Theories like the one described above are strongly interacting, and thus, cannot be treated as perturbative quantum field theories. One has to develop lattice calculations

and other non-perturbative tools in order to be able to compute in such theories. However, recently, there has emerged a special correspondence that relates strongly interacting four dimensional theories to weakly interacting five dimensional ones - the *AdS*-CFT correspondence [19, 20, 21, 22] first arose in the context of string theories describing the duality between type IIB string theory and classical supergravity. Later works have established that such a duality exists more generally and that many strongly interacting theories have a dual description in an extra dimensional context. Higgsless models in an extra dimension have thus emerged as viable theories of EWSB that are the analogues of technicolor theories. We turn our attention to these extra dimensional models in the next sections.

1.4 Extra dimensional theories

It is possible that our universe may have dimensions other than the customary 4-D space-time [12, 13, 14, 15, 16, 17, 18]. These extra dimensions must have to be compact, so we don't realize their existence in everyday life. This compact fifth dimension can be thought of as an interval, without loss of generality. For example, if the extra dimension is a circle of radius R, one could map it onto an interval $[0, 2\pi R]$ with periodic boundary conditions. If a reflection symmetry (a Z_2 symmetry) is imposed on top of the circle, we could map it onto the interval $[0, \pi R]$. The fields can have odd or even transformation properties under the Z_2 symmetry and the extra dimension is said to be "compactified" on an interval. A circle is a 1-D surface, S^1 - the process of imposing the Z_2 symmetry on top of this surface is called "Orbifolding", in particular, S^1/Z_2 orbifold. As we will see below, this picture naturally offers a rich spectrum of new, heavy particles that would be observable at energies greater than the inverse compactification radius, i.e., $E > 1/R$, where R is the radius or size of the extra dimension. Let us first try to understand the features of such a theory by

having the extra dimension populated by a scalar field, for simplicity.

1.4.1 Scalar field in the bulk

Consider a massless complex scalar field living in 5-D. The action for such a theory is given by:

$$S = \int d^5x \mathcal{L}(\vec{x}, z), \tag{1.32}$$

where z is the fifth dimension co-ordinate and the Lagrangian is given by:

$$\mathcal{L} = (\partial_\alpha \Phi)^\dagger (\partial_\alpha \Phi). \tag{1.33}$$

We will let z run from 0 to $2\pi R$, with the points $z = 0$ and $z = 2\pi R$ identified. This means that we are compactifying the extra dimension on a circle, and thus, we can expand Φ as a Fourier series in the following way:

$$\Phi(\vec{x}, z) = \sum_{n=-\infty}^{+\infty} \Phi^{(n)}(x) e^{(inz/R)}. \tag{1.34}$$

In this form, it is clear that $\Phi(\vec{x}, 0) = \Phi(\vec{x}, 2\pi R)$. Plugging back the solution, Eqn. (1.34) in the action, Eqn. (1.32), and integrating over z, we get:

$$\mathcal{L} = \sum_{n=-\infty}^{+\infty} (\partial_\alpha \Phi^{(n)})^\dagger (\partial_\alpha \Phi^{(n)}) - m_n^2 (\Phi^{(n)})^\dagger \Phi^{(n)}, \tag{1.35}$$

where

$$m_n^2 = \frac{n^2}{R^2}. \tag{1.36}$$

Thus, we see that we have ended up with a theory in which the lowest $n = 0$ state is massless and a tower of additional resonances whose masses are given by Eqn. (1.36). This tower is called the "Kaluza-Klein Resonances", or KK tower, for short.

Thus, this simple example demonstrates how a compactified extra dimensional theory naturally yields a rich spectrum of particles. Next, we apply this idea to gauge field theories.

1.4.2 Gauge theory in the bulk

Let us consider a gauge theory living in the bulk of the extra dimension, letting the group G be arbitrary. We will let the extra dimension be flat, i.e., the metric is given by $G^{MN} = (1, -1, -1, -1, -1)$.

The action for the extra dimensional gauge theory can be written as:

$$S_{\text{gauge}} = \int d^5x \left[-\frac{1}{4g_5^2} F^a_{MN} F^{aMN} - \frac{1}{4g_5^2 \xi} \left(\partial_\mu A^{a\mu} + \xi \partial_z A^{az} \right)^2 \right], \tag{1.37}$$

where

$$F^a_{MN} = \partial_M A^a_N - \partial_N A^a_M + f^a{}_{bc} A^b_M A^a_N. \tag{1.38}$$

and g_5 is the five dimensional gauge coupling and the second term in Eqn. (1.37) is the gauge fixing term. The form of the gauge fixing term is so chosen that it cancels the mixing between the gauge and Goldstone fields, $\partial_z A^a_\mu \partial_\mu A^{a5}_\mu$, that arises from the $F^a_{\mu z} F^{a\mu z}$. The variation of the action Eqn. (1.37) leads to the equations of motion:

$$\partial_M F^{aM\nu} - f^{abc} F^{bM\nu} A^c_M + \frac{1}{\xi} \partial^\nu \partial^\sigma A^a_\sigma - \partial^\nu \partial_z A^a_5 = 0, \tag{1.39}$$

$$\partial^\sigma F^a_{\sigma z} - f^{abc} F^b_{\sigma z} A^{c\sigma} + \partial_z \partial_\sigma A^{a\sigma} - \xi \partial_z^2 A^a_5 = 0. \tag{1.40}$$

The requirement that the boundary piece vanishes leads to the condition:

$$\left[F^a_{\nu z} \delta A^{a\nu} + \left(\partial_\sigma A^{a\sigma} - \xi \partial_z A^a_5 \right) \delta A^a_5 \right]_0^{\pi R} = 0. \tag{1.41}$$

The behavior of the fields at the boundaries of the extra dimension (the boundary

conditions) now have to be chosen. There are three choices that respect 4-D Lorentz invariance:

$$A^a_\mu = 0, \quad A^a_5 = \text{const.}, \tag{1.42}$$

$$A^a_\mu = 0, \quad \partial_z A^a_5 = 0, \tag{1.43}$$

$$F^a_{\mu z} = 0, \quad A^5_a = \text{const.}. \tag{1.44}$$

The choice of the boundary condition determines the pattern of symmetry breaking. Once we choose a particular breaking pattern, we can expand the gauge fields in KK modes like in the last section:

$$\begin{aligned} A^a_\mu(\vec{x}, z) &= \sum_n f_n(z) A^a_{n\mu}(x) \\ A^a_5(\vec{x}, z) &= \sum_n g_n(z) \pi^a_n(x). \end{aligned} \tag{1.45}$$

Thus, we see that the 5-D gauge field is decomposed into a vector and a 5-D scalar. In a realistic model, one lets the bulk gauge group be $SU(2)$ and the boundary conditions have to be chosen so that we have a zero mode that represents the W and the Z bosons, plus a tower of vector bosons. The Higgs mechanism still operates: the A_5 fields become the longitudinal components of these KK vector bosons, making them massive. Thus, the spectrum consists of the SM particles and their heavy copies. Let us briefly discuss a toy model with these features. We will let the bulk gauge group be $SU(2)$ and let the following boundary conditions break $SU(2)$ down to $U(1)$ at one end of the interval: At $z = 0$:

$$\partial_z A^a_\mu = 0, \tag{1.46}$$

$$A^a_5 = 0, \tag{1.47}$$

and at $z = \pi R$:

$$A_\mu^{1,2} = 0, \quad \partial_5 A_\mu^3 = 0 \tag{1.48}$$

$$\partial_z A_\mu^{1,2} = 0, \quad A_5^3 = 0. \tag{1.49}$$

We will work in the unitary gauge, $A_5^a = 0$. The KK expansions are:

$$A_\mu^\pm(\vec{x}, z) = \sum_n f_n(z) W_{n\mu}^\pm(x) \tag{1.50}$$

$$A_\mu^3(\vec{x}, z) = \sum_n g_n(z) Z_{n\mu}(x). \tag{1.51}$$

The eigenfunctions $f(z)$ and $g(z)$ are combinations of sines and cosines. Using the BCs, we can derive the following mass equations:

$$\cos\left(M_n^\pm \pi R\right) = 0, \tag{1.52}$$

$$\sin\left(M_n^0 \pi R\right) = 0 \tag{1.53}$$

where M_n^0 and $M_n^\pm$ are the masses of the neutral and charged gauge boson towers respectively. The solutions are given by:

$$M_n^\pm = \frac{n - 1/2}{R}, \quad n = 1, 2, ... \tag{1.54}$$

$$M_n^0 = \frac{n}{R}, \quad n = 0, 1, 2, ... \tag{1.55}$$

$$\tag{1.56}$$

We see that the lowest mode of the charged tower is a massive particle, which we can identify with the SM W boson. The $n = 0$ state of the neutral tower corresponds to the massless photon, and the $n = 1$ state can be identified with the Z boson. Of course, the precise W and Z mass relation does not come out - but our purpose here

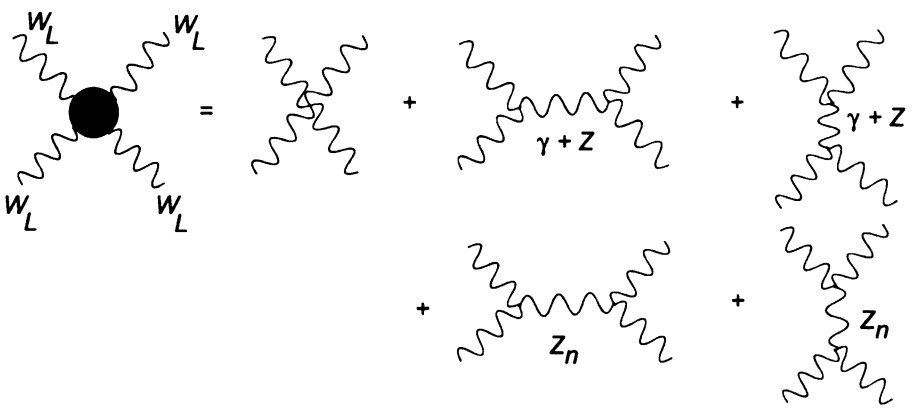

Figure 1.4: The Feynman diagrams for the longitudinal gauge boson scattering in extra dimensional model. Unitarity in this process is achieved by the exchange of the heavy vector boson instead of a Higgs.

is to develop a toy model that has the essential features of extra dimensional theories. Thus, we see that even in a toy model, one could choose the boundary conditions appropriately to get a rich particle spectrum in which the lowest KK modes can be identified with the SM particles, while the higher modes represent the KK resonances.

These KK resonances serve an important purpose. As explained in the beginning of the section, we have to ensure that the $W_L - W_L$ scattering amplitude is unitary, and the unitarization is carried out by the exchange of these heavy vector bosons in place of a Higgs in these theories. The Feynman diagrams for $W_L W_L \to W_L W_L$ is shown in Figure 1.4. The amplitude can be written in a generic form:

$$A = A^{(4)} \frac{E^4}{M_n^4} + A^{(2)} \frac{E^2}{M_n^2}. \tag{1.57}$$

The expressions for $A^{(1)}$ and $A^{(2)}$ can be derived to be:

$$A^{(4)} = i\left(g_{nnnn}^2 - \sum_k g_{nnk}^2\right)\left[f^{abe}f^{cde}(3+6\cos\theta-\cos^2\theta)+2(3-\cos^2\theta)f^{ace}f^{bde}\right] \tag{1.58}$$

$$A^{(2)} = \frac{i}{M_n^2}\left(4g_{nnnn}^2M_n^2 - 3\sum_k g_{nnk}^2M_k^2\right)\left[f^{ace}f^{bde} - \sin^2\frac{\theta}{2}f^{abe}f^{cde}\right]. \tag{1.59}$$

If the masses and couplings of the KK modes satisfy the following two sum rules:

$$g_{nnnn}^2 = \sum_k g_{nnk}^2 \tag{1.60}$$

$$g_{nnnn}^2M_n^2 = \frac{3}{4}\sum_k g_{nnk}^2M_k^2, \tag{1.61}$$

the pieces of the amplitude that grow as E^4 and E^2 are cancelled. (In the expressions for the amplitudes above, the first sum rule has already been used to simplify the form of $A^{(2)}$). Thus, we see that it is possible to maintain unitarity the exchange of new heavy vector states in a model with no physical scalar particle.

1.4.3 Fermions in 5-D

Now that we have seen a toy model to generate gauge boson masses in an extra dimensional theory, we will now investigate the problem of fermions living in an extra dimension. A 5-D Dirac spinor decomposes under the 4-D Lorentz subgroup into two two-component spinors:

$$\Psi = \begin{pmatrix} \Upsilon^\alpha \\ \bar{\psi}^{\dot{\alpha}} \end{pmatrix}. \tag{1.62}$$

In 5-D, the Dirac matrices read:

$$\Gamma^{\mu} = \begin{pmatrix} 0 & \sigma^{\mu} \\ \bar{\sigma}^{\mu} & 0 \end{pmatrix}, \quad \Gamma^{5} = i \begin{pmatrix} 1 & 0 \\ 0 & 1, \end{pmatrix} \tag{1.63}$$

where the σ's are the usual Pauli matrices. Now let us impose the Z_2 orbifold projection, $z \to -z$. In order to leave the 5-D Dirac equation invariant, Ψ has to satisfy:

$$\Psi(-z) = -i\Gamma^{5}\Psi(z), \tag{1.64}$$

i.e.,

$$\chi(-z) = \chi(z) \quad \text{and} \quad \psi(-z) = -\psi(z). \tag{1.65}$$

This suggests that χ and ψ can be written as:

$$\chi(x, z) = \sum_{n=0}^{\infty} \cos\left(\frac{nz}{R}\right) \chi^{(n)}(x), \tag{1.66}$$

$$\psi(x, z) = \sum_{n=0}^{\infty} \sin\left(\frac{nz}{R}\right) \psi^{(n)}(x) \tag{1.67}$$

Thus, we see that only χ has a KK zero mode.

We will now try recover this result using the "interval" approach. The 5-D action for Ψ reads:

$$S = \int d^{5}x \left[\frac{i}{2}\left(\bar{\Psi}\Gamma^{M}\partial_{M}\Psi - \partial_{M}\bar{\Psi}\Gamma^{M}\Psi\right) - m\bar{\Psi}\Psi\right]. \tag{1.68}$$

where the last term is a "bulk mass". The above action can be recast in 4-D components as:

$$S = \int d^{5}x \left[-i\bar{\chi}\bar{\sigma}^{\mu}\partial_{\mu}\chi - i\psi\sigma^{\mu}\partial_{\mu}\bar{\psi} + \left(\psi\overleftrightarrow{\partial_{z}}\chi - \bar{\chi}\overleftrightarrow{\partial_{z}}\bar{\psi}\right) + m\left(\psi\chi + \bar{\chi}\bar{\psi}\right)\right]. \tag{1.69}$$

where $\overleftrightarrow{\partial_z} = \frac{1}{2}(\overrightarrow{\partial_z} - \overleftarrow{\partial_z})$. The variation of this action leads to the equations of motion:

$$-i\bar{\sigma}^\mu \partial_\mu \chi - \partial_z \bar{\psi} + m\bar{\psi} = 0 \tag{1.70}$$

$$-i\sigma^\mu \partial_\mu \bar{\psi} + \partial_z \chi + m\chi = 0. \tag{1.71}$$

Requiring that the variation of the action at the boundary vanishes gives the condition:

$$-\chi\delta\psi + \psi\delta\chi + \delta\bar{\chi}\bar{\psi} - \bar{\chi}\delta\bar{\psi} = 0. \tag{1.72}$$

We also have to impose a boundary condition for Ψ in the form $f(\chi, \psi) = 0$ at the two boundaries of the interval, and this, along with the equations of motion, will fix all the arbitrary coefficients in the complete solution to the spinor equation. For instance, we can require that the spinor ψ vanishes on both boundaries. This would lead to:

$$(\partial_z + m)\chi|_{0,\pi R} = 0. \tag{1.73}$$

Solving the equations of motion with these boundary conditions would result in a zero mode for χ, but not ψ.

As in the case of gauge fields, we can expand the spinors in KK modes. Performing this KK decomposition gives us:

$$\chi = \sum_n g_n(z)\chi_n(x) \tag{1.74}$$

$$\psi = \sum_n f_n(z)\psi_n(x). \tag{1.75}$$

The fermions obey the Dirac equation:

$$-i\bar{\sigma}^\mu \partial_\mu \chi^{(n)} + m_n \bar{\psi}^{(n)} = 0 \tag{1.76}$$

$$-i\sigma^\mu \partial_\mu \bar{\psi}^{(n)} + m_n \chi^{(n)} = 0. \tag{1.77}$$

Substituting the KK decomposition into these equations gives:

$$g_n' + m g_n - m_n f_n = 0 \tag{1.78}$$

$$f_n' - m f_n + m_n g_n = 0. \tag{1.79}$$

We can combine these two coupled first order equations to form two uncoupled second order equations.

$$g_n'' + (m_n^2 - m^2) g_n = 0 \tag{1.80}$$

$$f_n'' + (m_n^2 - m^2) f_n = 0. \tag{1.81}$$

The solutions are simply sums of sines and cosines, whose coefficients are determined by reimposing the first order equations and the boundary conditions. For instance, if we impose $\psi = 0$ at both $z = 0$ and $z = \pi R$, we obtain:

$$f_n(z) = a_n \sin \frac{nz}{R}, \tag{1.82}$$

$$g_n(z) = \frac{a_n}{m_n} \left(\frac{n}{R} \cos \frac{nz}{R} - m \sin \frac{nz}{R} \right), \tag{1.83}$$

where

$$m_n = \sqrt{m^2 + \frac{n^2}{R^2}}, \tag{1.84}$$

and the coefficient a_n is fixed by the normalization condition:

$$\int_0^{\pi R} dz f_n^2(z) = 1. \tag{1.85}$$

The boundary conditions also allow for a zero mode for χ:

$$g_0(z) = \sqrt{\frac{2m}{1 - e^{-2m\pi R}}}\ e^{-mz}. \tag{1.86}$$

We see that the 5-D mass does not contribute to the mass of the lightest fermion (it stays massless). This is important - in a realistic theory, we should have all the SM fermions nearly massless (except the top-quark).

Now that we have discussed gauge theories and fermions in extra dimensions, let us move on to see if we can develop an understanding of the features of these theories based purely on physics in 4-D.

1.5 Deconstruction

As we have seen, compactified extra dimensions naturally have an associated KK tower. We would like to see if we can write down a simple gauge invariant Lagrangian to describe these KK modes without the full machinery of the extra dimension. This is done using the idea of "Deconstruction"[23, 24] - a manifestly 4-D description of 5-D physics.

Consider a gauge theory living in a slice of extra dimension. Now, if we imagine slicing up the extra dimension into an infinite number of segments, each plane is described by a 4-D gauge theory. So a 5-D gauge theory can be thought of as in infinite collection of 4-D gauge groups. Let us suppose the gauge group is $SU(2)$. We have to let the gauge symmetries be broken so the KK resonances become massive. We can do this by having a Higgs field, $\Phi(x)$, that transforms between two adjacent gauge groups $SU(2)$ groups as $(\bar{2}, 2)$. When the Higgs field develops a diagonal vev, i.e., $\langle\Phi\rangle = \begin{pmatrix} v & 0 \\ 0 & v \end{pmatrix}$, it breaks $SU(2) \times SU(2)$ down to the diagonal sub group, and thus we will have massive W and Z bosons plus their KK partners. But since our only goal is to break the gauge symmetry, we can do away with the scalar Higgs degree of freedom and employ a non-linear sigma model, in the spirit of the Higgsless Standard Model. Thus, the picture that emerges is one that is exactly like in Figure (1.3),

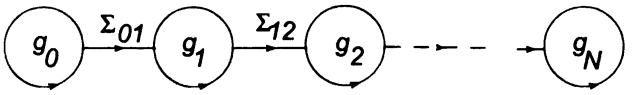

Figure 1.5: A deconstructed picture of the extra dimension. The 4-D gauge groups are connected by means of non-linear sigma model fields.

albeit with replicated gauge groups. This picture is called a "Moose" or "Quiver" diagram [25]. We show a general deconstructed model in Figure 1.5.

The non-linear sigma fields transform as fundamentals and anti-fundamentals under the adjacent gauge groups, $\Sigma_{i,i+1} \to U_i^{-1}\Sigma_{i,i+1}U_{i+1}$. The action for this theory can be written down by simply extending Eqn. (1.29) to include multiple sigma fields and gauge groups:

$$S = \int d^4x \sum_{i=1}^{\infty} -\frac{1}{2g_i^2}\mathrm{Tr}\left(F^{i\mu\nu}F^i_{\mu\nu}\right) + \int d^4x \sum_{i=1}^{\infty} -\frac{f_i^2}{4}\mathrm{Tr}\left|D_\mu\Sigma_{i,i+1}\right|^2, \qquad (1.87)$$

where the covariant derivative is given by:

$$D_\mu\Sigma_{i,i+1} = \partial_\mu\Sigma_{i,i+1} - iA_{i\mu}\Sigma_{i,i+1} + iA_{i+1\mu}\Sigma_{i,i+1}. \qquad (1.88)$$

To check that this picture is indeed right, let us look at the continuum limit, i.e., in the limit $N \to \infty$. In this limit, we should recover the full 5-D gauge theory. To do this, let us start by relabeling the couplings and the decay constants.

$$g_i = \sqrt{N+2}\,\kappa_i \qquad (1.89)$$

$$f_i = \sqrt{N+1}\,h_i \qquad (1.90)$$

with the constraints

$$\frac{1}{N+2}\sum_{i=0}^{N+1}\frac{1}{\kappa_i^2} = \frac{1}{N+1}\sum_{i=0}^{N+1}\frac{1}{h_i^2} = 1. \qquad (1.91)$$

which come from

$$\frac{1}{g^2} = \sum_{i=0}^{N+1} \frac{1}{g_i^2} \tag{1.92}$$

$$\frac{1}{f^2} = \sum_{i=0}^{N+1} \frac{1}{f_i^2} \tag{1.93}$$

Let us now define the dimensionless coordinate:

$$z_i = \frac{i}{N+1}, \tag{1.94}$$

and make the following identifications between 4-D and 5-D quantities:

$$\begin{aligned}
z_i &\to z, \\
\Delta z = \frac{1}{N+1} &\to dz, \\
\frac{1}{N+1} \sum_{i=0}^{N+1} &\to \int dz, \\
A_j^\mu(x) &\to A_j(x,z), \\
(N+1)\left[A_{j+1}^\mu(x) - A_j^\mu(x)\right] &\to \frac{\partial A_\mu}{\partial z}, \\
\kappa_i, h_i &\to \kappa(z), h(z), \\
\frac{1}{N+2} \sum_{i=0}^{N+1} \frac{1}{\kappa_i^2} &\to \int dz \frac{1}{\kappa^2(z)} = 1, \\
\frac{1}{N+1} \sum_{i=0}^{N+1} \frac{1}{h_i^2} &\to \int dz \frac{1}{h^2(z)} = 1.
\end{aligned}$$

Using the above replacements and working in the unitary gauge ($\Sigma_i = I$), the action, (Eqn. (1.87), becomes:

$$S_{\text{gauge}} = \int d^5x \left[-\frac{1}{2g^2\kappa^2(z)} \text{Tr}\left(F_{\mu\nu}F^{\mu\nu}\right) + \frac{f^2 h^2(z)}{4} \text{Tr}\left(F_{\mu z}F^{\mu z}\right) \right], \tag{1.95}$$

where

$$F_{\mu z} = \partial_z A_\mu, \tag{1.96}$$

since in the unitary gauge, $A_z = 0$. The above equation represents the action for a 5-D gauge in a "warped" or "curved" background, i.e., a geometry that is not flat (Note that if we had started with all the g_i's and f_i's the same, we would have ended up with the action for a gauge theory in a flat extra dimension, Eqn. (1.37)). Relabeling $g \to g\kappa$ and $f \to fh$, we see that this is reflected in the fact that the gauge couplings and f constants depend on the extra dimensional co-ordinate z. Thus, the process of deconstruction allows us to recover the complete 5-D theory in the continuum limit.

1.6 Deconstructed Higgsless Model

We will develop a deconstructed Higgsless model [26, 27, 28, 29] derived from a flat extra dimension, i.e., we will choose all the bulk gauge couplings and the decay constants, f, to be the same through the moose. When we integrate out all the heavy KK states, we should be left with an $SU(2) \times U(1)$ Higgsless standard model. We will thus choose the coupling at the first site to be g, which is almost the same as the SM $SU(2)$ coupling and, at the last site, we will gauge the $U(1)$ part of the $SU(2)$ and give it a SM-like hypercharge coupling g' - the couplings of the first and last site gauge groups being different from the rest of the moose is indicative of the boundary conditions imposed at the two ends of the extra dimension in the underlying 5-D theory. Thus, the gauge group of this N site moose is $\prod_{i=0}^{N-1} SU(2)_i \times U(1)$ (Figure 1.6). The sigma fields connecting two adjacent gauge groups transform, as before, as $\Sigma_{i,i+1} \to U_i^{-1} \Sigma_{i,i+1} U_{i+1}$. When the sigma fields develop a vev (f) and break every adjacent $SU(2) \times SU(2)$ groups down to the diagonal $SU(2)$, the lowest lying modes (which we identify as the SM W and Z bosons) and the KK tower get masses.

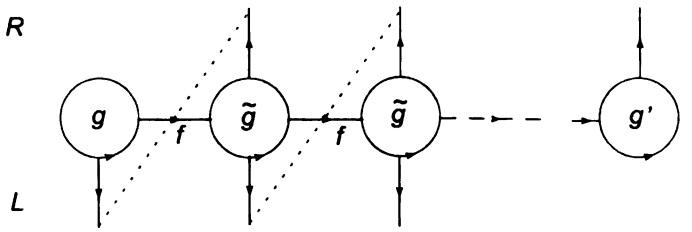

Figure 1.6: A deconstructed Higgsless model derived from a flat extra dimension. All the bulk gauge couplings are the same and so are the decay constants. The left and right handed fermions have Yukawa couplings to the sigma fields and also have a bulk Dirac mass term.

1.6.1 Gauge sector

The gauge sector Lagrangian reads:

$$\mathcal{L} = -\frac{1}{4}\sum_i W_i^{a\mu\nu} W^{ia\mu\nu} - \frac{1}{4} B^{\mu\nu} B_{\mu\nu} + \frac{f^2}{4}\sum_i \left| D_\mu \Sigma_{i,i+1} \right|^2, \tag{1.97}$$

where the covariant derivative is given by:

$$D_\mu \Sigma_{i,i+1} = \partial_\mu \Sigma_{i,i+1} + i\tilde{g} W_\mu^i \Sigma_{i,i+1} - i\tilde{g} \Sigma_{i,i+1} W_\mu^{i+1}, \tag{1.98}$$

and $\tilde{g}$ is the gauge coupling of the internal (or the bulk) $SU(2)$ groups. The mass terms for the gauge bosons can be derived from the last term of Eqn. (1.97) by working in the unitary gauge ($\Sigma = 1$). The charged gauge boson mass matrix is given by:

$$M_W^2 = \frac{\tilde{g}^2 f^2}{4} \begin{pmatrix} x^2 & -x & 0 & 0 & 0 & \cdots & 0 \\ -x & 2 & -1 & 0 & 0 & \cdots & 0 \\ 0 & -x & 2 & -1 & 0 & \cdots & 0 \\ \vdots & \vdots & \vdots & \vdots & \vdots & & \\ 0 & 0 & 0 & 0 & \cdots & -1 & 2. \end{pmatrix} \tag{1.99}$$

where $x = g/\tilde{g}$ is a small parameter. The matrix can be diagonalized perturbatively in x to yield the mass eigenvalues of the standard W boson and the KK resonances.

$$M_W^2 = \frac{g^2 f^2}{4(N+1)} \left[1 - \frac{N(2N+1)}{6(N+1)} x^2 + \cdots \right] \tag{1.100}$$

$$M_{W'}^2 = \tilde{g}^2 f^2 \left(\sin \frac{n\pi}{2(N+1)} \right)^2 + 2M_W^2 \left(\cos \frac{n\pi}{2(N+1)} \right)^2 . \tag{1.101}$$

In the continuum limit ($N \to \infty$), we see that the second term inside the parenthesis goes to zero. Thus, to recover the correct formula for the mass of the W gauge boson, f should scale like $v/\sqrt{N+1}$. Similarly, the neutral gauge boson mass matrix is given by:

$$M_Z^2 = \frac{\tilde{g}^2 f^2}{4} \begin{pmatrix} x^2 & -x & 0 & 0 & 0 & \cdots & 0 \\ -x & 2 & -1 & 0 & 0 & \cdots & 0 \\ 0 & -x & 2 & -1 & 0 & \cdots & 0 \\ \vdots & \vdots & \vdots & \vdots & \vdots & & \\ 0 & 0 & 0 & 0 & \cdots & 2 & y \\ 0 & 0 & 0 & 0 & \cdots & -y & y^2 \end{pmatrix} \tag{1.102}$$

where $y = g'/\tilde{g}$. The light and heavy eigenvalues are given by:

$$M_Z^2 = \frac{(g^2 + g'^2) f^2}{4(N+1)} \left[1 - \frac{N(2N+1)}{6(N+1)} (x^2 + y^2) + \frac{N x^2 y^2}{(x^2 + y^2} + \cdots \right] \tag{1.103}$$

$$M_{Z'}^2 = \tilde{g}^2 f^2 \left(\sin \frac{n\pi}{2(N+1)} \right)^2 + 2M_Z^2 \left(\cos \frac{n\pi}{2(N+1)} \right)^2 . \tag{1.104}$$

1.6.2 Fermion sector

To construct a realistic theory, we have to put in the fermions. In Figure (1.6), we show left (right) handed fermions as top (bottom) lines attached to each gauge

group. How do we write down mass terms for these fermions in the deconstructed language? In the spirit of Eqn.(1.68), we can write down a "bulk" mass term of the form $M\bar{\psi}\psi$. But the gauge symmetries also allow a term that couples fermions in adjacent sites - this "hopping" term ties left and right handed fermions through a Yukawa coupling to the sigma field and takes the form $\bar{\psi}_{Li}\Sigma_{i,i+1}\psi_{R,i+1}$. When the sigma field develops a vev, this becomes a mass term for the fermions. It was shown in [26, 27] that a Higgsless model with the light SM fermions localized on the branes (in the deconstructed picture, deriving the $SU(2)$ charge only from the first site) does not satisfy precision electroweak measurements. Thus, one has to allow the fermions to "delocalize", i.e., derive their $SU(2)$ charge from more than one site. In the 5-D picture, this correponds to the wavefunction of the fermion "leaking" into the bulk of the extra dimension. We write down the fermion Lagrangian below:

$$\begin{aligned} \mathcal{L}_{\text{fermions}} &= M_D \varepsilon_L \bar{\psi}_{L0}\Sigma_{01}\psi_{R1} + M_D \sum_i \bar{\psi}_{Li}\psi_{Ri} \\ &+ M_D \bar{\psi}_{LN}\Sigma_{N,N+1} \begin{pmatrix} \varepsilon_{uR} & \\ & \varepsilon_{dR} \end{pmatrix} \begin{pmatrix} u_{R2} \\ d_{R2} \end{pmatrix} + h.c. \end{aligned} \tag{1.105}$$

To get fermion flavor mixing, we could add generational indices to all the fermion fields, and choosing ε_L and M_D to be generation-diagonal, embed all the non-trivial flavor structure in the Yukawa matrix in the last term of Eqn. (1.106). Here, ε_L and ε_{fR} can be understood as the degree of delocalization of the left and right-handed fermions respectively. We will show how to determine the values of these parameters in the context of a model with only one extra $SU(2)$ group (a "three site model") in the next chapter. Diagonalizing the fermion mass matrix, we obtain the light and

heavy eigenvalues:

$$m_f = \frac{M_D \varepsilon_L \varepsilon_{fR}}{\sqrt{1 + \left(\frac{N\varepsilon_{fR}^2}{2}\right)}} \left[1 - \frac{12N + 6(N^2 - 2N)\varepsilon_{fR}^2 + (N^3 - 3N^2 + 2N)\varepsilon_{fR}^4}{48\left(1 + \frac{N\varepsilon_{fR}^2}{2}\right)} \right] \tag{1.106}$$

$$m_F = M_D. \tag{1.107}$$

Thus, a simple deconstructed model can be constructed without a physical Higgs boson in the spectrum. We have only sketched the general outline of such a theory in this section. We will construct simpler models in the next chapters and investigate their phenomenology in detail.

This thesis is organized as follows: in the next chapter, we will construct a simple model with only one site in the "bulk" (a three site model). In Chapter 3, we will look at a simple extension of the three site model by appealing to the idea of "top-color" that will enable us to have KK fermions in the spectrum that are light enough to be discovered at the LHC - we will investigate the phenomenology of these heavy fermions in detail and show that they are discoverable at the LHC for a wide range of masses. In Chapter 4, we will address the issue of unitarity in the process $t\bar{t} \to W_L^+ W_L^-$ in a family of deconstructed Higgsless models and show how the Appelquist-Chanowitz bound can be substantially weakened for a proper choice of the heavy fermion mass. Finally, in Chapter 5, we offer our conclusions.

Chapter 2

A Three Site Higgsless Model

2.1 A minimal model

Higgsless models, as we have seen, break the electroweak symmetry without requiring a fundamental scalar in the spectrum and the $W_L W_L$ scattering amplitude in these theories is unitarized by a tower of heavy gauge bosons, analagous to the SM W and Z bosons. Typically, these gauge bosons get progressively heavier and one can only see a few of the lowest lying resonances at the CERN LHC. Thus, it is phenomenologically useful to have an effective theory that retains only a few of the extra gauge bosons and yet captures all the phenomenologically interesting features of Higgsless models. In this chapter, we will present the Three Site Model [30], the simplest possible example of deconstructed Higgsless models of the kind described in the introduction. This chapter is based on work published in [30].

The model has the same color group as in the Standard Model and an extended $SU(2) \times SU(2) \times U(1)$ electroweak gauge group. Accordingly, there is one set of extra W' and Z' bosons that are heavy compared to their SM counterparts. This theory is in the same class as models of extended electroweak gauge symmetries [31, 32] motivated by models of hidden local symmetry [33, 34, 35, 36, 37]. We will

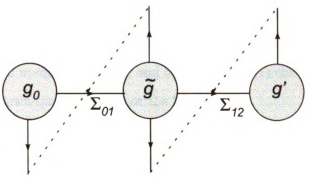

Figure 2.1: The three site model analyzed in this paper. g_0 and $\tilde{g}$ are the gauge couplings of the $SU(2)$ groups, while the coupling of the $U(1)$ is represented by g'. The left-handed fermions are denoted by the lower vertical lines (located at sites 0 and 1), and the right-handed fermions are denoted by the upper vertical lines (at sites 1 and 2). The dashed lines correspond to Yukawa couplings, as described in the text. As discussed below, we will take $\langle \Sigma_{01} \rangle = \langle \Sigma_{12} \rangle = \sqrt{2}\, v$.

also introduce a heavy fermionic partner for every SM fermion and these, along with the heavy gauge bosons, complete the extra particles in the spectrum. The scale of unitarity violation in the $W_L W_L$ scattering amplitude is delayed by the exchange of the W', as opposed to a tower of gauge bosons [43, 44, 45, 46, 47]. In Figure 2.1, we illustrate the model using "Moose notation" [25].

The model incorporates an $SU(2) \times SU(2) \times U(1)$ gauge group, and 2 nonlinear $(SU(2) \times SU(2))/SU(2)$ sigma models in which the global symmetry groups in adjacent sigma models are identified with the corresponding factors of the gauge group. The symmetry breaking between the middle $SU(2)$ and the $U(1)$ follows an $SU(2)_L \times SU(2)_R / SU(2)_V$ symmetry breaking pattern with the $U(1)$ embedded as the T_3-generator of $SU(2)_R$.

The left-handed fermions are $SU(2)$ doublets coupling to the groups at the first two sites, and which we will correspondingly label ψ_{L0} and ψ_{L1}. The right-handed fermions are an $SU(2)$ doublet at site 1, ψ_{R1}, and two singlet fermions, denoted in figure 2.1 as "residing" at site 2, u_{R2} and d_{R2}. The fermions ψ_{L0}, ψ_{L1}, and ψ_{R1}

have $U(1)$ charges typical of the left-handed doublets in the standard model, $+1/6$ for quarks and $-1/2$ for leptons. Similarly, the fermion u_{R2} has $U(1)$ charges typical for the right-handed up-quarks $(+2/3)$, and d_{R2} has the $U(1)$ charge associated with the right-handed down-quarks $(-1/3)$ or the leptons (-1).

In the analysis of a general linear moose model in Ref.[48], it was shown that a Higgsless model with localized fermions does not satisfy precision electroweak measurements. Thus, for these models to be viable, the fermions have to be "delocalized" - in the context of the three site model, this means that the fermions derive their $SU(2)$ charges from site 0 *and* site 1. (In an extra dimensional scenario, this is analagous to the "leakage" of the fermion wavefunction into the bulk). We will denote the amount of delocalization of the left(right) handed fermions by $\varepsilon_L(\varepsilon_R)$.

With the arrangement of fermions in Figure 2.1, we can write down Yukawa couplings linking adjacent left and right handed fermion fields via the non linear sigma model of the form $\bar{\psi}_L \Sigma \psi_R$. Thus, the fermion mass terms read:

$$\mathcal{L}_f = \lambda f_1 \bar{\psi}_{L0} \Sigma_1 \psi_{R1} + \sqrt{2}\tilde{\lambda} v \bar{\psi}_{R1} \psi_{L1} + f_2 \bar{\psi}_{L1} \Sigma_2 \begin{pmatrix} \lambda'_u & \\ & \lambda'_d \end{pmatrix} \begin{pmatrix} u_{R2} \\ d_{R2} \end{pmatrix} + h.c. \quad (2.1)$$

We will set the vev's of the sigma fields the same - $f_1 = f_2 = \sqrt{2}v$ (The reason for the $\sqrt{2}$ was explained in the introduction - for a Higgsless model derived from a flat extra dimension, the f constant should scale like $\sqrt{N+1}$ to recover the right continuum limit, and in the three site model, $N = 1$).

$$\mathcal{L}_f = M_D \left[\varepsilon_L \bar{\psi}_{L0} \Sigma_1 \psi_{R1} + \bar{\psi}_{R1} \psi_{L1} + \bar{\psi}_{L1} \Sigma_2 \begin{pmatrix} \varepsilon_{uR} & \\ & \varepsilon_{dR} \end{pmatrix} \begin{pmatrix} u_{R2} \\ d_{R2} \end{pmatrix} + h.c. \right] \quad (2.2)$$

We have set $\sqrt{2}\tilde{\lambda}v = M_D$ and set $\lambda/\tilde{\lambda} = \varepsilon_L$ and $\lambda'/\tilde{\lambda} = \varepsilon_R$. It is now straightforward to incorporate quark flavor and mixing in a minimal way. To get the SM quark flavor

mixing, we could add generational indices to each of the fermion fields, and, choosing ε_L and the mass term M_D to be generation-diagonal, embed all of the nontrivial flavor structure in the Yukawa matrix in the last term in Eqn. (2.2) – precisely as in the standard model; the only mixing parameters that appear are the ordinary Cabibbo-Kobayashi-Maskawa (CKM) angles and phase.

2.2 Masses and Eigenstates

This section reviews the mass eigenvalues and the wavefunctions of the gauge bosons and fermions of the three-site model. The gauge sector is the same as that of the BESS model [31]. Ref. [43] has also previously discussed the gauge boson eigenfunctions, but wrote them in terms of the parameters e, M_W, M_Z, $M_{W'}$, and $M_{Z'}$.

2.2.1 Gauge bosons

The gauge boson masses arise from the kinetic energy terms for the sigma fields:

$$\mathcal{L}_\Sigma = \frac{f^2}{4}\mathrm{Tr}[D_\mu \Sigma_{01}^\dagger D_\mu \Sigma_{01}] + \frac{f^2}{4}\mathrm{Tr}[D_\mu \Sigma_{12}^\dagger D_\mu \Sigma_{12}] \tag{2.3}$$

where the covariant derivatives are:

$$D_\mu \Sigma_{01} = \partial_\mu \Sigma_{01} + igW_\mu^0 \Sigma_{01} - i\tilde{g}\Sigma_{01} W_\mu^1 \tag{2.4}$$

$$D_\mu \Sigma_{01} = \partial_\mu \Sigma_{12} + i\tilde{g}W_\mu^1 \Sigma_{12} - ig'\Sigma_{12} W_\mu^2 \tag{2.5}$$

In the unitary gauge (with $\Sigma_{01} = \Sigma_{12} = 1$), Eqn. (2.3) gives terms quadratic in the gauge fields, for example,

$$\frac{f^2}{4}\mathrm{Tr}[D_\mu \Sigma_{01}^\dagger D_\mu \Sigma_{01}] \to \frac{f^2}{4}\left|-igW_\mu^0 + i\tilde{g}W_\mu^1\right|^2 \tag{2.6}$$

from which we can read off the mass matrix for the gauge bosons. We will work in the limit

$$x = g/\tilde{g} \ll 1 \ , \qquad y = g'/\tilde{g} \ll 1 \ , \tag{2.7}$$

in which case we expect a massless photon, light W and Z bosons, and a heavy set of bosons W' and Z'. Numerically, then, g and g' are approximately equal to the standard model $SU(2)_W$ and $U(1)_Y$ couplings. We also define an angle θ such that

$$\frac{g'}{g} = \frac{\sin\theta}{\cos\theta} \equiv \frac{s}{c} \tag{2.8}$$

The charged gauge-boson mass-squared matrix may be written in terms of the small parameter x as

$$\frac{\tilde{g}^2 v^2}{2} \begin{pmatrix} x^2 & -x \\ -x & 2 \end{pmatrix} \ . \tag{2.9}$$

Diagonalizing this matrix perturbatively in x, we find the light eigenvalue

$$M_W^2 = \frac{g^2 v^2}{4} \left[1 - \frac{x^2}{4} + \frac{x^6}{64} + \ldots \right] \ , \tag{2.10}$$

and the corresponding eigenstate

$$\begin{aligned} W^\mu &= v_W^0 \, W_0^\mu + v_W^1 \, W_1^\mu \\ &= \left(1 - \frac{x^2}{8} - \frac{5x^4}{128} + \ldots \right) W_0^\mu + \left(\frac{x}{2} + \frac{x^3}{16} - \frac{9x^5}{256} + \ldots \right) W_1^\mu \ . \end{aligned} \tag{2.11}$$

where $W_{0,1}$ are the gauge bosons associated with the $SU(2)$ groups at sites 0 and 1. Note that the light W is primarily located at site 0. The heavy eigenstate has an eigenvector orthogonal to that in Eqn. (2.11) and a mass

$$M_{W'}^2 = \tilde{g}^2 v^2 \left[1 + \frac{x^2}{4} + \frac{x^4}{16} + \ldots \right] \ , \tag{2.12}$$

Comparing Eqns. (2.10) and (2.12), we find

$$\frac{M_W^2}{M_{W'}^2} = \frac{x^2}{4} - \frac{x^4}{8} + \frac{x^6}{64} + \dots \ . \tag{2.13}$$

or, equivalently,

$$\left(\frac{g}{\tilde{g}}\right)^2 \equiv x^2 = 4\left(\frac{M_W^2}{M_{W'}^2}\right) + 8\left(\frac{M_W^2}{M_{W'}^2}\right)^2 + 28\left(\frac{M_W^2}{M_{W'}^2}\right)^3 + \dots \ , \tag{2.14}$$

which confirms that the W' boson is heavy in the limit of small x.

The neutral bosons' mass-squared matrix is

$$\frac{\tilde{g}^2 v^2}{2}\begin{pmatrix} x^2 & -x & 0 \\ -x & 2 & -xt \\ 0 & -xt & x^2 t^2 \end{pmatrix} \ , \tag{2.15}$$

where $t \equiv \tan\theta = s/c$. This matrix has a zero eigenvalue, corresponding to the massless photon, with an eigenstate which may be written

$$A^\mu = \frac{e}{g}W_0^\mu + \frac{e}{\tilde{g}}W_1^\mu + \frac{e}{g'}B^\mu \ , \tag{2.16}$$

where $W_{0,1}$ are the gauge bosons associated with the $SU(2)$ groups at sites 0 and 1, the B is the gauge boson associated with the $U(1)$ group at site 2, and the electric charge e satisfies

$$\frac{1}{e^2} = \frac{1}{g^2} + \frac{1}{\tilde{g}^2} + \frac{1}{g'^2} \ . \tag{2.17}$$

The light neutral gauge boson, which we associate with the Z, has a mass

$$M_Z^2 = \frac{g^2 v^2}{4c^2}\left[1 - \frac{x^2}{4}\frac{(c^2-s^2)^2}{c^2} + \frac{x^6}{64}\frac{(c^2-s^2)^4}{c^6} + \dots\right] \ , \tag{2.18}$$

with a corresponding eigenvector

$$Z^\mu = v_Z^0 W_0^\mu + v_Z^1 W_1^\mu + v_Z^2 B^\mu \tag{2.19}$$

$$v_Z^0 = c - \frac{x^2 c^3 (1 + 2t^2 - 3t^4)}{8} + \ldots \tag{2.20}$$

$$v_Z^1 = \frac{xc(1-t^2)}{2} + \frac{x^3 c^3 (1-t^2)^3}{16} + \ldots \tag{2.21}$$

$$v_Z^2 = -s - \frac{x^2 s c^2 (3 - 2t^2 - t^4)}{8} + \ldots \,. \tag{2.22}$$

The heavy neutral boson has a mass

$$M_{Z'}^2 = \tilde{g}^2 v^2 \left[1 + \frac{x^2}{4c^2} + \frac{x^4 (1-t^2)^2}{16} + \ldots \right] , \tag{2.23}$$

with the corresponding eigenvector

$$Z'^\mu = v_{Z'}^0 W_0^\mu + v_{Z'}^1 W_1^\mu + v_{Z'}^2 B^\mu \tag{2.24}$$

$$v_{Z'}^0 = -\frac{x}{2} - \frac{x^3 (1 - 3t^2)}{16} + \ldots \tag{2.25}$$

$$v_{Z'}^1 = 1 - \frac{x^2 (1 + t^2)}{8} + \ldots \tag{2.26}$$

$$v_{Z'}^2 = -\frac{xt}{2} + \frac{x^3 t (3 - t^2)}{16} + \ldots \,. \tag{2.27}$$

2.2.2 Fermions

Consider the fermion mass matrix

$$M_{u,d} = M_D \begin{pmatrix} \varepsilon_L & 0 \\ 1 & \varepsilon_{uR,dR} \end{pmatrix} \equiv \begin{pmatrix} m & 0 \\ M_D & m'_{u,d} \end{pmatrix} . \tag{2.28}$$

The notation introduced at the far right is used to emphasize that in the limit $M_D \gg m, m'$, the above matrix displays a "see-saw" form. In what follows, we will largely

be interested in the top- and bottom-quarks, and therefore in ε_{tR} and ε_{bR}.

Diagonalizing the top-quark seesaw-style mass matrix perturbatively in ε_L, we find the light eigenvalue

$$m_t = \frac{M_D \varepsilon_L \varepsilon_{tR}}{\sqrt{1+\varepsilon_{tR}^2}} \left[1 - \frac{\varepsilon_L^2}{2\left(\varepsilon_{tR}^2+1\right)^2} + \ldots \right]. \tag{2.29}$$

This is precisely the same form as found in a continuum model [51]. For the bottom-quark, we find the same expression with $\varepsilon_{tR} \to \varepsilon_{bR}$, and therefore (neglecting higher order terms in ε_{bR}^2)

$$\frac{m_b}{m_t} \approx \frac{\varepsilon_{bR}}{\varepsilon_{tR}} \sqrt{1+\varepsilon_{tR}^2} \tag{2.30}$$

The heavy eigenstate (T) corresponding to the top-quark has a mass

$$m_T = M_D \sqrt{1+\varepsilon_{tR}^2} \left[1 + \frac{\varepsilon_L^2}{2\left(\varepsilon_{tR}^2+1\right)^2} + \ldots \right]. \tag{2.31}$$

and similarly for the heavy eigenstate corresponding to the bottom-quark (B) with $\varepsilon_{tR} \to \varepsilon_{bR}$ (or, equivalently, $m_t' \to m_b'$).

The left- and right-handed light mass eigenstates of the top quark are

$$\begin{aligned} t_L &= t_L^0 \psi_{L0}^t + t_L^1 \psi_{L1}^t \\ &= \left(-1 + \frac{\varepsilon_L^2}{2(1+\varepsilon_{tR}^2)^2} + \frac{(8\varepsilon_{tR}^2 - 3)\varepsilon_L^4}{8(\varepsilon_{tR}^2+1)^4} + \ldots \right) \psi_{L0}^t \\ &+ \left(\frac{\varepsilon_L}{1+\varepsilon_{tR}^2} + \frac{(2\varepsilon_{tR}^2 - 1)\varepsilon_L^3}{2(\varepsilon_{tR}^2+1)^3} + \ldots \right) \psi_{L1}^t \end{aligned} \tag{2.32}$$

$$\tag{2.33}$$

and

$$
\begin{aligned}
t_R &= t_R^1 \psi_{R1}^t + t_R^2 t_{R2} \\
&= \left(-\frac{\varepsilon_{tR}}{\sqrt{1+\varepsilon_{tR}^2}} + \frac{\varepsilon_{tR}\varepsilon_L^2}{(1+\varepsilon_{tR}^2)^{5/2}} + \ldots \right) \psi_{R1}^t \\
&+ \left(\frac{1}{\sqrt{1+\varepsilon_{tR}^2}} + \frac{\varepsilon_{tR}^2\varepsilon_L^2}{(1+\varepsilon_{tR}^2)^{5/2}} + \ldots \right) t_{R2} \ , \qquad (2.34)
\end{aligned}
$$

and similarly for the left- and right-handed b-quarks with $\varepsilon_{tR} \to \varepsilon_{bR}$. Here we denote the upper components of the $SU(2)$ doublet fields as $\psi_{L0,L1,R1}^t$; clearly the smaller the value of ε_L (ε_{tR}), the more strongly the left-handed (right-handed) eigenstate will be concentrated at site 0 (site 2). The left- and right-handed heavy fermion mass eigenstates are the orthogonal combinations

$$
\begin{aligned}
T_L &= T_L^0 \psi_{L0}^t + T_L^1 \psi_{L1}^t \qquad (2.35) \\
&= \left(-\frac{\varepsilon_L}{1+\varepsilon_{tR}^2} - \frac{(2\varepsilon_{tR}^2 - 1)\varepsilon_L^3}{2(\varepsilon_{tR}^2+1)^3} + \ldots \right) \psi_{L0}^t \\
&+ \left(-1 + \frac{\varepsilon_L^2}{2(1+\varepsilon_{tR}^2)^2} + \frac{(8\varepsilon_{tR}^2 - 3)\varepsilon_L^4}{8(\varepsilon_{tR}^2+1)^4} + \ldots \right) \psi_{L1}^t \qquad (2.36) \\
T_R &= T_R^1 \psi_{R1}^t + T_R^2 t_{R2} \ , \qquad (2.37) \\
&= \left(-\frac{1}{\sqrt{1+\varepsilon_{tR}^2}} - \frac{\varepsilon_{tR}^2\varepsilon_L^2}{(1+\varepsilon_{tR}^2)^{5/2}} + \ldots \right) \psi_{R1}^t \\
&+ \left(-\frac{\varepsilon_{tR}}{\sqrt{1+\varepsilon_{tR}^2}} + \frac{\varepsilon_{tR}\varepsilon_L^2}{(1+\varepsilon_{tR}^2)^{5/2}} + \ldots \right) t_{R2} \ , \qquad (2.38)
\end{aligned}
$$

and similarly for the left- and right-handed heavy B quarks with $\varepsilon_{tR} \to \varepsilon_{bR}$.

Analogous results follow for the other ordinary fermions and their heavy partners, with the appropriate ε_{fR} substituted for ε_{tR} in the expressions above. As mentioned

before, ε_L is flavor universal whose value is dictated by ideal fermion delocalization, which we will explain in the next section. We will choose ε_R for each fermion in accordance with $m_f \approx M_D \varepsilon_L \varepsilon_{fR}$. In the limit $m_f \to 0$, ε_{fR} is very small.

2.3 Couplings

2.3.1 Ideal fermion delocalization

We mentioned before that for higgsless models to satisfy precision electroweak data, the fermions have to be delocalized. Most tree-level corrections to precision observables come necessarily from the coupling of SM fermions to heavy gauge bosons, and this suggests that a phenomenologically efficient means of delocalization is one that will render this coupling zero. The coupling of the heavy W' to SM fermions is of the form $\sum_i g_i (\psi_{f_i})^2 \psi_{W_i'}$. Thus choosing the light fermion profile such that $(\psi_{f_i})^2$ is proportional to ψ_{W_i} would make this coupling automatically vanish because the heavy and light W fields are orthogonal to one another [49]. Thus we require:

$$g_i (\psi_i^f)^2 = g_W v_W^i \tag{2.39}$$

We will refer the above as Ideal Fermion Delocalization (IFD) [49]. In the three-site model, if we write the wavefunction of a delocalized left-handed fermion $f_L = f_L^0 \psi_{L0}^f + f_L^1 \psi_{L1}^f$ then ideal delocalization imposes the following condition (having taken the ratio of the separate constraints for $i = 0$ and $i = 1$):

$$\frac{g (f_L^0)^2}{\tilde{g} (f_L^1)^2} = \frac{v_W^0}{v_W^1} \,. \tag{2.40}$$

Based on our general expressions for fermion mass eigenstates (Eqns. (2.32) and (2.34)) and the W mass eigenstate (Eqn.(2.11)), it is clear that Eqn.(2.40) relates

the flavor-independent quantities x and ε_L to the flavor-specific ε_{fR}. Hence, if we construe this as an equation for ε_L and solve perturbatively in the small quantity x, we find

$$\varepsilon_L^2 \to (1+\varepsilon_{fR}^2)^2 \left[\frac{x^2}{2} + \left(\frac{1}{8} - \frac{\varepsilon_{fR}^2}{2}\right) x^4 + \frac{5\,\varepsilon_{fR}^4\, x^6}{8} + \ldots\right] . \tag{2.41}$$

Note that, as we will see, ε_{fR} is only substantial for the top-quark - and so ideal delocalization for the light fermions corresponds to the case $\varepsilon_{fR} = 0$. Regardless of the precise value of ε_{fR} involved, it is immediately clear that ideal delocalization implies $\varepsilon_L = \mathcal{O}(x)$. Since $x \ll 1$, this justifies the expansions used above in diagonalizing the fermion mass matrix. We will now derive the fermion couplings to light and heavy gauge boson imposing this condition.

2.3.2 Charged currents

We will start by computing the left handed coupling of the W to the fermions. Throughout this section and the next, we will be writing down the couplings specifically for the top-bottom doublet. The couplings for other fermions can simply read off by the replacement $\varepsilon_{tR} \to \varepsilon_{fR}$. Also, we will work in the limit $\varepsilon_{bR} \to 0$, which simply means that the couplings are computed in the $m_b \to 0$ limit.

$$g_L^{Wtb} = g t_L^0 b_L^0 v_W^0 + \tilde{g} t_L^1 b_L^1 v_W^1 \tag{2.42}$$

which can be evaluated to be:

$$g_L^{Wtb} = g\left(1 - \frac{3\varepsilon_{tR}^4 + 4\varepsilon_{tR}^2 + 3}{8(\varepsilon_{tR}^2+1)^2}\, x^2 + \frac{3\varepsilon_{tR}^8 + 16\varepsilon_{tR}^6 + 50\varepsilon_{tR}^4 + 8\varepsilon_{tR}^2 + 15}{128(\varepsilon_{tR}^2+1)^4}\, x^4 + \ldots\right) . \tag{2.43}$$

The corresponding equation for the coupling of standard model fermions other than the top-quark to the W may be obtained by taking $\varepsilon_{tR} \to 0$ in the equation above, yielding

$$g_L^W = g\left(1 - \frac{3}{8}x^2 + \frac{15}{128}x^4 + \ldots\right) . \tag{2.44}$$

Combining this with eqns. (2.8), (2.10), (2.17), and (2.18) we find

$$g_L^W = \frac{e}{\sqrt{1 - \dfrac{M_W^2}{M_Z^2}}}\left[1 + \mathcal{O}(s^2 x^4)\right] , \tag{2.45}$$

which shows that the W-fermion couplings (for fermions other than top) are of very nearly standard model form, as consistent with ideal delocalization. Eqn. (2.44) corresponds to a value of G_F

$$\sqrt{2}G_F = \frac{(g_L^W)^2}{4M_W^2} = \frac{1}{v^2}\left(1 - \frac{x^2}{2} + \frac{x^4}{4} + \ldots\right). \tag{2.46}$$

The W also couples to the heavy partners of the ordinary fermions. Here, we quote the results for the T and B fermions; analogous results follow for other generations when ε_{tR} is replaced by the appropriate ε_{qR}. There is a diagonal WTB coupling of the form

$$g_L^{WTB} = gT_L^0 B_L^0 v_W^0 + \tilde{g}T_L^1 B_L^1 v_W^1 , \tag{2.47}$$

$$= \frac{g}{2}\left(1 - \frac{\varepsilon_{tR}^4 - 6\varepsilon_{tR}^2 - 5}{8(\varepsilon_{tR}^2 + 1)^2}x^2 + \ldots\right) \tag{2.48}$$

$$= \frac{g_L^W}{2}\left(1 + \frac{\varepsilon_{tR}^4 + 6\varepsilon_{tR}^2 + 4}{4(\varepsilon_{tR}^2 + 1)^2}x^2 + \ldots\right) , \tag{2.49}$$

where $T_L^{0,1}$ and $B_L^{0,1}$ are the heavy-fermion analogs of the components $t_L^{0,1}$ and $b_L^{0,1}$. There are also smaller off-diagonal couplings involving one heavy and one ordinary

fermion

$$g_L^{WTb} = gT_L^0 b_L^0 v_W^0 + \tilde{g} T_L^1 b_L^1 v_W^1 \ , \tag{2.50}$$

$$= \frac{g(1-\varepsilon_{tR}^2)}{2\sqrt{2}(\varepsilon_{tR}^2+1)} \left(x + \mathcal{O}(x^3)\right) \ , \tag{2.51}$$

and

$$g_L^{WtB} = gt_L^0 B_L^0 v_W^0 + \tilde{g} t_L^1 B_L^1 v_W^1 \ , \tag{2.52}$$

$$= \frac{g(1+2\varepsilon_{tR}^2)}{2\sqrt{2}(\varepsilon_{tR}^2+1)} \left(x + \mathcal{O}(x^3)\right) \ , \tag{2.53}$$

Because ψ_R is a doublet under $SU(2)_1$, the three-site model includes right-handed couplings of the W

$$\mathcal{L}_{WR} \propto W_\mu^+ \left[\tilde{g}\, v_W^1 (\bar{\psi}_{R1} \tau^- \gamma^\mu \psi_{R1})\right] + h.c. \ . \tag{2.54}$$

Note that the right-handed fermions exist only on sites 1 and 2 while the W is limited to sites 0 and 1; hence, the right-handed coupling comes entirely from the overlap at site 1. For the tb doublet we find

$$g_R^{Wtb} = \tilde{g}\, t_R^1 b_R^1 v_W^1 \tag{2.55}$$

$$= \frac{g}{2} \frac{\varepsilon_{tR}}{\sqrt{1+\varepsilon_{tR}^2}} \frac{\varepsilon_{bR}}{\sqrt{1+\varepsilon_{bR}^2}} \left(1 + \mathcal{O}(x^2)\right) \tag{2.56}$$

$$\approx \frac{g}{2} \frac{m_b}{m_t} \frac{\varepsilon_{tR}^2}{1+\varepsilon_{tR}^2} \ , \tag{2.57}$$

where reaching the last line requires use of Eqn.(2.30). We thus see that the right handed coupling for all fermions vanishes in the limit $m_f \to 0$. The W also has

right-handed couplings to T and B, for which we compute the diagonal coupling

$$g_R^{WTB} = \tilde{g} T_R^1 B_R^1 v_W^1 \tag{2.58}$$

$$= \frac{g}{2\sqrt{1+\varepsilon_{tR}^2}} \left(1 + \frac{\varepsilon_{tR}^4 + 6\varepsilon_{tR}^2 + 1}{8(\varepsilon_{tR}^2+1)^2} x^2 + \ldots \right) \tag{2.59}$$

and the off-diagonal coupling

$$g_R^{WtB} = \tilde{g} t_R^1 B_R^1 v_W^1 \tag{2.60}$$

$$= \frac{g\,\varepsilon_{tR}}{2\sqrt{1+\varepsilon_{tR}^2}} \left(1 + \frac{\varepsilon_{tR}^4 + 2\varepsilon_{tR}^2 - 3}{8(\varepsilon_{tR}^2+1)^2} x^2 + \ldots \right) \tag{2.61}$$

As in the case of g_R^{Wtb}, the right-handed coupling g_R^{WTb} turns out to be proportional to ε_{bR}, and is therefore very small. Other right-handed Wff' couplings involving the light standard fermions are straightforward to deduce from eqn. (2.56) and clearly suppressed by the small values of ε_{fR}. Similarly, the off-diagonal $g_R^{WFf'}$ are proportional to small ε_{fR}. The diagonal $g_R^{WFF'}$ are analogous in form to (2.59).

2.3.3 Neutral Currents

We will now compute the Z coupling to fermions. Like the W, the Z may couple to a pair of ordinary or heavy-partner fermions, or to a mixed pair with one ordinary and one heavy-partner fermion. The left-handed coupling of the light Z-boson to quark fields may be written

$$\mathcal{L}_{ZL} \propto g v_Z^0 (\bar{\psi}_{L0} \frac{\tau^3}{2} \gamma^\mu \psi_{L0}) Z_\mu + \tilde{g} v_Z^1 (\bar{\psi}_{L1} \frac{\tau^3}{2} \gamma^\mu \psi_{L1}) Z_\mu$$
$$+ \frac{g'}{6} v_Z^2 \left(\bar{\psi}_{L0} \gamma^\mu \psi_{L0} + \bar{\psi}_{L1} \gamma^\mu \psi_{L1} \right) . \tag{2.62}$$

where the first two terms give rise to the left-handed "T_3" coupling and the last term (proportional to g') gives rise to the left-handed hypercharge coupling. The expression for leptons would be similar, replacing hypercharge 1/6 with $-1/2$.

Similarly, the right-handed coupling of the Z to quark fields is

$$\mathcal{L}_{ZR} \propto \tilde{g}\, v_Z^1 (\bar{\psi}_{R1} \frac{\tau^3}{2} \gamma^\mu \psi_{R1}) Z_\mu + \frac{g'}{6}\, v_Z^2 (\bar{\psi}_{R1} \gamma^\mu \psi_{R1}) Z_\mu$$
$$g'\, v_Z^2 \left(\frac{2}{3} \bar{u}_{R2} \gamma^\mu u_{R2} - \frac{1}{3} \bar{d}_{R2} \gamma^\mu d_{R2} \right) Z_\mu \ , \tag{2.63}$$

where the last three terms arise from the hypercharge. For leptons, $1/6 \to -1/2$ in the second term, $2/3 \to 0$ in the third term (for neutrinos), and $-1/3 \to -1$ in the last term for the charged leptons.

The left handed T_3 coupling of the light fermion field to the Z is given by:

$$g_{3L}^{Zff} = g (f_L^0)^2 v_Z^0 + \tilde{g} (f_L^1)^2 v_Z^1 \tag{2.64}$$
$$= gc \left(1 - \frac{x^2 c^2 \left(3 + 6t^2 - t^4 \right)}{8} + \ldots \right) . \tag{2.65}$$

The coupling of left-handed light fermions to hypercharge arises from the overlap between the fraction of the Z wavefunction arising from site 2 (the locus of hypercharge) and the left-handed fermion wavefunctions which are limited to sites 0 and 1:

$$g_{YL}^{Zff} = g' v_Z^2 \left[(f_L^0)^2 + (f_L^1)^2 \right] = g' v_Z^2 \tag{2.66}$$
$$= -g's \left(1 + \frac{x^2 c^2 (3 - 2t^2 - t^4)}{8} + \ldots \right) . \tag{2.67}$$

The left-handed coupling of the top-quark to T_3 is

$$g_{3L}^{Ztt} = g(t_L^0)^2 v_Z^0 + \tilde{g}(t_L^1)^2 v_Z^1 \tag{2.68}$$

$$= g_{3L}^{Zff}\left(1 + \frac{\varepsilon_{tR}^2(2+\varepsilon_{tR}^2)}{4c^2(1+\varepsilon_{tR}^2)^2}x^2 + \ldots\right) \tag{2.69}$$

and the corresponding right handed coupling is:

$$g_{3R}^{Ztt} = (\tilde{g}v_Z^1 - g' v_Z^2)(t_R^1)^2 \tag{2.70}$$

$$= \frac{g}{2c}\frac{\varepsilon_{tR}^2}{1+\varepsilon_{tR}^2}(1 + \mathcal{O}(x^2)) \; . \tag{2.71}$$

The left and right handed couplings to hypercharge can be evaluated:

$$g_{YL}^{Ztt} = g' v_Z^2 \left[(t_L^0)^2 + (t_L^1)^2\right] = g_{YL}^{Zqq} \tag{2.72}$$

$$g_{YR}^{Ztt} = g' v_Z^2 \left[(t_R^1)^2 + (t_R^2)^2\right] = g_{YR}^{Zqq} \; . \tag{2.73}$$

The T_3 couplings of the Z to a pair of heavy-partner fermions or an off-diagonal pair can all be similarly computed. We give the result for the top-bottom pair and their heavy partners below: (The couplings for the other generations can be read off by replacing $\epsilon_{tR} \to \epsilon_{fR}$).

$$
\begin{aligned}
g_{3L}^{Ztt} &= cg - \frac{1}{8}c^3 g(3+6t^2-t^4)\,x^2 + \frac{g\varepsilon_{tR}^2(2+\varepsilon_{tR}^2)}{4\,c(1+\varepsilon_{tR}^2)^2}\,x^2 \\
g_{3R}^{Ztt} &= \frac{g\varepsilon_{tR}^2}{2c(\varepsilon_{tR}^2+1)}\left(1+\frac{-3(\varepsilon_{tR}^2+1)^2+8c^2\varepsilon_{tR}^2(\varepsilon_{tR}^2+2)-4c^4(\varepsilon_{tR}^2+1)^2}{8c^2(\varepsilon_{tR}^2+1)^2}x^2\right) \\
g_{3L}^{ZTT} &= -\frac{1}{2}cg\left(t^2-1\right)+\frac{cg\left(4\left(t^2+1\right)-c^2\left(\varepsilon_{tR}^2+1\right)^2\left(t^2-1\right)^3\right)}{16\left(\varepsilon_{tR}^2+1\right)^2}x^2 \\
g_{3R}^{ZTT} &= \frac{g}{2c(\varepsilon_{tR}^2+1)} \\
&+ g\frac{\left(-3(\varepsilon_{tR}^2+1)^2+8c^2(\varepsilon_{tR}^4+3\varepsilon_{tR}^2+1)-4c^4(\varepsilon_{tR}^2+1)^2\right)}{16c^3(\varepsilon_{tR}^2+1)^3}x^2 \\
g_{3L}^{ZtT} &= \frac{g}{2\sqrt{2}c(\varepsilon_{tR}^2+1)}x \\
&+ g\frac{\left((\varepsilon_{tR}^2+1)^2+c^2(\varepsilon_{tR}^4+6\varepsilon_{tR}^2-3)-4c^4(\varepsilon_{tR}^2+1)^2\right)}{16\sqrt{2}c^3(\varepsilon_{tR}^2+1)^3}x^3 \\
g_{3R}^{ZtT} &= \frac{g\varepsilon_{tR}}{2c(\varepsilon_{tR}^2+1)} \\
&+ g\varepsilon_{tR}\frac{\left(-3(\varepsilon_{tR}^2+1)^2+4c^2(2\varepsilon_{tR}^4+5\varepsilon_{tR}^2+1)-4c^4(\varepsilon_{tR}^2+1)^2\right)}{16c^3(\varepsilon_{tR}^2+1)^3}x^2
\end{aligned}
$$

The hypercharge couplings of the Z to a pair of left-handed or right-handed heavy-partner fermions follow the pattern of the ordinary fermions:

$$g_{YR}^{ZFF} = g' v_Z^2 = g_{YL}^{ZFF}\ , \tag{2.74}$$

and the hypercharge coupling of the Z to an off-diagonal (flavor-conserving) fF pair always vanishes

$$g_{YL}^{ZfF} = g_{YR}^{ZfF} = 0\ . \tag{2.75}$$

because the F and f wavefunctions are orthogonal.

Weak mixing angle: Before closing this section, let us calculate the "Z standard" weak mixing angle. Using Eqns. (2.17) and (2.18) and the relation

$$\sqrt{2}G_F = \frac{(g_L^W)^2}{4M_W^2} = \frac{1}{v^2}\left(1 - \frac{x^2}{2} + \frac{x^4}{4} + \ldots\right), \tag{2.76}$$

we can calculate:

$$\begin{aligned} s_Z^2 c_Z^2 &\equiv \frac{e^2}{4\sqrt{2}G_F M_Z^2} \\ &= s^2c^2 + s^2(c^2 - s^2)\left(c^2 - \frac{1}{4}\right)x^2 + O(x^4), \end{aligned} \tag{2.77}$$

where $s_Z \equiv \sin\theta_W|_Z$ and $c_Z \equiv \cos\theta_W|_Z$. The relationship between the weak mixing angle $\theta_W|_Z$ and the angle θ defined in Eq. (2.8) is expressed as follows:

$$s_Z^2 = s^2 + \Delta, \quad c_Z^2 = c^2 - \Delta, \tag{2.78}$$

$$\Delta \equiv s^2\left(c^2 - \frac{1}{4}\right)x^2 + O(x^4). \tag{2.79}$$

In other words, s^2 and s_Z^2 differ by corrections of order x^2.

2.4 Phenomenological bounds

The three site model has the following parameters in addition to the SM: $\varepsilon_L, \varepsilon_{fR}$ and M_D. We are interested in finding bounds on physical parameters, in particular, $M_{W'}$, the mass of the gauge boson and M_D, the mass scale of the heavy fermions.

2.4.1 g_{ZWW} and $M_{W'}$

Experimental constraints on the ZWW vertex in the three-site model turn out to provide useful bounds on the fermion delocalization parameter ε_L.

To leading order, in the absence of CP-violation, the triple gauge boson vertices may be written in the Hagiwara-Peccei-Zeppenfeld-Hikasa triple-gauge-vertex notation [58]

$$\begin{aligned}\mathcal{L}_{TGV} &= -ie\frac{c_Z}{s_Z}\left[1+\Delta\kappa_Z\right]W_\mu^+W_\nu^-Z^{\mu\nu} - ie\left[1+\Delta\kappa_\gamma\right]W_\mu^+W_\nu^-A^{\mu\nu} \\ &- ie\frac{c_Z}{s_Z}\left[1+\Delta g_1^Z\right](W^{+\mu\nu}W_\mu^- - W^{-\mu\nu}W_\mu^+)Z_\nu \\ &- ie(W^{+\mu\nu}W_\mu^- - W^{-\mu\nu}W_\mu^+)A_\nu \ .\end{aligned} \tag{2.80}$$

where the two-index tensors denote the Lorentz field-strength tensor of the corresponding field. In the standard model, $\Delta\kappa_Z = \Delta\kappa_\gamma = \Delta g_1^Z \equiv 0$.

As noted in ref. [59], in any vector-resonance model, such as the Higgsless models considered here, the interactions (2.80) come from re-expressing the nonabelian couplings in the kinetic energy terms in the original Lagrangian in terms of the mass-eignestate fields. In this case one obtains equal contributions to the deviations of the first and third terms, and the second and fourth terms in Eqn. (2.80). In addition the coefficient of the fourth term is fixed by electromagnetic gauge-invariance, and therefore in these models we find

$$\Delta\kappa_\gamma \equiv 0 \qquad \Delta\kappa_Z \equiv \Delta g_1^Z \ . \tag{2.81}$$

Computing the ZWW coupling explicitly in the three-site model yields

$$g_{ZWW} = g(c_W^0)^2 c_Z^0 + \tilde{g}(c_W^1)^2 c_Z^1 \tag{2.82}$$

$$= g\,c\left(1 - \frac{x^2 c^2(1+2t^2-t^4)}{4} + \ldots\right) \tag{2.83}$$

$$= g_{3L}^{Zff}\left(1 + \frac{x^2}{8c^2} + \ldots\right) , \tag{2.84}$$

thus, the deviation of the coupling from the SM value is given by:

$$\Delta g_1^Z = \frac{x^2}{8c^2} \tag{2.85}$$

The 95% C.L. upper limit from LEP-II is $\Delta g_1^Z < 0.028$ [52]. Approximating $c^2 \approx \cos^2\theta_W \approx 0.77$, we find the bound on x

$$x \leq 0.42\sqrt{\frac{\Delta g_1^Z}{0.028}} , \tag{2.86}$$

and hence, from eqn. (2.13),

$$M_{W'} \approx \frac{2}{x} M_W \geq 380\,\mathrm{GeV}\sqrt{\frac{0.028}{\Delta g_1^Z}} . \tag{2.87}$$

This lower bound on $M_{W'}$ translates into an upper bound on ε_L through the IFD condition, Eqn. (2.41). Finally, we recall that, in the absence of a Higgs boson, $W_L W_L$ spin-0 isospin-0 scattering would violate unitarity at a scale of $\sqrt{8\pi}v$ and that exchange of the heavy electroweak bosons is what unitarizes WW scattering in Higgsless models. Hence, $M_{W'} \leq 1.2$ TeV in the three-site model. This, along with Eq. (2.87) constrains ε_L to lie in the range

$$0.095 \leq \varepsilon_L \leq 0.30 . \tag{2.88}$$

2.4.2 $\Delta\rho$ and M_D

The isospin violating ρ parameter is defined as the ratio of isotriplet neutral current and charged current interactions at zero momentum. Neglecting the exchange of heavy gauge bosons, as appropriate in the case of ideal fermion delocalization, ρ can also be expressed in terms of the masses of the W and Z bosons as follows:

$$\rho = \frac{M_W^2}{M_Z^2 \cos^2\theta}. \tag{2.89}$$

At tree level in the SM, ρ is one - the reason for this is an *accidental symmetry* in the Higgs sector of the SM. To see what this symmetry is, let us start by writing the components of this Higgs field as [53]:

$$\phi = \begin{pmatrix} \phi^+ \\ \phi^0 \end{pmatrix} \tag{2.90}$$

Then, $i\sigma_2\phi^*$ is also an $SU(2)_L$ doublet with components:

$$i\sigma_2\phi^* = \begin{pmatrix} \phi^{0*} \\ -\phi^- \end{pmatrix}. \tag{2.91}$$

This lets us define the Higgs matrix field:

$$\Phi = \frac{1}{\sqrt{2}} \begin{pmatrix} \phi^{0*} & \phi^+ \\ -\phi^- & \phi^0 \end{pmatrix}. \tag{2.92}$$

Now we can rewrite the Higgs Lagrangian as:

$$\mathcal{L}_{\text{Higgs}} = -\mu^2 \text{Tr}\left(D_\mu\Phi\right)^\dagger \left(D^\mu\Phi\right) - V(\Phi), \tag{2.93}$$

where the potential is given by:

$$V(\Phi) = -\mu^2 \mathrm{Tr}\Phi^\dagger\Phi + \lambda \mathrm{Tr}(\Phi^\dagger\Phi)^2. \tag{2.94}$$

and the covariant derivative is:

$$D_\mu\Phi = \left(\partial_\mu\Phi + i\frac{g}{2}\sigma.W_\mu\Phi - i\frac{g'}{2}B_\mu\Phi\sigma_3\right). \tag{2.95}$$

Now, in the limit $g' \to 0$, the Higgs Lagrangian has an $SU(2)_L \times SU(2)_R$ global symmetry. Under this symmetry, matrix field transforms as:

$$\Phi \to L\Phi R^\dagger. \tag{2.96}$$

When the Higgs field develops a vev,

$$\langle\Phi\rangle = \frac{1}{\sqrt{2}}\begin{pmatrix} v & 0 \\ 0 & v \end{pmatrix}, \tag{2.97}$$

it breaks both $SU(2)_L$ and $SU(2)_L$, leaving only the diagonal subgroup $SU(2)_{L+R} = SU(2)_V$ unbroken. Thus, there are three massless Goldstone bosons generated that are eaten by the W and the Z to make them massive. It is this accidental $SU(2)$ global symmetry, called the *custodial symmetry*, that guarantees the relation between the W and the Z masses (Eqn. (2.89)) in the SM. In the fermionic sector, the $SU(2)_L \times SU(2)_R$ symmetry guarantees that the masses of the up and down components of a fermion doublet have equal masses. Significant fermionic one loop corrections to the ρ parameter arise from the breaking of this custodial isospin symmetry, thus making the up and down type fermions non-degenerate. The largest correction comes from

the top-bottom doublet and is given by [55]:

$$\rho = 1 + \frac{3G_F}{8\pi^2\sqrt{2}}\left[m_t^2 + m_b^2 - 2\frac{m_t^2 m_b^2}{m_t^2 - m_b^2}\ln\frac{m_t^2}{m_b^2}\right]. \tag{2.98}$$

For the other fermion doublets, the up and down type components have almost the same mass and hence the correction vanishes.

In the three site model, in addition to the SM t and b quark contribution, the existence of the T and B quarks gives rise to new contributions to $\Delta\rho$. We will evaluate this correction and use this and m_t to constrain M_D.

Since ε_L is flavor independent, it cannot contribute to custodial symmetry violation and hence we will work in the limit $\varepsilon_L \to 0$ to extract only the leading contribution in ε_{tR}. The corrections due to the heavy top-bottom doublet arises out of vacuum polarization diagrams (symbol $\Pi(0)$, where the 0 indicates that these are evaluated at zero momentum) shown in Fig. (2.2). In particular, the formula for $\Delta\rho$ is given by:

$$\Delta\rho = \frac{4}{v^2}\left[\Pi_{11}(0) - \Pi_{33}(0)\right]. \tag{2.99}$$

Note that the subscripts 11 and 33 in this formula refer to the W_1 and W_3 bosons that couple to the fermions. The W_1 and W_3 are *not* mass eigenstates. Subsequently, we have defined quantities like Π_{LL}, and the subscripts here should be understood as the currents to which the bosons couple, for example, Π_{LL} refers to the coupling to two left handed currents. We will call the vacuum polarization diagrams with left handed currents Π_{LL}. Similarly, we will also define Π_{RR} (only right handed currents) and Π_{LR} (with both left and right handed currents). At zero momentum

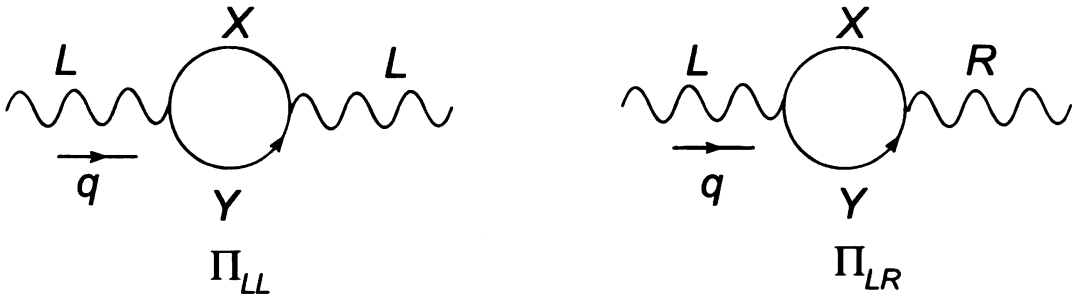

Figure 2.2: One-loop contributions to $\Delta\rho$ arise from vacuum polarization diagrams involving two left handed fermionic currents (left) and mixed left and right handed currents (right). The RR piece is the same as the LL piece. The X and Y indicate the type of fermions in the loop. We compute the leading contribution in the limit $\varepsilon_L \to 0$ and $g' \to 0$.

these functions are [54]

$$\Pi_{LL}(0) = \frac{1}{16\pi^2}\left[(m_X^2 + m_Y^2)E - 2\left(m_X^2 b_1(m_X, m_Y; 0) + m_Y^2 b_1(m_Y, m_X; 0)\right)\right] \tag{2.100}$$

$$\Pi_{LR}(0) = \frac{1}{16\pi^2}\left[-2m_X m_Y E + 2m_X m_Y b_0(m_X, m_Y; 0)\right], \tag{2.101}$$

where

$$b_0(m_X, m_Y; q^2) = \int_0^1 dx \log\left(\frac{x\, m_X^2 + (1-x)m_Y^2 - x(1-x)q^2}{\mu^2}\right) \tag{2.102}$$

$$b_1(m_X, m_Y; q^2) = \int_0^1 dx\, x \log\left(\frac{x\, m_X^2 + (1-x)m_Y^2 - x(1-x)q^2}{\mu^2}\right) \tag{2.103}$$

Here E is the divergent part of the loop diagram from dimensional regularization, $E = \frac{2}{\varepsilon} - \gamma + \log(4\pi) - \log(\mu^2)$ ($\varepsilon = 4 - d$), and μ is the renormalization mass scale. The RR piece has the same form as the LL piece. We will treat the LL, RR and the LR pieces separately and show explicitly that the divergences cancel and compute the finite part. For simplicity, we will relabel $b(m_1, m_2, 0)$ as simply $b(1, 2, 0)$. We will be concentrating on the top-bottom doublet and their heavy partners, as they

codify maximum flavor violation.

LL diagrams: The vacuum polarization amplitude with left handed external currents at zero momentum is given by:

$$\Pi_{LL}(0) = -\frac{4}{(4\pi)^2}\left[\frac{-1}{4}\left(m_1^2+m_2^2\right)E + \frac{1}{2}\left(m_2^2 b_1(120) + m_1^2 b_1(210)\right)\right] \quad (2.104)$$

There are contributions due to (t,b), (t,B), (T,b) and (T,B) fermions in the loop. The divergent part is thus given by:

$$\begin{aligned}\Pi_{11}(0)_{\rm div} = \frac{E}{(4\pi)^2}\Big[&2(g_{tb}^L)^2\left(m_t^2+m_b^2\right) + 2(g_{tB}^L)^2\left(m_t^2+m_B^2\right)\\ &+2(g_{Tb}^L)^2\left(m_T^2+m_b^2\right) + 2(g_{TB}^L)^2\left(m_T^2+m_B^2\right)\Big]. \end{aligned} \quad (2.105)$$

Plugging in the couplings, we find the the divergent part of $\Pi_{11}(0)$ is:

$$\Pi_{11}(0)_{\rm div} = \frac{E}{(4\pi)^2}\left[\frac{m_t^2}{2} + \frac{1}{8}\left(m_T^2+m_B^2\right)\right]. \quad (2.106)$$

which cancels the divergent contribution from the $\Pi_{33}(0)$ piece:

$$\begin{aligned}\Pi_{33}(0)_{\rm div} &= \frac{E}{(4\pi)^2}\Big[2(g_{tt}^L)^2 m_t^2 + 2(g_{TT}^L)^2 m_T^2 + 2(g_{BB}^L)^2 m_B^2\\ &\quad +2(g_{tT}^L)^2\left(m_t^2+m_T^2\right) + 2(g_{bB}^L)^2 m_B^2\Big]\\ &= \frac{E}{(4\pi)^2}\left[\frac{m_t^2}{2} + \frac{1}{8}\left(m_T^2+m_B^2\right)\right] \end{aligned} \quad (2.107)$$

To evaluate the finite part, we will consider two cases. $m_1 = m_2$ and $m_1 \neq m_2$.

$$\mathbf{m_1 = m_2} : \Pi_{LL}(0)_{\text{finite}} = \frac{-2}{(4\pi)^2} m^2 \log m^2 \tag{2.108}$$

$$\mathbf{m_1 \neq m_2} : \Pi_{LL}(0)_{\text{finite}} = \frac{1}{2(4\pi)^2 \left(m_1^2 + m_2^2\right)} \left[m_1^4 - m_2^4 - 2m_1^4 \log m_1^2 + 2m_2^4 \log m_2^2\right] \tag{2.109}$$

We recall that to the order we are interested in, $M_B = M_D$ and $M_T = M_D\sqrt{1+\varepsilon_{tR}^2}$. Evaluating the finite contributions due to $\Pi_{11}(0)$ and $\Pi_{33}(0)$, we get:

$$\Pi_{11}(0)_{\text{finite}} = -\frac{4}{(4\pi)^2}\left[-\frac{m_t^2}{16}\left(1 - 2\log m_t^2\right) + \frac{M_D^2}{192}\left(6\varepsilon_{tR}^2 + 2\varepsilon_{tR}^4 + 12\log M_D^2 + 6\varepsilon_{tR}^2 \log M_D^2\right)\right] \tag{2.110}$$

and

$$\Pi_{33}(0)_{\text{finite}} = -\frac{4}{(4\pi)^2}\left[\frac{m_t^2}{8}\log m_t^2 + \frac{1}{16}M_D^2 \log M_D^2 + \frac{1}{32}M_D^2\varepsilon_{tR}^2 + \frac{1}{64}M_D^2\varepsilon_{tR}^4 + \frac{1}{32}M_D^2\varepsilon_{tR}^2 \log M_D^2\right] \tag{2.111}$$

and thus the finite part of the difference in the vacuum polarization amplitude for the LL piece is given by:

$$\left(\Pi_{11}(0) - \Pi_{33}(0)\right)_{\text{finite}} = \frac{4}{(4\pi)^2}\frac{m_t^2}{16} + \frac{4}{(4\pi)^2}\frac{M_D^2\varepsilon_{tR}^4}{192}. \tag{2.112}$$

We recognize the first term as the SM contribution to the one loop correction to the ρ parameter [55] and the second term is due to the heavy top-bottom doublet.

RR diagrams: As before, the divergent pieces of Π_{11} and Π_{33} are equal and

cancel.

$$\Pi_{11}(0)_{\rm div} = \Pi_{33}(0)_{\rm div} = \frac{E}{(4\pi)^2}\left[\frac{\varepsilon_{tR}^2}{8}\left(m_t^2 + m_B^2\right) + \frac{1}{8}\left(m_T^2 + m_B^2\right)\left(1 - \varepsilon_{tR}^2\right)\right]. \tag{2.113}$$

Using Eqn. (2.108), we can evaluate the finite contributions due to the RR currents:

$$\Pi_{11}(0)_{\rm finite} = -\frac{4}{(4\pi)^2}\left[\frac{1}{16}M_D^2 \log M_D^2 + \frac{M_D^2}{64}\varepsilon_{tR}^2 - \frac{M_D^2}{192}\varepsilon_{tR}^4\right] \tag{2.114}$$

$$\Pi_{33}(0)_{\rm finite} = -\frac{4}{(4\pi)^2}\left[\frac{1}{16}M_D^2 \log M_D^2 + \frac{M_D^2}{64}\varepsilon_{tR}^2 - \frac{M_D^2}{128}\varepsilon_{tR}^4\right] \tag{2.115}$$

Thus, the finite contribution from the vacuum polarization diagrams involving two right handed currents is given by:

$$(\Pi_{11}(0) - \Pi_{33}(0))_{\rm finite} = \frac{4}{(4\pi)^2}\frac{5M_D^2\varepsilon_{tR}^4}{384}. \tag{2.116}$$

LR diagrams: The LR diagrams are evaluated to be (Ref. [54]):

$$\Pi_{LR}(0) = -\frac{2}{(4\pi)^2}\left[m_1 m_2 E - m_1 m_2 b_0(120)\right]. \tag{2.117}$$

The divergent part of Π_{11} can now be evaluated:

$$\Pi_{11}(0)_{\rm div} = -\frac{2E}{(4\pi)^2}\left[2m_t m_B (g_{tB}^R)(g_{tB}^L) + 2m_T m_B (g_{TB}^L)(g_{TB}^R)\right]. \tag{2.118}$$

In the above formula, we have omitted terms proportional to m_b. Plugging in the couplings, we see that:

$$\Pi_{11}(0)_{\rm div} = -\frac{2E}{(4\pi)^2}\left[2m_T m_B\left(\frac{1}{16}\right)\left(1 - \frac{\varepsilon_{tR}^2}{2}\right)\right]. \tag{2.119}$$

It can be easily shown that the divergent part of Π_{33} exactly cancels this. We now proceed to compute the finite contributions.

$$\begin{aligned}\Pi_{11}(0)_{\text{finite}} &= \frac{2}{(4\pi)^2}2(g_{tB}^L)(g_{tB}^R)m_t m_B b_0(m_t, m_B, 0) \\ &+ \frac{2}{(4\pi)^2}2(g_{TB}^L)(g_{TB}^R)m_T m_B b_0(m_T, m_B, 0) \\ &= \frac{2}{(4\pi)^2}\left[\frac{M_D^2}{8}\log M_D^2 + \frac{M_D^2\varepsilon_{tR}^2}{16} + \varepsilon_{tR}^4\left(-\frac{M_D^2}{48} + \frac{M_D^2\log M_D^2}{16}\right)\right]\end{aligned} \tag{2.120}$$

$$\begin{aligned}\Pi_{33}(0)_{\text{finite}} &= \frac{2}{(4\pi^2)}\left[(g_{tt}^L)(g_{tt}^R)m_t^2 b_0(m_t, m_t, 0) + (g_{TT}^L)(g_{TT}^R)m_T^2 b_0(m_T, m_T, 0)\right. \\ &\left.+(g_{BB}^L)(g_{BB}^R)m_B^2 b_0(m_B, m_B, 0) + 2(g_{tT}^L)(g_{tT}^R)m_t m_T b_0(m_t, m_T, 0)\right] \\ &= \frac{2}{(4\pi)^2}\left[\frac{M_D^2}{8}\log M_D^2 + \frac{M_D^2\varepsilon_{tR}^2}{16} + \varepsilon_{tR}^4\left(-\frac{M_D^2}{32} + \frac{M_D^2\log M_D^2}{16}\right)\right].\end{aligned} \tag{2.121}$$

Thus, we see that the finite contribution due to the LR diagrams is:

$$(\Pi_{11}(0) - \Pi_{33}(0))_{\text{finite}} = \frac{4}{(4\pi)^2}\frac{M_D^2\varepsilon_{tR}^4}{192}. \tag{2.122}$$

The total fermionic contribution to $\Delta\rho$ in the three site model is obtained by adding Eqns. (2.112), (2.116) and (2.122) and is given by (after subtracting out the SM contribution and multiplying by a factor of 3 for color):

$$\Delta\rho = \frac{1}{16\pi^2 v^2}M_D^2\varepsilon_{tR}^4. \tag{2.123}$$

The W' and Z' contributions to $\Delta\rho$ are discussed in [56]. The phenomenological bounds on the value of $\Delta\rho$ depend (since they include the one-loop standard model

corrections) on the reference Higgs mass chosen. We are interested in the bounds on $\Delta\rho$ corresponding to Higgs masses between about 380 GeV (from Eqn.(2.87)) and the unitarity bound 1.2 TeV [56]. Current bounds (see, for example, Langacker and Erler in [57]) yield (approximately) $\Delta\rho \leq 2.5 \times 10^{-3}$, at 90% C.L., assuming the existence of a moderately heavy (340 GeV) Higgs boson, while it is relaxed to approximately $\Delta\rho \leq 5 \times 10^{-3}$ in the case of a heavy (1000 GeV) Higgs boson. We therefore expect that the upper bound on $\Delta\rho$ in the three site model varies from approximately 2.5×10^{-3} to 5×10^{-3}. For $\alpha T = 5 \times 10^{-3}$, we find the upper bound

$$\varepsilon_{tR} < 0.94 \left(\frac{v}{M}\right)^{1/2}. \tag{2.124}$$

Our upper limit on ε_{tR} and our knowledge of the top quark mass allow us to derive a lower bound on M. Our expression (2.29) for m_t reminds us that

$$m_t = \frac{\varepsilon_L \varepsilon_{tR} M}{\sqrt{1+\varepsilon_{tR}^2}}. \tag{2.125}$$

For a given value of M_D, the existence of an upper bound on ε_{tR} implies that there is a *smallest* allowed value of ε_L, which we denote ε_L^*

$$\varepsilon_L^* = 1.26 \left(\frac{2.5 \times 10^{-3}}{\alpha T}\right)^{1/4} \frac{m_t}{\sqrt{vM}} \sqrt{1 + 0.63 \left(\frac{\alpha T}{2.5 \times 10^{-3}}\right)^{1/2} \frac{v}{M}}. \tag{2.126}$$

Since eqn. (2.88) requires $\varepsilon_L^* < 0.30$, for $\alpha T = 2.5 \times 10^{-3}$ we find that M_D must be greater than 2.3 TeV, and for $\alpha T = 5 \times 10^{-3}$ we find that M_D must be greater than 1.8 TeV. The joint range of M_D and $M_{W'}$ is summarised in Fig. (2.3), for both values of αT. Using $M > 1.8$ TeV and the bound in Eqn. (2.124), we see that $\varepsilon_{tR} < 0.35$. The right handed Wtb coupling contributes to the process $b \to s\gamma$, and this gives an upper bound on ε_{tR} of 0.67, which is superceded by this limit.

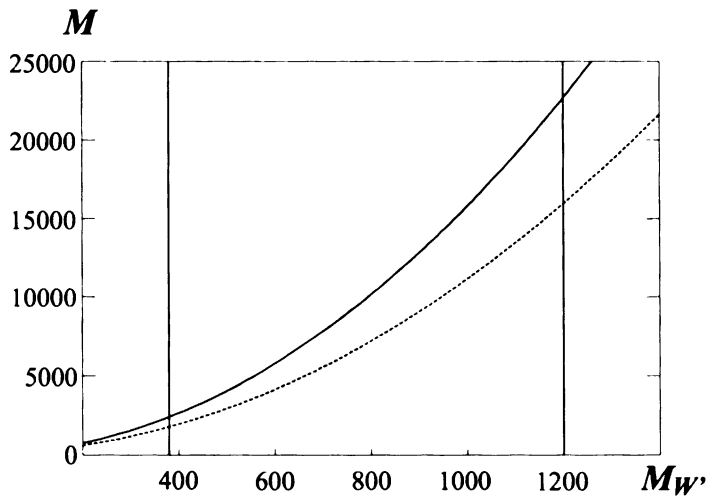

Figure 2.3: Phenomenologically acceptable values of M_D and $M_{W'}$ in GeV for $\alpha T = 2.5 \times 10^{-3}$ (solid curve) and 5×10^{-3} (dashed curve). The region bounded by the lines $380\,\text{GeV} < M_{W'} < 1200\,\text{GeV}$ and above the appropriate curve is allowed. For a given M_D and $M_{W'}$, the value of ε_{tR} is determined by Eqn. (2.125).

2.5 Remarks

In this chapter, we have described in detail a minimal deconstructed Higgsless model that is simple, in the sense that there is only one extra set of vector bosons instead of the infinite tower of vector bosons present in the continuum limit. Likewise, there need be only a single heavy fermion partner for each of the standard model fermions, instead of a tower of such states. The three site model serves as a convenient framework to understand many important ideas in Higgsless models, like the concept of ideal fermion delocalization. After deriving the mass eigenstates and couplings, we investigated the phenomenological bounds on the mass scales of the gauge and fermionic sector by appealing to precision low energy measurements. We found that the lower bound of M'_W is around 380 GeV, which makes its discovery at the CERN LHC a realistic possibility. However, the scale that sets the mass of fermions, M_D has a lower bound exceeding a TeV, because of the twin requirements of getting

the correct value of the top quark mass and having a phenomenologically acceptable value for $\Delta\rho$. This renders the discovery of the heavy fermions rather difficult. It is interesting to explore avenues to relax these constraints, so we could have extra fermions that are light enough to have a strong discovery potential. This, however, will involve extending the three site model in some specific way so as to free M_D from the constraints of m_t and $\Delta\rho$ and this will be the subject of the next chapter.

Chapter 3

Triangle Moose Model

In Chapter 2, we presented the details of the three site model [30], a maximally deconstructed version of a higgsless extra dimensional model, with only one extra $SU(2)$ gauge group, as compared to the SM. Thus, there are three extra gauge bosons, which contribute to unitarizing the $W_L W_L$ scattering in place of a higgs. (The LHC phenomenology of these extra vector bosons can be found in [60]). Also incorporated in the three site model is a heavy Dirac partner for every SM fermion. The presence of these new fermions, in particular, the heavy top and bottom quarks, gives rise to new one loop contributions to $\Delta\rho$. Low energy precision measurements require $\Delta\rho$ to be $< \mathcal{O}(10^{-3})$ and so, the combination of parameters ε_{tR} and M_D have to be tuned to both make $\Delta\rho$ small and obtain the large top quark mass. These twin constraints push the heavy quark mass into the multi TeV range, too high to be seen at the LHC. Our goal in this chapter is to construct a model that retains the features of the higgsless mechanism, but allows for Dirac fermions that are lighter. To achieve this, we separate top quark mass generation from the rest of electroweak symmetry breaking, by analogy with top color models.

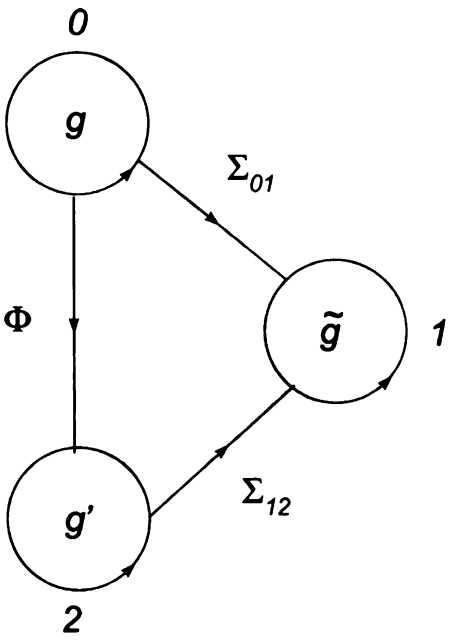

Figure 3.1: The gauge structure of the model in Moose notation [25]. g and g' are approximately the SM $SU(2)$ and hypercharge gauge couplings while $\tilde{g}$ represents the "bulk" gauge coupling. The left (right) handed light fermions are mostly localized at site 0 (2) while their heavy counterparts are mostly at site 1. The links connecting sites 0 and 1 and sites 1 and 2 are non linear sigma model fields while the one connecting sites 0 and 2 is the top Higgs field.

3.1 The Model

The electroweak gauge structure of the model is the same as that in the three site model and is $SU(2) \times SU(2) \times U(1)$ (shown using the "Moose Notation" in Figure (3.1)), with the SM fermions deriving their $SU(2)$ charges mostly from site 0 (which is most closely associated with the SM $SU(2)_W$) and the bulk fermions mostly from site 1. The extended electroweak gauge structure of the theory is the same as that of the BESS models [31, 32], motivated by models of hidden local symmetry (with $a \neq 1$) [33, 34, 35, 36, 37]. The non linear sigma field Σ_{01} is responsible for breaking the $SU(2) \times SU(2)$ gauge symmetry down to $SU(2)$. The left handed fermions are $SU(2)$ doublets residing at sites 0 (ψ_{L0}) and 1 (ψ_{L1}), while the right handed fermions are a

doublet under $SU(2)_1(\psi_{R1})$ and two $SU(2)$ singlet fermions at site 2 (u_{R2} and d_{R2}). The fermions ψ_{L0}, ψ_{L1}, and ψ_{R1} have $SU(2)$ charges typical of the left-handed $SU(2)$ doublets in the SM, $+1/6$ for quarks and $-1/2$ for leptons. Similarly, the fermion u_{R2} has $U(1)$ charge typical for the right-handed up-quarks ($+2/3$) and d_{R2} has the $U(1)$ charge typical for the right-handed down-quarks ($-1/3$).

Our goal is to separate top quark mass generation from the rest of electroweak symmetry breaking. We do this by introducing a "top Higgs" field Φ, motivated by top-color models [38, 39], and let the top quark couple preferentially to the top Higgs via the Lagrangian:

$$\mathcal{L}_{top} = -\lambda_t \bar{\psi}_{L0} \Phi t_R + h.c. \tag{3.1}$$

Thus, the model incorporates two non-linear sigma fields (the Higgsless sector) and a top Higgs field that couples to the top quark. We point out that electroweak symmetry breaking goes through via a Higgsless mechanism - we will see in the next section that the W and Z gauge boson masses are dominated by the vev of the non-linear sigma model fields and that the top Higgs link only has a sub-dominant contribution. Using the *AdS*-CFT correspondence [19, 20, 21, 22], this model can be thought of as being dual to Top-Color assisted Technicolor (TC_2) theories [7, 40, 41].

The top Higgs field can be written as:

$$\phi = e^{i\pi^a \sigma^a / f} \begin{pmatrix} 0 \\ \frac{f+H(x)}{\sqrt{2}} \end{pmatrix}. \tag{3.2}$$

$H(x)$ is the physical top Higgs and the π's are the associated Goldstone bosons that are *not* eaten. Thus, the spectrum consists, in addition to the SM particles and their heavy copies, a top-Higgs boson and three uneaten top-pions, π^0, π^+, and π^-. We assume that Extended Technicolor (ETC) dynamics [7] induces "plaquette" terms that align the technicolor vacuum with the topcolor vacuum and give mass to the top

pions. The mass term can be written down as:

$$\mathcal{L}_\pi = 4\pi\kappa v^3 \mathrm{Tr}\left(\Phi\Sigma_{01}\Sigma_{12}^\dagger\right), \tag{3.3}$$

where κ is a dimensionless parameter.

The top Higgs field is described by the Lagrangian:

$$\mathcal{L}_\Phi = \frac{f^2}{4} D_\mu\Phi^\dagger D_\mu\Phi - V(\Phi). \tag{3.4}$$

The potential $V(\Phi)$ is minimized at $\langle\Phi\rangle = f$. When the field Φ develops a non zero vacuum expectation value, Eqn.(3.1) generates a top quark mass term. We choose the vacuum expectation value associated with the non linear signal model fields to be $F = \sqrt{2}\,v\,\cos\omega$ (for simplicity, we choose the vev of both the non linear sigma model fields to be the same) and the one associated with the top Higgs sector to be $f = \langle\Phi\rangle = v\,\sin\omega$ (where ω is a small parameter).

The mass terms for all the light fermions arise from Yukawa couplings of the fermionic fields with the non linear sigma fields and is the same as that in the three site model discussed in the previous chapter.

$$\mathcal{L} = M_D\left[\varepsilon_L\bar{\psi}_{L0}\Sigma_{01}\psi_{R1} + \bar{\psi}_{R1}\psi_{L1} + \bar{\psi}_{L1}\Sigma_{12}\begin{pmatrix}\varepsilon_{uR} & 0\\ 0 & \varepsilon_{dR}\end{pmatrix}\begin{pmatrix}u_{R2}\\ d_{R2}\end{pmatrix}\right]. \tag{3.5}$$

We have denoted the Dirac mass (that sets the scale of the heavy fermion mass) to be M_D. One can see that flavor violation (in all but the top-quark sector) is encoded in the last term. Here, ε_L is a parameter that describes the degree of delocalization of the left handed fermions and is flavor universal. The delocalization parameter for the right handed fermions, ε_{fR}, can be tuned to realize the mass difference between the up and down type fermions. For our phenomenological study, we will, for the

most part, assume that all the fermions (except the top) are massless and hence will set this parameter to zero. It will turn out that even for the top quark, ε_{tR} can be small since its mass is dominated by the top Higgs contribution (see Eqn.(1)). We will see in Section VI that the top quark mass does not severely constrain $\Delta\rho$, and correspondingly, there will exist no tension between the heavy quark mass, M_D, and one loop contributions to $\Delta\rho$, as in the three site model. This enables us to have heavy quarks in this model that are light enough to be found at the LHC - we will investigate this point in Section VII.

3.2 Masses and Eigenstates

In addition to the SM γ, Z and W bosons, we also have the heavy partners, W' and Z' because of the extra $SU(2)$ group. The canonically normalized kinetic energy terms of the gauge fields can be written down in the usual way:

$$\mathcal{L}_{KE} = -\frac{1}{4}F^0_{\mu\nu}F^{0\mu\nu} - \frac{1}{4}F^1_{\mu\nu}F^{1\mu\nu} - \frac{1}{4}B_{\mu\nu}B^{\mu\nu}. \tag{3.6}$$

In this section, we review the masses and wave functions of the gauge bosons, which are almost the same as the ones for the three site model, except for small ω dependent factors.

3.2.1 Charged Gauge Bosons

The masses of the gauge bosons come from the kinetic terms of the sigma fields:

$$\mathcal{L}_{\text{gauge}} = \frac{F^2}{4}\text{Tr}[D_\mu\Sigma_{01}^\dagger D_\mu\Sigma_{01}] + \frac{F^2}{4}\text{Tr}[D_\mu\Sigma_{12}^\dagger D_\mu\Sigma_{12}] + \frac{f^2}{4}\text{Tr}[D_\mu\Phi^\dagger D_\mu\Phi], \tag{3.7}$$

where the gauge covariant derivatives are:

$$D_\mu \Sigma_{01} = \partial_\mu \Sigma_{01} + igW_\mu^0 \Sigma_{01} - i\tilde{g}\Sigma_{01} W_\mu^1 \tag{3.8}$$

$$D_\mu \Sigma_{01} = \partial_\mu \Sigma_{12} + i\tilde{g}W_\mu^1 \Sigma_{12} - ig'\Sigma_{12} W_\mu^2. \tag{3.9}$$

and Σ_{01} and Σ_{12} are unitary 2×2 matrix fields.

Let us write the gauge couplings in the following form:

$$g_0 = \frac{e}{\sin\theta\cos\phi} \quad \tilde{g} = \frac{e}{\sin\theta\sin\phi} \quad g' = \frac{e}{\cos\theta}. \tag{3.10}$$

We will find the mass eigenvalues and eigenvectors perturbatively in the small parameter $\sin\phi$, which we will call x.

From the above Lagrangian, one can get the mass matrix for the gauge bosons by working in the unitary gauge ($\Sigma = 1$) and collecting the coefficients of the terms quadratic in the gauge fields. The charged gauge boson mass matrix is thus given by:

$$M_W^2 = \frac{e^2 v^2}{4x^2 \sin^2\theta} \begin{pmatrix} \frac{x^2(1+\cos^2\omega)}{1-x^2} & -\frac{2x\cos^2\omega}{\sqrt{1-x^2}} \\ -\frac{2x\cos^2\omega}{\sqrt{1-x^2}} & 4\cos^2\omega \end{pmatrix}. \tag{3.11}$$

This matrix can be diagonalized perturbatively in x. We find the light W has the following mass and eigenvector:

$$M_W^2 = \frac{e^2 v^2}{4\sin^2\theta}\left(1 + \frac{3x^2}{4}\right) \tag{3.12}$$

$$W^\mu = v_w^0 W_0^\mu + v_w^1 W_1^\mu = \left(1 - \frac{x^2}{8}\right) W_0^\mu + \frac{1}{2} x W_1^\mu. \tag{3.13}$$

Here, W_0 and W_1 are the gauge bosons associated with sites 0 and 1. Since x is small, we note that the light W resides primarily at site 0. (The above formulas are

valid to $\mathcal{O}(x^2)$, as are all the other eigenvalues and couplings in this chapter).

The heavy W eigenvector is orthogonal to the above and has a mass:

$$M_{W'}^2 = \frac{e^2 v^2 \cos^2\omega}{4\sin^2\theta\, x^2}\left(4 + x^2\right). \tag{3.14}$$

To leading order, the relation between the light and heavy W boson masses is

$$\frac{M_W^2}{M_{W'}^2} = \frac{x^2}{4\cos^2\omega}. \tag{3.15}$$

3.2.2 Neutral gauge bosons

The neutral gauge bosons' mass matrix is given by:

$$M_Z^2 = \frac{e^2 v^2}{4x^2\sin^2\theta}\begin{pmatrix} \frac{x^2(1+\cos^2\omega)}{1-x^2} & -\frac{2x\cos^2\omega}{\sqrt{1-x^2}} & -\frac{x^2\sin^2\omega\tan\theta}{\sqrt{1-x^2}} \\ -\frac{2x\cos^2\omega}{\sqrt{1-x^2}} & 4\cos^2\omega & -2x\,\cos^2\omega\,\tan\theta \\ -\frac{x^2\sin^2\omega\tan\theta}{\sqrt{1-x^2}} & -2x\cos^2\omega\tan\theta & x^2(1+\cos^2\omega)\tan^2\theta \end{pmatrix} \tag{3.16}$$

This mass matrix has a zero eigenvalue (the photon), the eigenvector of which may be written exactly as:

$$A^\mu = \frac{e}{g}W_0^\mu + \frac{e}{\tilde{g}}W_1^\mu + \frac{e}{g'}B^\mu. \tag{3.17}$$

Requring that this state be properly normalized, we get the relation between the couplings:

$$\frac{1}{e^2} = \frac{1}{g^2} + \frac{1}{\tilde{g}^2} + \frac{1}{g'^2}. \tag{3.18}$$

The light Z boson has the mass

$$M_Z^2 = \frac{e^2 v^2}{4 \sin^2\theta \cos^2\theta}\left(1 + x^2\left(1 - \frac{\sec^2\theta}{4}\right)\right), \tag{3.19}$$

and the corresponding eigenvector

$$Z^\mu = v_z^0 W_0^\mu + v_z^1 W_1^\mu + v_z^2 B^\mu, \tag{3.20}$$

where

$$v_z^0 = \frac{1}{8}(4(-2+x^2)\cos\theta - 3x^2\sec\theta) \tag{3.21}$$

$$v_z^1 = \frac{1}{2}x(-2\cos^2\theta + 1)\sec\theta \tag{3.22}$$

$$v_z^2 = \sin\theta - \frac{1}{2}x^2\sec\theta\tan\theta. \tag{3.23}$$

The heavy neutral vector boson, which we call Z', has a mass and eigenvector

$$M_{Z'}^2 = \frac{e^2 v^2 \cos^2\omega}{4\sin^2\theta\, x^2}\left(4 + x^2\sec^2\theta\right) \tag{3.24}$$

$$Z'^\mu = v_{z'}^0 W_0^\mu + v_{z'}^1 W_1^\mu + v_{z'}^2 B^\mu, \tag{3.25}$$

where

$$v_{z'}^0 = \frac{1}{2}x \tag{3.26}$$

$$v_{z'}^1 = -1 + \frac{1}{8}x^2\sec^2\theta \tag{3.27}$$

$$v_{z'}^2 = \frac{1}{2}x\ \tan\theta. \tag{3.28}$$

For small x, it is seen that the Z' is mainly at site 1, while the Z is at sites 0 and 2, as one would expect.

3.3 Fermions and Ideal delocalization

In this section, we will review the masses and wave functions of the light fermions and their heavy partners. We will then discuss how to "ideally delocalize" the light fermions, which will make the tree level value of the S parameter vanish [49].

3.3.1 Masses and wave functions

Working in the unitary gauge ($\Sigma_{01} = \Sigma_{12} = 1$), the mass matrices of the light quarks and their Dirac fermion partners can be derived from Eqn.(1) and are given by:

$$M_{u,d} = M_D \begin{pmatrix} \varepsilon_L & 0 \\ 1 & \varepsilon_{uR,dR} \end{pmatrix}. \tag{3.29}$$

The subscripts $u(d)$ denote up (down) quarks and M_D is the Dirac mass, introduced in Eqn. (3.5). Diagonalizing the matrix perturbatively in ε_L, we find the light eigenvalue:

$$m_u = \frac{M_D \varepsilon_L \varepsilon_{uR}}{\sqrt{1+\varepsilon_{uR}^2}} \left[1 - \frac{\varepsilon_L^2}{2(1+\varepsilon_{uR}^2)} + ... \right]. \tag{3.30}$$

Note that m_f is proportional to the flavor-specific parameter ε_{fR}, where f is any light SM fermion (except the top). The heavy Dirac quark has a mass:

$$m_U = M_D \sqrt{1+\varepsilon_{uR}^2} \left[1 + \frac{\varepsilon_L^2}{2(1+\varepsilon_{uR}^2)^2} + ... \right]. \tag{3.31}$$

The left and right handed eigenvectors of the light quarks are

$$\begin{aligned} u_L =& u_L^0 \psi_{L0} + u_L^1 \psi_{L1} \\ =& \left(-1 + \frac{\varepsilon_L^2}{2(1+\varepsilon_{uR}^2)^2} \right) \psi_{L0} + \left(\frac{\varepsilon_L}{1+\varepsilon_{uR}^2} \right) \psi_{L1} \end{aligned} \tag{3.32}$$

$$
\begin{aligned}
u_R =& u_R^1 \psi_{R1} + u_R^2 u_{R2} \\
=& \left(-\frac{\varepsilon_{uR}}{\sqrt{1+\varepsilon_{uR}^2}} + \frac{\varepsilon_L^2 \varepsilon_{uR}}{(1+\varepsilon_{uR}^2)^{5/2}} \right) \psi_{R1} + \left(\frac{1}{\sqrt{1+\varepsilon_{uR}^2}} + \frac{\varepsilon_L^2 \varepsilon_{uR}^2}{(1+\varepsilon_{uR}^2)^{5/2}} \right) u_{R2}.
\end{aligned}
\tag{3.33}
$$

The left and right handed eigenvectors of the heavy partners are orthogonal to Eqn.(3.32) and Eqn.(3.33):

$$
\begin{aligned}
U_L =& U_L^0 \psi_{L0} + U_L^1 \psi_{L1} \\
=& \left(-\frac{\varepsilon_L}{1+\varepsilon_{uR}^2} \right) \psi_{L0} + \left(-1 + \frac{\varepsilon_L^2}{2(1+\varepsilon_{uR}^2)^2} \right) \psi_{L1}
\end{aligned}
\tag{3.34}
$$

$$
\begin{aligned}
U_R =& U_R^1 \psi_{R1} + U_R^2 u_{R2} \\
=& \left(-\frac{1}{\sqrt{1+\varepsilon_{uR}^2}} - \frac{\varepsilon_L^2 \varepsilon_{uR}^2}{(1+\varepsilon_{uR}^2)^{5/2}} \right) \psi_{R1} + \left(-\frac{\varepsilon_{uR}}{\sqrt{1+\varepsilon_{uR}^2}} + \frac{\varepsilon_L^2 \varepsilon_{uR}}{(1+\varepsilon_{uR}^2)^{5/2}} \right) u_{R2}.
\end{aligned}
\tag{3.35}
$$

In the above expressions, U and D stand for the heavy up and down quarks respectively. The masses and eigenvectors of other fermions can be obtained by the replacement $\varepsilon_{uR} \to \varepsilon_{fR}$.

3.3.2 Ideal fermion delocalization

The leading *tree level* contributions to precision measurements in Higgsless models come necessarily from the coupling of standard model fermions to the heavy gauge bosons. It was shown in [49] that it is possible to delocalize the light fermions in such a way that they do not couple to these heavy fields and thus minimize the deviations in precision electroweak parameters. The coupling of the heavy W' to SM fermions is

of the form $\sum_i g_i(\psi_{f_i})^2 \psi_{W_i'}$. Thus choosing the light fermion profile such that $(\psi_{f_i})^2$ is proportional to ψ_{W_i} would make this coupling automatically vanish because the heavy and light W fields are orthogonal to one another. This procedure (called Ideal fermion delocalization) also equates the coupling of the W to two light fermions to the SM value. Thus, an equivalent way to impose ideal fermion delocalization (IFD) is to demand that the tree level $g_{We\nu}$ coupling (say) equal the SM value.

We will use the latter procedure to implement IFD. The deviation of the $g_{We\nu}$ coupling from the SM value can be parametrized in terms of the Peskin-Takeuchi parameters [42] S, T and U parameters as [50]:

$$g_{We\nu} = \frac{e}{s}\left[1 + \frac{\alpha S}{4s^2} - \frac{c^2\alpha T}{2s^2} - \frac{(c^2 - s^2)\alpha U}{8s^2}\right]. \tag{3.36}$$

where $c = \cos\theta_w = M_W/M_Z$ and $s = \sin\theta_w = \sqrt{1-c^2}$ are the "mass defined" angles. It was shown in [48] that at tree level, in models of this kind, the parameters T and U have negligible values that are $\mathcal{O}(x^4)$, and so we can impose ideal fermion delocalization by requiring S to vanish at tree level (which would make $g_{We\nu}$ the SM value, from Eqn. (3.36)).

In computing the couplings, we will use the mass defined angles. (We will indicate this by a suffix w in all the couplings). From Eqns.(3.12) and (3.19), we can see that $\sin\theta_w$ is related to $\sin\theta$ defined implicitly in the couplings in Eqn. (3.10) by:

$$\sin\theta_w = \left(1 - \frac{x^2}{8}\right)\sin\theta. \tag{3.37}$$

Using the W and the fermion wave functions, we can calculate the coupling $g_{We\nu}$ as

$$g_{We\nu} = \frac{e}{\sin\theta_w}\left(1 + \frac{x^2}{4} - \frac{\varepsilon_L^2}{8}\right). \tag{3.38}$$

Thus, we find the ideal fermion delocalization condition in the model to be:

$$\varepsilon_L^2 = \frac{x^2}{2}. \tag{3.39}$$

Note that this relation is the same as the one obtained in the three site model.

3.4 Light Fermion couplings to the gauge bosons

3.4.1 Charged Currents

Now that we have the wave functions of the vector bosons and the fermions, we can compute the couplings between these states. Since all the light fermions are approximately massless, we set ε_{fR} for all the light fermions to zero in this section. We will calculate all couplings to $\mathcal{O}(x^2)$. We begin with the left handed Wud coupling.

$$g_L^{Wud} = g_0 v_w^0 u_L^0 d_L^0 + \tilde{g} v_w^1 u_L^1 d_L^1 = \frac{e}{\sin\theta_w}. \tag{3.40}$$

This result follows from the fact that we have implemented ideal fermion delocalization in the model.

All other charged current couplings (both left and right handed) can be similarly computed. The couplings in this model are only very slightly different from the ones in the three site model. The difference is attributable to the fact that the expansion parameter we have chosen, x, is $\sin\phi$, as opposed to $\tan\phi$ in the three site model. We

now summarize the results:

$$g_L^{Wud} = g_0 v_w^0 u_L^0 d_L^0 + \tilde{g} v_w^1 u_L^1 d_L^1 = \frac{e}{\sin\theta_w} \tag{3.41}$$

$$g_L^{WUd}(= g_L^{WuD}) = g_0 v_w^0 U_L^0 d_L^0 + \tilde{g} v_w^1 U_L^1 d_L^1 = \frac{e\,x}{2\sqrt{2}\sin\theta_w} \tag{3.42}$$

$$g_L^{WUD} = g_0 v_w^0 U_L^0 D_L^0 + \tilde{g} v_w^1 U_L^1 D_L^1 = \frac{e}{2\,\sin\theta_w}\left(1 + \frac{3}{8}x^2\right) \tag{3.43}$$

$$g_R^{Wud} = \tilde{g} v_w^1 u_R^1 D_R^1 = 0 \tag{3.44}$$

$$g_R^{WUd}(= g_R^{WuD}) = \tilde{g} v_w^1 U_R^1 D_R^1 = 0 \tag{3.45}$$

$$g_R^{WUD} = \tilde{g} v_w^1 U_R^1 D_R^1 = \frac{e}{2\sin\theta_w}\left(1 - \frac{1}{8}x^2\right) \tag{3.46}$$

$$g_L^{W'ud} = g_0 v_{w'}^0 u_L^0 d_L^0 + \tilde{g} v_{w'}^1 u_L^1 d_L^1 = 0 \tag{3.47}$$

$$g_L^{W'Ud}(= g_L^{W'uD}) = g_0 v_{w'}^0 U_L^0 d_L^0 + \tilde{g} v_{w'}^1 U_L^1 d_L^1 = -\frac{e}{\sqrt{2}\,\sin\theta_w} \tag{3.48}$$

$$g_L^{W'UD} = g_0 v_{w'}^0 U_L^0 D_L^0 + \tilde{g} v_{w'}^1 U_L^1 D_L^1 = \frac{e}{x\sin\theta_w}\left(1 - \frac{3}{4}x^2\right) \tag{3.49}$$

$$g_R^{W'ud} = \tilde{g} v_{w'}^1 u_R^1 d_R^1 = 0 \tag{3.50}$$

$$g_R^{W'Ud}(= g_R^{W'uD}) = \tilde{g} v_{w'}^1 U_R^1 d_R^1 = 0 \tag{3.51}$$

$$g_R^{W'UD} = \tilde{g} v_{w'}^1 U_R^1 D_R^1 = \frac{e}{x\sin\theta_w}\left(1 - \frac{1}{4}x^2\right) \tag{3.52}$$

Two comments are in order. The right handed $WUd, W'ud$ couplings are zero in the limits in which we are working ($\varepsilon_{uR} = \varepsilon_{dR} = 0$). The right handed coupling of W with two heavy fields arises, in this limit, solely from site 1 and is not zero. The left and right-handed W' coupling to two heavy fermions is enhanced by a factor $1/x$ relative to $g_{L,R}^{WUD}$, with x being the small expansion parameter. Thus, for very small values of x, this coupling becomes large and consequently, $\Gamma(W')/M_{W'} \gg 1$. We therefore exclude the region $M_{W'} \geq 2M_D$ of the $M_D - M_{W'}$ parameter space in our phenomenological study of the heavy quark production in Section 3.6.

3.4.2 Neutral Currents

We can now calculate the coupling of the fermions to the neutral bosons. All the charged fermions couple to the photon with their standard electric charges.

$$g_{L\gamma ee} = g_{R\gamma ee} = g(e/g)(e_L^0)^2 + \tilde{g}(e/\tilde{g})(e_L^1)^2 = e. \tag{3.53}$$

We will be calculating the couplings in the "$T_3 - Q$" basis. To do this we use the standard relation between the three quantum numbers: $Q = T_3 + Y$. Since the fermions derive their $SU(2)$ charge from more than one site, we will calculate, for example, the T_3 coupling of two light fields to the Z as $\sum_i g_i (v_{f_i})^2 v_z^i$. The left handed Z coupling to SM fermions is calculated to be:

$$\begin{aligned} g_{LZuu} &= \left(g_0 v_Z^0 (u_L^0)^2 + \tilde{g} v_Z^1 (u_L^1)^2\right) T_3 + g' v_Z^2 \left((u_L^0)^2 + (u_L^1)^2\right)(Q - T_3) \\ &= -\frac{e}{\sin\theta_w \cos\theta_w}\left(T_3 - Q\sin^2\theta_w\right). \end{aligned} \tag{3.54}$$

All the other couplings can be similarly computed and we summarize the results

below:

$$g_L^{Zuu} = -\frac{e}{\sin\theta_w \cos\theta_w}\left(T_3 - Q\sin^2\theta_w\right) \tag{3.55}$$

$$g_L^{ZuU} = -\frac{e\,x}{2\sqrt{2}\sin\theta_w\cos\theta_w}T_3 \tag{3.56}$$

$$g_L^{ZUU} = -\frac{e}{\sin\theta_w\cos\theta_w}\left(\frac{1}{2}\left(1+\frac{x^2}{8}(4-\sec^2\theta_w)\right)T_3 - Q\sin^2\theta_w\right) \tag{3.57}$$

$$g_R^{Zuu} = e(Q-T_3)\tan\theta_w \tag{3.58}$$

$$g_R^{ZuU} = 0 \tag{3.59}$$

$$g_R^{ZUU} = -\frac{e}{\sin\theta_w\cos\theta_w}\left(\frac{1}{2}(1-\frac{x^2}{8})\,T_3 - Q\sin^2\theta_w\right) \tag{3.60}$$

$$g_L^{Z'uu} = -\frac{1}{2}\,x\sec\theta_w\tan\theta_w\,(T_3-Q) \tag{3.61}$$

$$g_L^{Z'uU} = \frac{e}{\sqrt{2}\sin\theta_w}\left(1-\frac{x^2}{8}\tan^2\theta_w\right)T_3 \tag{3.62}$$

$$g_L^{Z'UU} = -\frac{e}{x\sin\theta_w}\left[1-\frac{3x^2}{8}(2\sec^2\theta_w - 3\tan^2\theta_w)\right]T_3 + \frac{1}{2}\,e\,x\,\frac{\sin^2\theta_w}{\cos\theta_w}\,Q \tag{3.63}$$

$$g_R^{Z'uu} = \frac{ex}{2}\sec\theta_w\tan\theta_w(Q-T_3) \tag{3.64}$$

$$g_R^{Z'uU} = 0 \tag{3.65}$$

$$g_R^{Z'UU} = -\frac{e}{x\sin\theta_w}\left[1-\frac{x^2}{8}(2\sec^2\theta_w - 5\tan^2\theta_w)\right]T_3 + \frac{1}{2}\,e\,x\,\frac{\sin^2\theta_w}{\cos\theta_w}\,Q \tag{3.66}$$

While ideal fermion delocalization makes $g_{W'ud}$ zero, in the case of the neutral currents, the corresponding $g_{Z'uu}$ is seen to have a small hypercharge coupling. (The T_3 portion is, of course, zero). Also, g_L^{ZuU} is seen to have only a T_3 coupling because the term multiplying $Q - T_3$ (hypercharge) vanishes due to the orthogonality of the fermion wave functions. In the limit $\cos\theta_w \to 1$, g_L^{ZuU} is seen to correspond exactly to the off diagonal coupling of the W, g_L^{WuD}. As in the case of charged currents, the coupling of two heavy quarks to the Z' is enhanced by a factor $1/x$. This makes $\Gamma(Z')/M_{Z'} \gg 1$ for small values of x, and hence we will restrict ourself to the region

$M_{Z'} \leq 2M_D$ in our phenomenogical analysis in Section 3.6.

3.5 The Top quark

The top quark in the model has different properties than the light quarks since its mass is generated by the top Higgs. This section reviews the masses and eigenstates of the top quark and proceeds to analyze the delocalization pattern of the top and bottom quarks.

3.5.1 Masses and wave functions

The top quark mass matrix may be read from Eqns. (3.1) and (3.5) and is given by:

$$\begin{pmatrix} M_D\varepsilon_{Lt} & \lambda_t v \sin\omega \\ M_D & M_D\varepsilon_{tR} \end{pmatrix}. \tag{3.67}$$

Let us define the parameter

$$a = \frac{\lambda_t\, v \sin\omega}{M_D}, \tag{3.68}$$

in terms of which the above matrix can be written as:

$$M_t = M_D \begin{pmatrix} \varepsilon_{Lt} & a \\ 1 & \varepsilon_{tR} \end{pmatrix}. \tag{3.69}$$

Note that we have introduced the left handed delocalization parameter ε_{Lt}, that is technically distinct from the one for the light fermions. We will see in the next subsection that $\varepsilon_{Lt} = \varepsilon_L$ is the preferred value, i.e., the top quark is delocalized in exactly the same way as the light quarks.

Diagonalizing the top quark mass matrix perturbatively in ε_{Lt} and ε_{tR}, we can find the light and heavy eigenvalues:

$$m_t = \lambda_t v \sin\omega \left[1 + \frac{\varepsilon_{Lt}^2 + \varepsilon_{tR}^2 + \frac{2}{a}\varepsilon_{Lt}\varepsilon_{tR}}{2(-1+a^2)}\right], \tag{3.70}$$

$$M_t = M_D \left[1 - \frac{\varepsilon_{Lt}^2 + \varepsilon_{tR}^2 + 2a\varepsilon_{Lt}\varepsilon_{tR}}{2(-1+a^2)}\right]. \tag{3.71}$$

Thus, we see that m_t depends mainly on v and only slightly on ε_{tR}, in contrast to the light fermion mass, Eqn. (3.30), where the dominant term is ε_{fR} dependent.

The wave functions of the left and right handed top quark are:

$$\begin{aligned} t_L &= t_L^0 \psi_{L0}^t + t_L^1 \psi_{L1}^t \\ &= \left(1 - \frac{\varepsilon_{Lt}^2 + a^2\varepsilon_{tR}^2 + 2a\varepsilon_{Lt}\varepsilon_{tR}}{2(-1+a^2)^2}\right)\psi_{L0}^t + \left(\frac{\varepsilon_{Lt} + a\varepsilon_{tR}}{-1+a^2}\right)\psi_{L1}^t \end{aligned} \tag{3.72}$$

$$\begin{aligned} t_R &= t_R^1 \psi_{R1}^t + t_R^2 t_{R2} \\ &= \left(1 - \frac{a^2\varepsilon_{Lt}^2 + \varepsilon_{tR}^2 + 2a\varepsilon_{Lt}\varepsilon_{tR}}{2(-1+a^2)^2}\right)\psi_{R1}^t + \left(\frac{a\varepsilon_{Lt} + \varepsilon_{tR}}{-1+a^2}\right) t_{R2}. \end{aligned} \tag{3.73}$$

The left and right handed heavy top wave functions are the orthogonal combinations:

$$\begin{aligned} T_L &= T_L^0 \psi_{L0}^t + T_L^1 \psi_{L1}^t \\ &= \left(\frac{\varepsilon_{Lt} + a\varepsilon_{tR}}{-1+a^2}\right)\psi_{L0}^t + \left(-1 + \frac{\varepsilon_{Lt}^2 + a^2\varepsilon_{tR}^2 + 2a\varepsilon_{Lt}\varepsilon_{tR}}{2(-1+a^2)^2}\right)\psi_{L1}^t \end{aligned} \tag{3.74}$$

$$\begin{aligned} T_R &= T_R^1 \psi_{R1}^t + T_R^2 t_{R2} \\ &= \left(\frac{a\varepsilon_{Lt} + \varepsilon_{tR}}{-1+a^2}\right)\psi_{R1}^t + \left(-1 + \frac{a^2\varepsilon_{Lt}^2 + \varepsilon_{tR}^2 + 2a\varepsilon_{Lt}\varepsilon_{tR}}{2(-1+a^2)^2}\right) t_{R2}. \end{aligned} \tag{3.75}$$

3.5.2 $Zb\bar{b}$ and choice of ε_{Lt}

Since the (left-handed) bottom is the $SU(2)$ partner of the (left-handed) top, it is delocalized in exactly the same way as t_L. Thus, we can compute the tree level value of the $Zb_L\bar{b}_L$coupling and use it to constrain ε_{Lt}. This coupling is given by:

$$\begin{aligned} g_{LZbb} &= \left(g_0 v_Z^0 (b_L^0)^2 + g_1 v_Z^1 (b_L^1)^2\right) T_3 + \tilde{g} v_Z^2 \left((b_L^0)^2 + (b_L^1)^2\right)(Q - T_3) \\ &= -\frac{e}{\sin\theta_w \cos\theta_w}\left((1 + \frac{x^2}{4} - \frac{\varepsilon_{Lt}^2}{2})T_3 - Q\sin^2\theta_w\right). \end{aligned} \tag{3.76}$$

Now this exactly corresponds to the tree-level SM value provided that ε_{Lt} satisfies

$$\varepsilon_{Lt}^2 = \frac{x^2}{2}. \tag{3.77}$$

We see that this matches the delocalization condition for the light quarks, Eqn. (3.39). Thus, we see that the left-handed top quark is to be delocalized in exactly the same way as the light fermions if we are to avoid significant tree-level corrections to the SM $Zb_L\bar{b}_L$ value. Henceforth, we shall be choosing this value for ε_{Lt}.

3.5.3 $\Delta\rho$ and M_D

The contribution of the heavy top-bottom doublet to $\Delta\rho$ can be evaluated in this model in the same way as in the three site model discussed in Chapter 2 and the result is the same as in Eqn. (2.123). We give it below:

$$\Delta\rho = \frac{M_D^2 \varepsilon_{tR}^4}{16\pi^2 v^2}. \tag{3.78}$$

The important difference now is that, since the top quark mass is dominated by the vev of the top Higgs instead of M_D (see Eqn. (3.70)), ε_{tR} could be as low as the ε_R

of any light fermion. Thus, there is no constraint between the twin goals of getting a large top quark mass and having an experimentally admissible value of $\Delta\rho$. This enables us to have heavy fermions in this model that are light enough to be seen at the LHC. We explore this in detail in the next section.

3.6 Heavy fermion phenomenology at hadron colliders

We are now prepared to investigate the collider phenomenology of this model. As we have just seen, there is no tension between getting the correct values of the top quark mass and the ρ parameter in this model. Thus, the mass of the heavy quark does not necessarily lie in the TeV range as in the three site model discussed in Chapter 2 [30]. This enables us to investigate the phenomenology of these heavy quarks for M_D of the order of hundreds of GeV. The current CDF lower bounds on heavy up (decaying via charged currents) and down type quarks (decaying via neutral currents) are 284 GeV and 270 GeV respectively at 95% C.L. [61]. Thus, in our phenomenological analysis, we will be concentrating on quarks whose masses are between 300 GeV and 1 TeV.

Let us recall that the diagonal coupling of the heavy W' or Z' with two heavy fermions is enhanced by a factor $1/x$, where $x = \sin\phi$ is our small expansion parameter. Thus, if the masses are such that the heavy gauge bosons can decay to two heavy fermions, then we are in a situation where $\Gamma_{W'}/M_{W'} > 1$, rendering perturbative analysis invalid. Thus, for perturbative consistency, we will always stay in the region of the $M_{W'} - M_D$ parameter space where $M_{W',Z'} \leq 2M_D$. We will study both pair and single production channels.

3.6.1 Heavy fermion decay

The heavy fermions in the model decay to a vector boson and a light fermion. If the heavy fermion is massive enough, the vector boson could even be the W' or Z' in the theory (Fig. 3.2). (The situation changes slightly for the heavy top quark, for which decay into top pions is allowed).

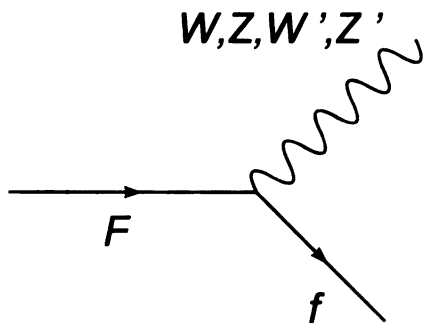

Figure 3.2: The decay modes of the heavy quarks in the theory. The decay rate is controlled by the off-diagonal left handed coupling of the vector boson to a heavy fermion and the corresponding light fermion (the corresponding right handed coupling vanishes in the limit of massless light fermions).

In the limit that the mass of the light fermion is zero, the rate of decay to charged gauge bosons is given by:

$$\Gamma = \frac{g_{VFf}^2}{32\pi}\frac{M_D^3}{m_V^2}\left(1-\frac{m_V^2}{M_D^2}\right)^2\left(1+2\frac{m_V^2}{M_D^2}\right). \tag{3.79}$$

In the limit that the Dirac mass is much higher than the W and W' boson masses, the terms in the parentheses can be approximated by 1. Thus, in this limit, the decay width is determined by the factor g_{VFf}^2/M_V^2. This can be evaluated for the W and

the W' couplings to be:

$$g^2_{WQq}/m^2_W \approx \frac{\left(e^2x^2/8\sin^2\theta_w\right)}{\left(e^2v^2/4\sin^2\theta_w\right)}$$
$$\sim \frac{x^2}{v^2}. \tag{3.80}$$
$$g^2_{W'Qq}/m^2_{W'} \approx \frac{\left(e^2/2\sin^2\theta_w\right)}{\left(e^2v^2/4\sin^2\theta_w x^2\right)}$$
$$\sim \frac{x^2}{v^2}. \tag{3.81}$$

Thus, we see that in this limit, the decay of the heavy fermion into W and W' become equally important because $g^2_{WQq}/m^2_W \approx g^2_{W'Qq}/m^2_{W'}$. This is further illustrated in Figure (3.3).

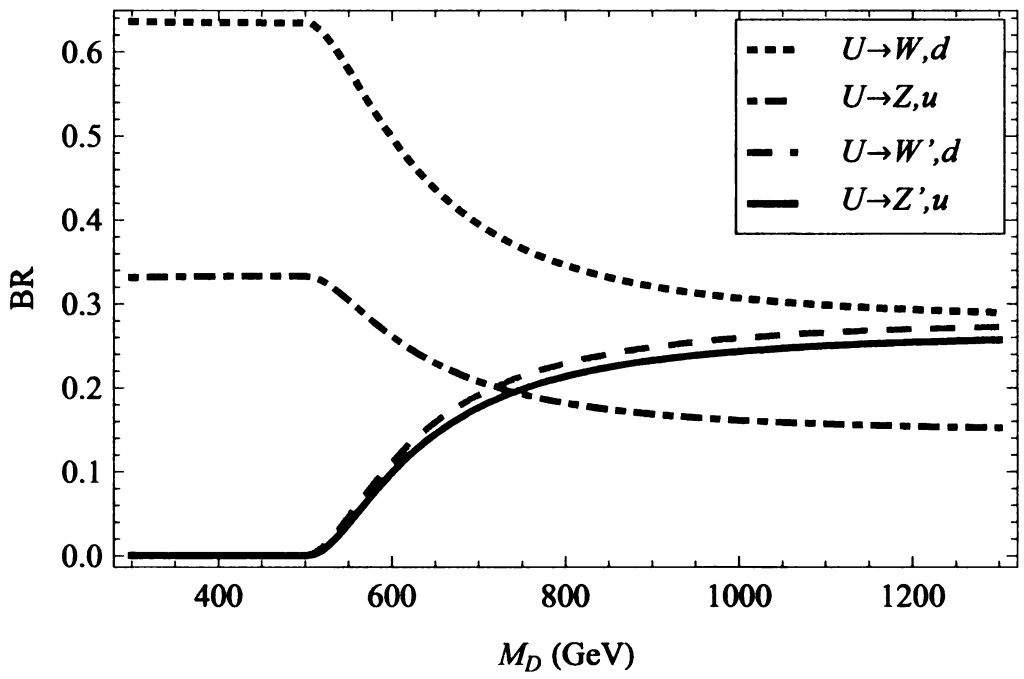

Figure 3.3: The plot of the branching ratio of the heavy quark into the charged and neutral gauge bosons. The masses of the W' and Z' gauge bosons were taken to be 500 GeV each.

3.6.2 Heavy quarks at the LHC

Our goal in this section is to analyze the possible discovery modes of the heavy quarks at the LHC. We will show that it is possible to discover them at 5σ level for a large range in the $M_{W'} - M_D$ parameter space. We will consider both the (QCD dominated) pair production and the (electroweak) single production of the heavy quarks. Each produced quark immediately decays to either a SM gauge boson plus a light quark (for $M_D < M_{W'}$) or a heavy gauge boson plus a light quark (for $M_D > M_{W'}$). We will consider the first possiblity in the pair production scenario (subsection 1) and the second in the single production analysis (subsection 2) and show that these cover much of the $M_D - M_{W'}$ parameter space. For our phenomenological analysis, we used the CalcHEP package [62].

Pair production: $pp \to Q\bar{Q} \to WZqq \to lll\nu jj$

We first consider the process $pp \to Q\bar{Q}$ at the LHC. Pair production of heavy quarks occurs via gluon fusion and quark annihilation processes (Figure 3.4). In Figure 3.5, we present the production cross section as a function of Dirac mass for a single flavor. We see that the cross-section for the gluon fusion process is higher than its counterpart for low values of M_D. However, as M_D increases, the $q\bar{q}$ channel starts to dominate. This is because the parton distribution function (pdf) of the gluon falls rapidly with increasing parton momentum fraction, x.

Each heavy quark decays to a vector boson and a light fermion. For $M_D < M_{W',Z'}$, the decay is purely to the standard model gauge bosons. The decay to heavy gauge bosons opens up for $M_D > M_{W',Z'}$, and we will analyze this channel while discussing single production of heavy fermions in the next subsection. Here, we look at the signal in the case where one of the heavy quarks decays to a Z and the other decays to a W, with the gauge bosons subsequently decaying leptonically. Thus, the final state is $pp \to Q\bar{Q} \to lll\nu jj$.

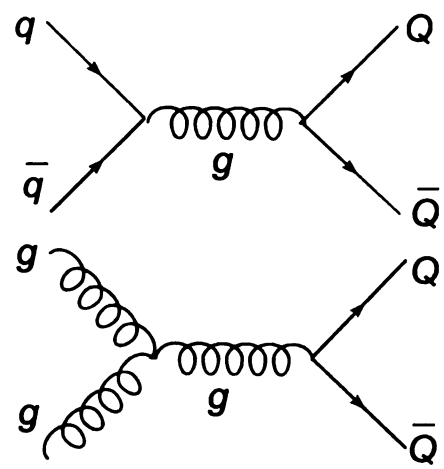

Figure 3.4: (a). Pair production of the heavy quarks occurs through $\bar{q}q$ annihilation and gluon fusion.

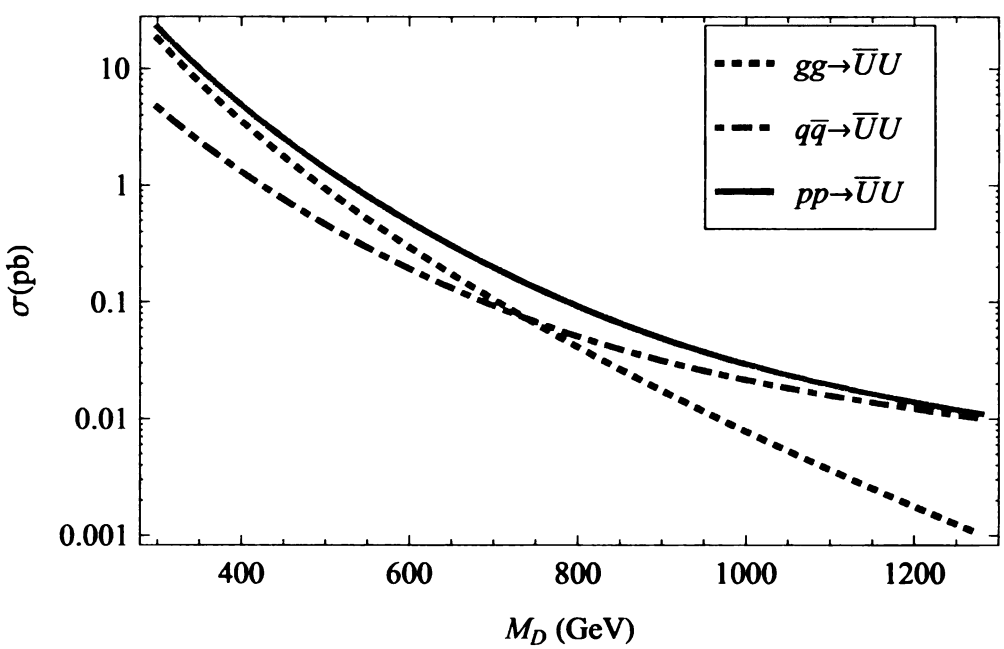

Figure 3.5: The cross section for pair production (for one flavor) as a function of the Dirac mass. As can be seen from the figure, for low values of M_D, the cross section for the gluon fusion channel is higher than the quark annihilation process. As M_D increases, the quark annihilation process becomes equally important because the pdf of the gluon falls rapidly with increasing parton momentum fraction, x.

To enhance the signal to background ratio, we have imposed a variety of cuts. We note that the the two jets in the signal should have a high p_T ($\sim M_D/2$), since they each come from the 2-body decay of a very heavy fermion. Thus, imposing strong p_T cuts on the outgoing jets can eliminate much of the SM background without affecting the signal too much. We also expect the η distribution of the jets to be largely central (see Figure 3.6), which suggests an η cut: $|\eta| \leq 2.5$. Lastly, we will impose a separation cut on the jets to avoid IR divergences in our computations.

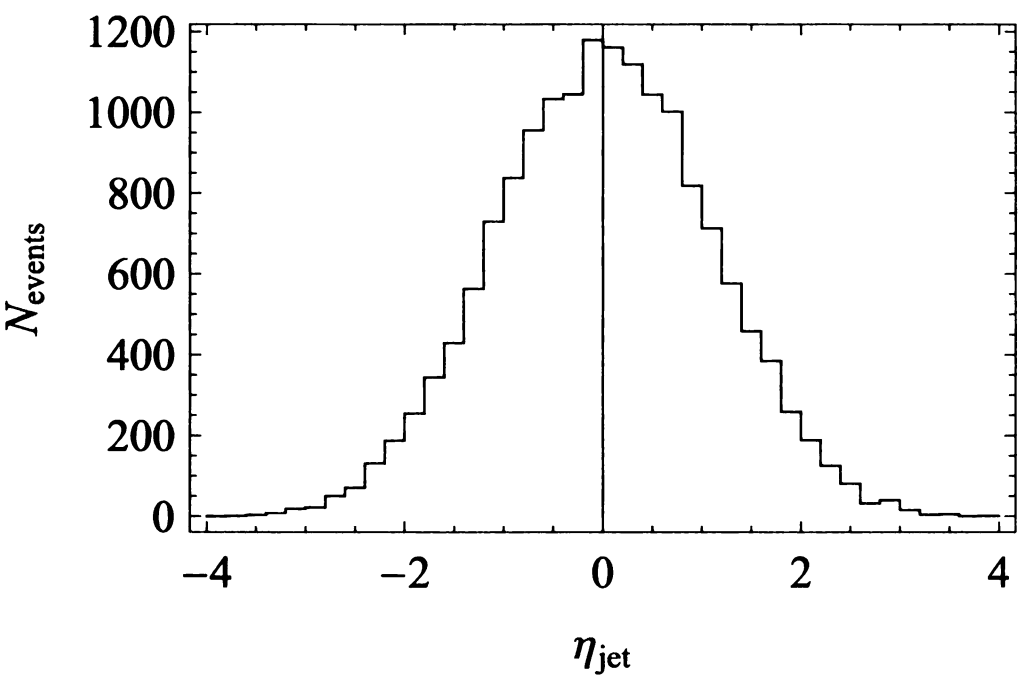

Figure 3.6: The η distribution of the outgoing hard jets for the process $pp \to Q\bar{Q} \to WZqq \to lll\nu jj$, corresponding to $M_D = 700$ GeV and $M_{W'} = 500$ GeV for a luminosity of 100 fb^{-1}. One can see that the events are in the central region: $-2.5 < \eta < 2.5$. The slight asymmetry in the shape of the curve is because we add the distributions corresponding to the jets from both the Q and the $\bar{Q}$ decays.

We also impose p_T cuts on the leptons and missing energy (Table 3.3). In reconstructing the heavy fermion mass, we have a choice between reconstructing the Q and the $\bar{Q}$. We let one of them decay to W, j and the other to Z, j with the $W's$ and

Kinematic variable	Cuts
p_T(jets)	>100 GeV
p_T(leptons)	>15 GeV
$\|\Delta R\|$(jets)	$\geq$0.4
Missing E_T	>15 GeV
$\|\eta_{jets}\|$	$\leq$ 2.5
M_{ll}	89 GeV< M_{ll} < 93 GeV

Table 3.1: The complete set of cuts employed to enhance the signal to background ratio in the process $pp \rightarrow Q\bar{Q} \rightarrow WZqq \rightarrow lll\nu jj$.

$Z's$ further decaying to leptons. Since the leptonic decay of W involves neutrinos, it is more conveniant to use the $Z.j$ combination (to avoid the two fold ambiguity in determing momenta when one uses neutrinos). One could simply identify the leptons that came out of the Z and construct the invariant mass of the lepton pair with the outgoing jet. Thus, we will impose the cut $(M_Z - 2)\text{GeV} < M_{ll} < (M_Z + 2)\text{GeV}$. We present the complete set of cuts in Table 3.3.

When generating the signal events, we included 4 flavors of heavy quarks. We do not consider the heavy top and bottom in this analysis. Including them would further enhance the signal, but since the top quark couples to the uneaten top pions, the branching ratios to gauge bosons would be different from that of the heavy partners of the first two generations. In Figure 3.6, we present the invariant mass distribution (of jet +2 leptons) for two different values of M_D (with $M_{W'}$= 500 GeV) with the cuts (Table 3.3) imposed. Since one cannot distinguish between the jets from the Q and $\bar{Q}$ decays, we added the distributions corresponding to each jet, i.e., the invariant mass distribution was constructed by identifying the leptons from the decay of the Z and combining that with both jets separately and adding the two distributions. This enhances the number of signal events, but also creates the small off-peak events in the distributions (Figure 3.6). We checked that for the M_D values we are interested in, these off-peak events are not big enough to compete with the signal. This can be directly seen from Figure 3.6 - the fluctuation around the signal peaks is just too

small to overwhelm the signal.

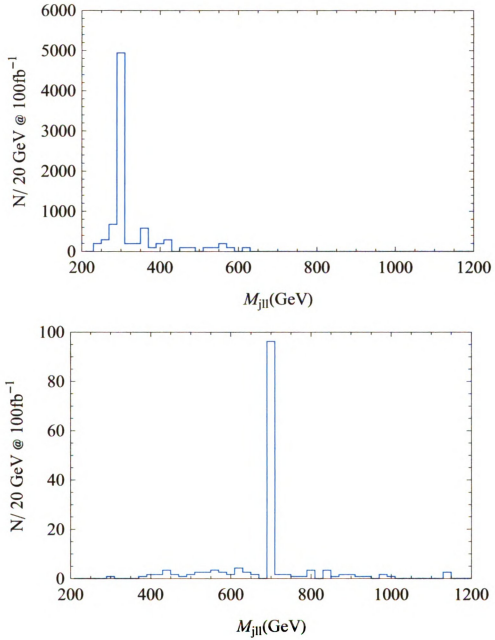

Figure 3.7: Predicted signal invariant mass distributions M_{llj} for $M_D = 300$ GeV and $M_D = 700$ GeV for a fixed $M_{W'} = 500$ GeV. The small off peak events arise because we added the distributions corresponding to the jets from both Q and $\bar{Q}$ decays.

In each of the plots, the signal distribution is clearly seen to peak at the value of M_D. We estimate the size of the peak by counting the signal events in the invariant mass window:

$$(M_D - 10)\text{GeV} < M_{jll} < (M_D + 10)\text{GeV}. \tag{3.82}$$

To analyze the SM background, we fully calculated the irreducible $pp \to ZWjj$ process and subsequently decayed the W and Z leptonically. Once we imposed all the cuts discussed above on the final state $lll\nu jj$, we find that the cuts entirely eliminate the background for the range of M_D values of interest to us. The most effective cut for reducing the SM background is the strong p_T cut imposed on both the jets.

We find there is an appreciable number of signal events in the region of parameter space where $Q \to Vq$ decays are allowed but $Q \to V'q$ decays are kinematically forbidden. The precise number is controlled by the branching ratio of the heavy fermion into the standard model vector bosons. In Fig 3.8, we present a contour plot of the number of expected events in the $M_D - M_{W'}$ plane for a fixed luminosity of 100 fb^{-1}.

Since the SM background is negligible, we can take 10 events to represent a 5σ discovery (this is the minimum number of events required to report discovery). Thus, we see that this process spans almost the entire parameter space. However, as may be seen from Figure 3.8, the region where $M_D \geq 900$ GeV and $M_{W'} \leq M_D$ will not yield enough signal events for the discovery of the heavy quark. In order to explore this region, we will now investigate the single production channel where the heavy quark decays to a heavy gauge boson.

Single production: $pp \to Qq \to W'qq' \to WZqq'$

The single production channel of heavy fermions is electroweak in nature, in contrast to pair production where gluon fusion is important. But the smaller cross sections

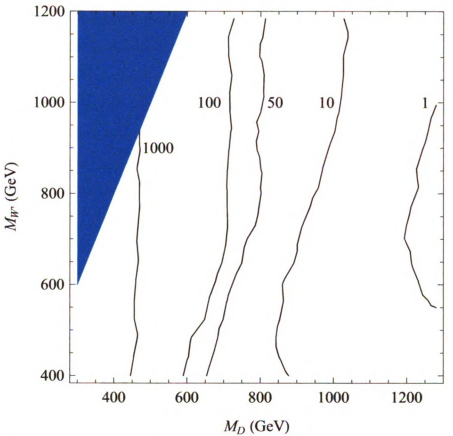

Figure 3.8: Contour plot of number of events in the pair production case for a fixed integrated luminosity of 100 fb^{-1}. The shaded region corresponds to $M_{W'} > 2M_D$ and is non perturbative and is excluded from our analysis, as discussed in the beginning of this section.

can be compensated if we exploit the fact that the u and d are valence quarks, and hence their parton distribution functions do not fall as sharply as the gluon's for large x (parton momentum fraction). Also, there is less phase space suppression in the single production channel than in the pair production case. Thus, we analyze the processes $[u, u \to u, U]$, $[d, d \to d, D]$ and $[u, d \to u, D]$. These occur through a t channel exchange of Z and Z' (Figure 3.8). In Figure 3.9, we show the cross section for the single production of one flavor of the heavy quark as a function of the Dirac mass. Since we want to look at the region of parameter space where $M_{W'}$ is smaller

than M_D, we let the heavy quark decay to a W'. (One can also consider decays to Z'. The only (small) difference would be that the Z' does not decay to a pair of W's 100% of the time - the ideal fermion delocalization condition only makes the T_3 coupling of the Z to SM fermions zero, but there is a small non zero hypercharge coupling proportional to x). The W' decays 100% of the time to a W and Z, because its coupling to two SM fermions is zero in the limit of ideal fermion delocalization (see Eqn.(3.39)). We constrain both the Z and W to decay leptonically so the final state is $lll jj \not{E}_T$.

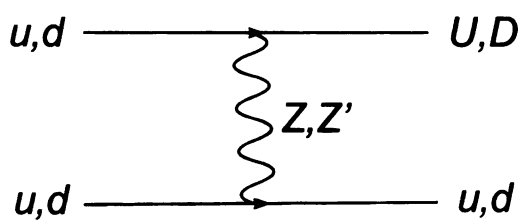

Figure 3.9: Feynman diagram for the t channel single production of the heavy fermion via the exchange of the Z and the Z' bosons.

As in the case of pair production, we expect the jet from the decay of the heavy quark to have a large p_T, and hence we will impose a strong p_T cut on the hard jet. Also, as before, this jet is going to be largely in the central direction and hence one can impose the same η cut (Table 3.3) on the hard jet. We also impose the same p_T cuts on the leptons and missing energy as in Table 3.3. Also, we expect the η distribution of the soft jet to be in the forward region, $2 < |\eta| < 4$. And finally, we impose a separation cut, ΔR, on the outgoing jets. We present the complete set of cuts in Table 3.4.

The leptonic W decay introduces the usual two fold ambiguity in determining the neutrino momentum and hence, we did a transverse mass analysis of the process,

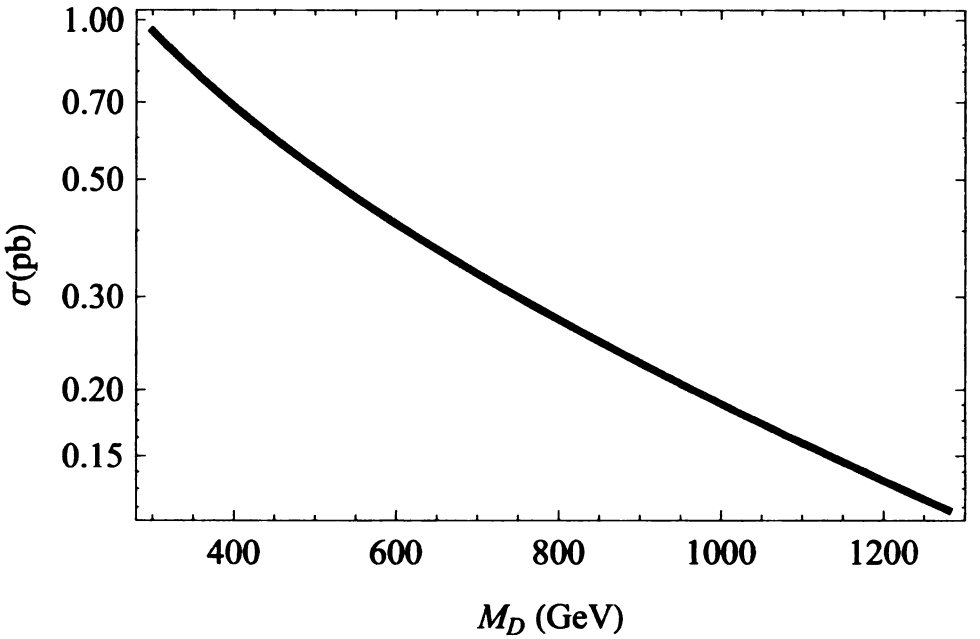

Figure 3.10: Cross section for the t channel single production of the heavy fermion as a function of the Dirac mass M_D. It is seen to fall more gradually as compared to that of the pair production case.

defining the transverse mass variable of interest as:

$$M_T^2 = \left(\sqrt{M^2(lllj) + p_T^2(lllj)} + |p_T(miss)|\right)^2 - |\overrightarrow{p_T}(lllj) + \overrightarrow{p}_T(miss)|^2 \quad (3.83)$$

The signal to background ratio increases appreciable after applying the transverse mass cut. We expect the distribution to fall sharply at M_D in the narrow width approximation, and indeed we find that there are typically few or no events beyond $M_D + 20$ GeV in the distributions. Thus, we have chosen the following cut on the transverse mass variable:

$$(M_D - 200)\text{GeV} < M_T < (M_D + 20)\text{GeV}. \quad (3.84)$$

In Figure 3.9, we show a few example transverse mass distributions of the signal with the cuts (Table 3.4) imposed. The distributions can be seen to fall off sharply

Kinematic variable	Cuts
p_T(hard jet)	>100 GeV
p_T(soft jet)	>15 GeV
p_T(leptons)	>15 GeV
$\|\Delta R\|$(jets)	$\geq$0.4
Missing E_T	>15 GeV
$\|\eta_{hardjet}\|$	$\leq$2.5
$\|\eta_{softjet}\|$	2< $\|\eta\|$ <4

Table 3.2: The complete set of cuts employed to enhance the signal to background ratio in the process $pp \rightarrow Qq \rightarrow W'q'q \rightarrow WZq'q \rightarrow lll\nu jj$.

at M_D.

We show a contour plot of the number of signal events for an intergrated luminosity of 100 fb^{-1} in Figure (3.12). It is seen that there are no events in the $M_D < M_{W'}$ region because we allow the heavy quarks to decay to W' and hence are considering only the region $M_D > M_{W'}$. Also, in the region of interest, one can see that there is an appreciable number of events.

The SM background for this process, $pp \rightarrow WZjj \rightarrow jjl\nu ll$, was calculated summing over the u, d, c, s and gluon jets and the first two families of leptons. Since we apply a stong p_T cut on only one of the jets (unlike in the pair production case), there is a non zero SM background. We show the SM transverse mass distribution in Figure 3.13.

The luminosity necessary for a 5 σ discovery can be calculated by requiring $(N_{signal}/\sqrt{N_{BG}}) \geq 5$, as per a Gaussian approximation to a Poisson distribution. It is instructive to look at the results of this analysis by combining it with the previous pair production case, as the two cover the $M_{W'} < M_D$ and $M_{W'} > M_D$ regions of the $M_{W'} - M_D$ parameter space respectively. Thus, we present a combined plot of the required luminosity for a 5 σ discovery of these heavy vector quarks at the LHC in Figure (3.14).

One can see that almost the entire parameter space is covered, with the pair and

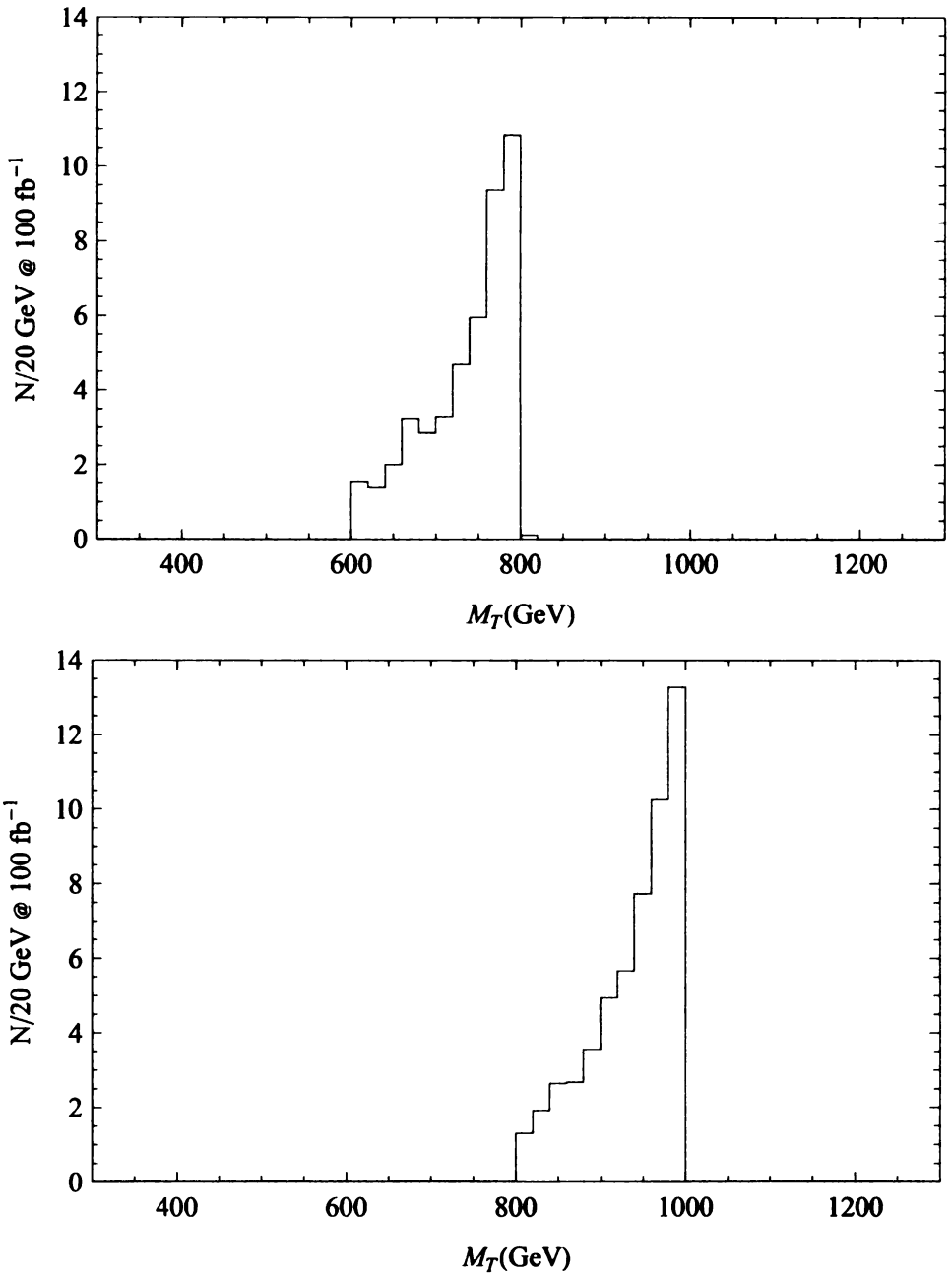

Figure 3.11: The transverse mass distribution for the single production of a heavy quark in the model, for M_D = 800 GeV and 1 TeV, for a fixed $M_{W'}$ = 500 GeV. It is seen that the signal falls sharply at M_D.

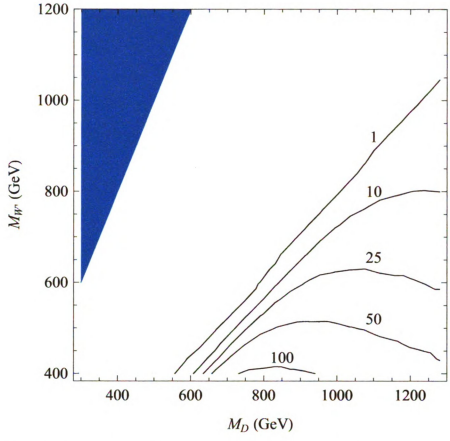

Figure 3.12: Contour plot of the number of signal events for the single production channel for an integrated luminosity of 100 fb^{-1}. The shaded region is where $M_{W'} > 2M_D$ and is non perturbative. One can see there is a considerable number of events in the low $M_{W'}$ region of the parameter space.

single production channels nicely complementing each other. Before we conclude, however, we would like to comment briefly on how our analysis compares with other models with vector quarks.

3.7 Related Vector Quark Models

There are other BSM theories that feature heavy quarks with vector-like couplings, as in the present model. In this section, we would like to briefly explain how our phe-

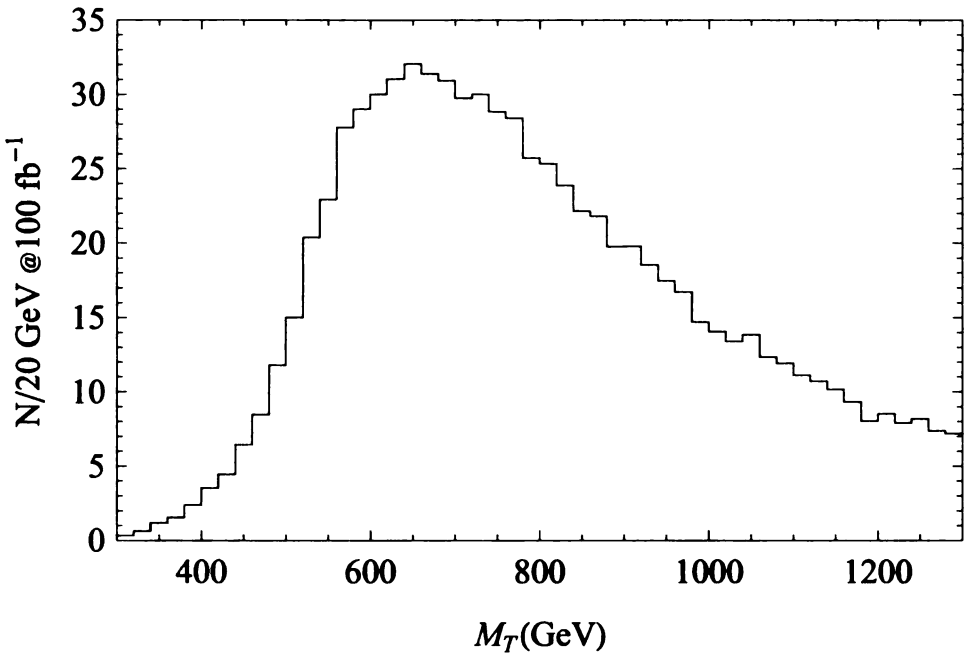

Figure 3.13: The SM background for the single production channel, $pp \to WZjj \to jjl\nu ll$, calculated by summing over the u, d, c, s and gluon jets and the first two families of leptons, and with the cuts in Table 3.4 imposed. The bin size is 20 GeV.

nomenological analysis compares with these. One important feature of deconstructed Higgsless models of the kind discussed in this paper is ideal fermion delocalization, which does not allow the heavy gauge bosons in the theory to couple to two standard model fermions. This constrains the W' to decay only to W and Z, thus providing a tool to distinguish this class of models from others. There are, however, certain features of this model that are generic, like the vector nature of the heavy quark couplings.

In the context of Little Higgs Models [63], there have been studies of the LHC phenomenology of the T-odd heavy quarks [64]. The cross sections for the production of heavy T-quark pairs are comparable to the ones in our study. However, in those models, the heavy T-quark necessarily decays to a heavy photon (due to constraints of conserving T parity). Also, in [65], the authors study the pair production of

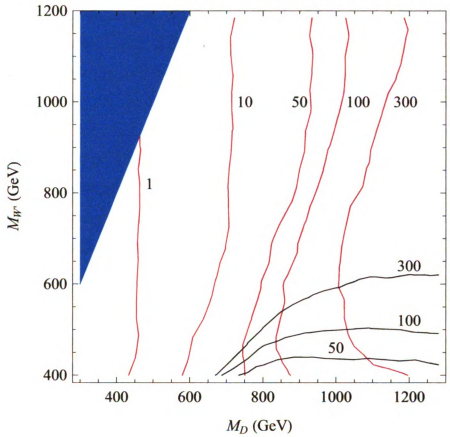

Figure 3.14: Luminosity required for a 5 σ discovery of the heavy vector fermions at the LHC in the single (blue) and pair (red) production channels. The shaded portion is non perturbative and not included in the study. It is seen that the two channels are complementary to one another and allow almost the entire region to be covered in 300 fb^{-1}.

heavy partners of the 1st and 2nd generation quarks in the context of the Littlest Higgs Models [66, 67, 68, 69, 70]. They consider decays exclusively to the heavy gauge bosons in the theory, which then decay to the standard model gauge bosons plus a heavy photon. Thus, the final state, though still $lljj\not{E}_T$, is kinematically different. In particular, strong cuts on the missing energy are now an important part of the analysis, because part of $\not{E}_T$ is due to the heavy photons. Ref.[71] presents a comprehensive study of the production and decay of heavy quarks by separating out the partners of the 3rd generation from the others and analyzing them separately. The authors let the heavy quark decay to a SM W boson and a light quark, but in their analysis, they neglect the mass of the W boson compared to its momentum (since it is highly boosted). Thus, when the W decays to a $l\nu$ pair, the direction of the neutrino momentum can be approximated to be parallel to that of the charged lepton, which enables them to recontruct the full neutrino momentum and create a invariant mass peak for the heavy quark (as opposed to a transverse mass analysis).

In the context of the three site model, the authors of [72] consider the single production of the heavy top quark. As mentioned before, the heavy top in this model is necessarily around a few TeV's and the paper concludes that the most viable scenario at the LHC is the subprocess $qb \rightarrow q'T \rightarrow q'Wb$ with the W decaying leptonically.

Ref. [73] presents a model independent analysis of the discovery prospects of heavy quarks at the Tevatron. The authors write down generic charged and neutral current interactions mixing the heavy and the light fermions and proceed to analyze both the pair and single production of these heavy quarks, with decays to the SM gauge bosons. Understandably, the Tevatron reach is much lower than that of the LHC.

3.8 Remarks

In this chapter, we presented a minimal extension of the three site model to lift the constraint that exists between getting the top quark mass right and having the ρ parameter under experimental bounds. This we did by separating the third generation quarks from the light ones, and having the top quark mass arise from the vev of a 'top Higgs'. This enabled us to have additional vector-like quarks in the model that are light enough to be discovered at the LHC, without affecting the tree level couplings of the three site model too much. We encoded the model in CalcHEP and analyzed the phenomenology of the heavy quarks. We first considered pair production ($pp \to Q\bar{Q} \to WZjj \to lll\nu jj$) of these heavy fermions. We found that the 5σ reach of the pair production channel was $\approx$ 1 TeV, but for high Dirac masses, this channel is viable only if the W' mass is in the TeV region also. This is because, in the $M_D > M_{W'}$ region, there is the possibility of heavy quark decay into W' and the signal is dominated by the branching ratio of the heavy quark into a W and light quark. The single production channel ($pp \to Qj \to W'jj \to WZjj \to lll\nu jj$) complements this nicely because we choose to decay the heavy quark to a W' and hence are necessarily in the region $M_{W'} < M_D$. By combining both these analyses, we were able to cover most of the $M_D - M_{W'}$ parameter space between $M_D \approx$ 300 GeV and $M_D \approx$ 1200 GeV. We conclude that the reach at the LHC for the vector quarks in this theory can be $\approx$ 1.3 TeV (for a 5σ discovery) for an appropriate choice of $M_{W'}$.

In doing the phenomenology, we have implicitly assumed that the value of the fermion mass M_D could be anything higher than the experimental lower bounds. But clearly, in low energy effective theories like the one discussed in this chapter, the masses of particles cannot be arbitrarily high, since the theory itself breaks down at some scale. Thus, it is interesting to see whether we can determine an *upper* bound

for the fermion mass scale. We will address this question in the next chapter.

Chapter 4

Unitarity and Bounds on the Scale of Fermion Mass Generation

The mechanism of electroweak symmetry breaking must give mass to two very different classes of particles: the electroweak gauge bosons and the fermions. In the standard model, the scalar Higgs doublet couples directly to both classes of particles. Moreover, the gauge and Yukawa couplings through which the Higgs interacts, respectively, with gauge bosons and fermions are proportional to the masses generated for those states when the scalar doublet acquires a vacuum expectation value. Nonetheless, in considering physics beyond the standard model, the possibility remains that the gauge boson and fermion masses are generated through different mechanisms. In particular, it is possible that electroweak symmetry breaking is transmitted to the fermions via some intermediary physics specifically associated with fermion mass generation. This Chapter is based on work published in [74].

Appelquist and Chanowitz [75] have shown (see also [76, 77]) that the tree-level, spin-0 scattering amplitude for fermion-anti-fermion pairs to scatter into longitudinally-polarized electroweak gauge bosons grows linearly with energy below the scale of the physics responsible for transmitting electroweak symmetry breaking to the fermions.

As the amplitude must be unitary, one can derive an *upper* bound on the scale of fermion mass generation by finding the energy at which the amplitude would grow to be of order 1/2 . The rate of energy growth is proportional to the mass of the fermions involved. The most stringent bound, therefore, arises from top-quark annihilation, and the bound on the scale of top-quark mass generation is found to be of order a few TeV.For light fermions, the scattering of fermions into many gauge-bosons yields a stronger result than the Appelquist-Chanowitz bound [78, 79]. For the top-quark, however, two-body final states yield the strongest bound.

As emphasized by Golden [77], the interpretation of the Appelquist-Chanowitz (AC) bound on the scale of top-quark mass generation can be problematic: longitudinal electroweak gauge-boson elastic scattering itself grows quadratically with energy [80, 81, 3, 4, 82] below the scale of the physics responsible for electroweak gauge-boson mass generation. As the scale of the physics responsible for electroweak symmetry breaking is also bounded by of order a TeV, it can be difficult to be sure that the violation of unitarity in fermion annihilation is truly independent of the violation of unitarity in the gauge-boson sector. The standard model illustrates this difficulty, as in that case the Higgs boson is responsible for restoring unitarity in *both* the fermion annihilation and gauge-boson scattering processes.

In this chapter, we will discuss unitarity violation and the resulting bounds on the scale of top-quark mass generation in the context of deconstructed Higgsless models. It is straightforward to generalize the three site model to an arbitrary number of sites [83]. In the continuum limit (the limit in which the number of sites goes to infinity), this model reproduces the five-dimensional model introduced in [51].

A fermion field in a general compactified five-dimensional theory gives rise to a tower of Kaluza-Klein (KK) modes, the lightest of which can (under chiral boundary conditions) be massless in the absence of electroweak symmetry breaking. The lightest states can therefore be identified with the ordinary fermions. The massive Kaluza-

Klein fermion modes are, however, massive Dirac fermions from the four-dimensional point of view. Correspondingly, the fermions in a deconstructed Higgsless model include both chiral and vector-like electroweak states [30, 83], and generation of the masses of the ordinary fermions in these models involves the mixing of the chiral and vector states [84, 50]. As we will demonstrate, the scale of top-quark mass generation in these models depends on the masses of the vector-like fermions (the "KK" modes), as well as on the number of sites in the deconstructed lattice.

What is particularly interesting about deconstructed Higgsless models, in this context, is that one *can* distinguish between the unitarity-derived bounds on the scales of gauge-boson and top-quark mass generation. We will demonstrate that, for an appropriate number of deconstructed lattice sites, spin-0 top-quark annihilation to longitudinally-polarized gauge-bosons remains unitary at tree-level up to energies much higher than the naive AC bound if the vector-like fermions are light. However the AC bound is reproduced as the mass of the vector-like fermion is increased. Therefore, for fixed top-quark and gauge-boson masses, the bound on the scale of fermion mass generation interpolates smoothly between the AC bound and one that can, potentially, be much higher as the mass of the vector-like fermion varies. The unitarity bounds on elastic scattering of longitudinal electroweak gauge bosons in Higgsless models [85], however, depend only on the masses of the gauge-boson KK modes. In this sense, the bound on the scale of fermion mass generation is *independent* of the bound on the scale of gauge-boson mass generation.

While our discussion is restricted to deconstructed Higgsless models, many models of dynamical electroweak symmetry breaking incorporate the mixing of chiral and vector fermions to accommodate top-quark mass generation. Examples include the top-quark seesaw model [86, 87, 88], and models in which the top mixes with composite fermions arising from a dynamical electroweak symmetry breaking sector [89, 90, 91]. Indeed, the fermion delocalization required to construct a realistic Higgs-

less model is naturally interpreted, in the context of AdS/CFT duality [19, 20, 21, 22], as mixing between fundamental and composite fermions [92]. As chiral-vector fermion mixing is the basic feature required for our results, we expect similar effects in these other models.

In the next section, to set notation and make contact with the literature, we reproduce [77] the Appelquist-Chanowitz bound in the electroweak chiral Lagrangian [93, 94, 95, 96, 97] - which may be interpreted as a "two-site" Higgsless model. In section three, we introduce the $n(+2)$ site Higgsless models that we will use for our calculations. Section four contains our calculations and primary results. The last section summarizes our findings.

4.1 The Appelquist-Chanowitz Bound

In the standard model (SM), the helicity non-conserving process $t_+\bar{t}_+ \to W_L^+W_L^-$ receives contributions at tree level from the diagrams in Figure 4.1.

We are interested in the behavior of the amplitude for large center of mass energy, $\sqrt{s} \gg M_W, m_t$. This allows us to expand the amplitude in the small parameters M_W^2/s and m_t^2/s. Practically, this means that we use the following leading order approximations. For the longitudinal polarization of the W gauge boson, we use

$$\varepsilon_{W_L}^{\mu} \simeq \frac{k_{W_L}^{\mu}}{M_W}, \tag{4.1}$$

where $k_{W_L}^{\mu}$ is the four-momentum of the corresponding boson. For the spinor chain in the s channel, we use

$$\bar{v}_+ (\not{k}_1 - \not{k}_2)(g_L P_L + g_R P_R) u_+ \simeq m_t \sqrt{s} \cos\theta (g_L + g_R) \tag{4.2}$$

$$\bar{v}_- (\not{k}_1 - \not{k}_2)(g_L P_L + g_R P_R) u_- \simeq -m_t \sqrt{s} \cos\theta (g_L + g_R) \ , \tag{4.3}$$

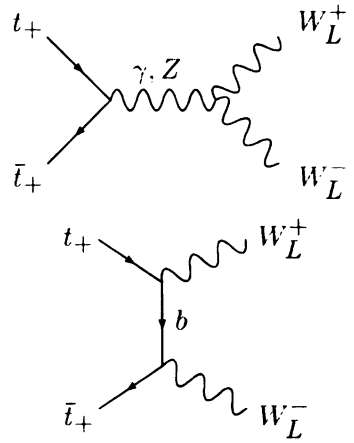

Figure 4.1: The diagrams that contribute to the process $t_+\bar{t}_+ \to W_L^+W_L^-$ in the Higgsless SM. There are analogous diagrams for the process $t_-\bar{t}_- \to W_L^+W_L^-$. Each diagram has an amplitude that grows linearly with $\sqrt{s}$ for all energies. However, most (but not all) of this linear $\sqrt{s}$ growth cancels when the diagrams are summed. The remaining piece that grows linearly with $\sqrt{s}$ comes from the t channel diagram, and it eventually surpasses the unitarity bound. In the SM, this unitarity violation is eliminated by the contribution of the Higgs in the s channel.

where k_1^μ and k_2^ν are the momenta of the outgoing bosons, and for the spinor chain in the t channel we find

$$\bar{v}_+ \not{k}_2 (\not{p}_1 - \not{k}_1) \not{k}_1 g_L P_L u_+ \simeq \frac{m_t t\sqrt{s}}{2} (1 + \cos\theta) g_L \tag{4.4}$$

$$\bar{v}_- \not{k}_2 (\not{p}_1 - \not{k}_1) \not{k}_1 g_L P_L u_- \simeq -\frac{m_t t\sqrt{s}}{2} (1 + \cos\theta) g_L \tag{4.5}$$

where

$$P_L = \frac{1}{2}(1 - \gamma_5) \tag{4.6}$$

$$P_R = \frac{1}{2}(1 + \gamma_5) \tag{4.7}$$

are chirality projection operators, and g_L and g_R are chiral electroweak coupling constants.

Since the $t\bar{t} \to W^+W^-$ amplitude is the same for each color and only differs

by a sign for the opposite helicity, we get the largest amplitude by considering the incoming state

$$|\psi\rangle = \frac{1}{\sqrt{6}}\Big(\quad |\bar{t}_{1+}t_{1+}\rangle + |\bar{t}_{2+}t_{2+}\rangle + |\bar{t}_{3+}t_{3+}\rangle \\ - |\bar{t}_{1-}t_{1-}\rangle - |\bar{t}_{2-}t_{2-}\rangle - |\bar{t}_{3-}t_{3-}\rangle \quad \Big) . \tag{4.8}$$

where the numerical subscripts (1,2, and 3) label the three different colors. The state we consider here differs from that chosen by [75], as we include both combinations of incoming helicities. This state allows us to derive a slightly stronger bound, *c.f.* Eqn (4.23). Putting the pieces together gives the scattering amplitude

$$\mathcal{M} = \frac{\sqrt{6}\, m_t \sqrt{s} \cos\theta}{2M_W^2} \times \left(2 g_{tt\gamma} g_{\gamma WW} + g_{LttZ} g_{ZWW} + g_{RttZ} g_{ZWW} - g_{LtbW}^2 \right) \\ + \frac{\sqrt{6}\, m_t \sqrt{s}}{2M_W^2} g_{LtbW}^2 . \tag{4.9}$$

for $\sqrt{s} \gg M_W, m_t$, where the electroweak couplings are given by:

$$g_{tt\gamma} = \frac{2}{3} e , \tag{4.10}$$

$$g_{\gamma WW} = e , \tag{4.11}$$

$$g_{LttZ} = \frac{e}{\sin\theta_W \cos\theta_W} \left(\frac{1}{2} - \frac{2}{3} \sin^2\theta_W \right) , \tag{4.12}$$

$$g_{RttZ} = \frac{e}{\sin\theta_W \cos\theta_W} \left(-\frac{2}{3} \sin^2\theta_W \right) , \tag{4.13}$$

$$g_{ZWW} = \frac{e \cos\theta_W}{\sin\theta_W} , \tag{4.14}$$

$$g_{LtbW} = \frac{e}{\sqrt{2} \sin\theta_W} . \tag{4.15}$$

Our expression here differs in the sign of the term proportional to g_{LtbW}^2 from that given in [75], and is correct for the top-quark which is the $T_3 = +1/2$ member of an electroweak doublet. The corresponding expression in [75], which is from [98, 99], is

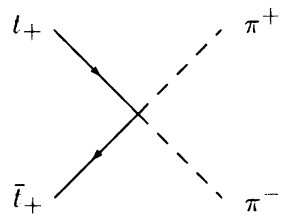

Figure 4.2: The diagram that contributes linear growth in $\sqrt{s}$ to the process $t_+\bar{t}_+ \to \pi^+\pi^-$ in the Higgsless SM, where we have used the equivalence theorem to replace the longitudinally polarized gauge-boson by the corresponding "eaten" Goldstone Bosons. There is an analogous diagram for the process $t_-\bar{t}_- \to \pi^+\pi^-$.

correct for the *lower* member of an electroweak doublet with $T_3 = -1/2$. With these couplings, we find the identity

$$2g_{tt\gamma}g_{\gamma WW} + g_{LttZ}g_{ZWW} + g_{RttZ}g_{ZWW} - g^2_{LtbW} = 0\,. \tag{4.16}$$

The remaining amplitude is, therefore,

$$\mathcal{M} = \frac{\sqrt{6}\,m_t\sqrt{s}}{2M_W^2}g^2_{LtbW}. \tag{4.17}$$

which grows linearly with $\sqrt{s}$ for $\sqrt{s} \gg M_W, m_t$. We note that since $g_{LtbW} = g/\sqrt{2}$ and $M_W = gv/2$, where g is the weak coupling and $v \simeq 246\,\mathrm{GeV}$ is the weak scale, our expression for M simplifies to [75]

$$\mathcal{M} = \frac{\sqrt{6}\,m_t\sqrt{s}}{v^2}\,. \tag{4.18}$$

We can check this result using the equivalence theorem [3, 100], where one replaces the longitudinal gauge-bosons by the corresponding "eaten" Nambu-Goldstone Bosons. In this limit, the only diagram that contributes to the $J = 0$ amplitude is shown in Figure 4.2. The leading order approximations

$$\bar{v}_+u_+ \simeq \sqrt{s} \qquad \bar{v}_-u_- \simeq -\sqrt{s}, \tag{4.19}$$

combined with the four point coupling

$$g_{tt\pi^+\pi^-} = \frac{m_t}{v^2}, \tag{4.20}$$

yield the same amplitude as in Eqn. (4.18)

$$\mathcal{M} = \frac{\sqrt{6}\, m_t \sqrt{s}}{v^2} \,. \tag{4.21}$$

Note that the potential s-channel contribution, illustrated in Figure 4.3, does *not* contribute in the $J = 0$ channel.

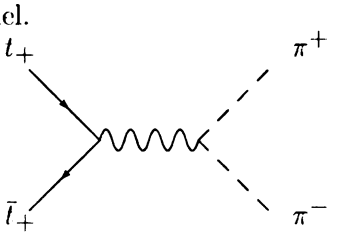

Figure 4.3: This diagram, corresponding to s-channel Z-boson exchange in the equivalence-theorem limit, *does not* contribute to the $J = 0$ partial wave scattering amplitude for the process $t_+\bar{t}_+ \to \pi^+\pi^-$ in the Higgsless SM.

The $J = 0$ partial wave is extracted from Eqn. (4.18) as

$$a_0 = \frac{1}{32\pi} \int_{-1}^{1} d\cos\theta \; \mathcal{M} = \frac{m_t \sqrt{6s}}{16\pi v^2} \tag{4.22}$$

To satisfy partial wave unitarity, this tree-level amplitude must be less than 1/2, the maximum value for the real part of any amplitude lying in the Argand circle. This produces the bound

$$\sqrt{s} \lesssim \frac{8\pi v^2}{m_t \sqrt{6}} \approx 3.5\,\text{TeV} \,. \tag{4.23}$$

Our result differs numerically from that given in [75], as we include both helicity channels in Eq. 4.8, and bound the amplitude by 1/2 rather than 1. One may obtain a slightly stronger upper bound by considering an isosinglet, spin-0, final state

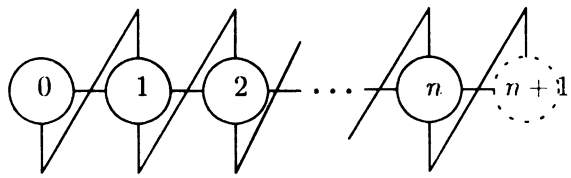

Figure 4.4: Moose [25] diagram of the $n(+2)$ site model. Each solid (dashed) circle represents an $SU(2)$ ($U(1)$) gauge group. Each horizontal line is a non-linear sigma model. Vertical lines are fermions, and diagonal lines represent Yukawa couplings.

($I = J = 0$) of gauge-bosons [76]. This amounts to a reduction in the value of the upper bound in Eqn. (4.23) by a factor of $\sqrt{2/3} \approx 0.8$.

4.2 The $n(+2)$ Site Deconstructed Higgsless Model

We will be studying the Higgsless model introduced in [83], denoted the $n(+2)$ site model. As we will discuss in subsection 4.2.1, the gauge sector is an $SU(2)^{n+1} \times U(1)$ extended electroweak group; the label n thus denotes how many extra $SU(2)$ groups the model contains relative to the Standard Model. The electroweak chiral lagrangian [93, 94, 95, 96, 97] can be obtained by setting $n = 0$ while the Higgsless Three Site Model [30], which has one extra $SU(2)$ group, can be obtained by setting $n = 1$. This model may be schematically represented by a "Moose" diagram [25] as shown in Figure 4.4. After discussing the gauge sector, we examine the fermion sector (subsection 4.2.2), the "eaten Nambu-Goldstone bosons" (subsection 4.2.3) and then the couplings that are relevant to our calculation of $t\bar{t} \to W^+W^-$.

4.2.1 Gauge Boson Sector

The gauge group of the $n(+2)$ site model, as illustrated in Figure 4.4, is

$$G = SU(2)_0 \times \prod_{j=1}^{n} SU(2)_j \times U(1)_{n+1} \tag{4.24}$$

where $SU(2)_0$ is represented by the leftmost circle and has coupling g; the gauge groups $SU(2)_j$ are represented consecutively by the internal circles and have a common coupling $\tilde{g}$. Common couplings for the "internal" $SU(2)$ groups corresponds to a continuum model with spatially independent gauge-coupling [51]. Qualitatively, our results do not depend on this assumption and should apply in any case in which the mass of the W-boson is much less than that of the first gauge-boson KK mode. The $U(1)_{n+1}$ is represented by the dashed circle at the far right and has coupling g'. The coupling $\tilde{g}$ is taken to be much larger than g, so we expand in the small quantity

$$x = \frac{g}{\tilde{g}}. \tag{4.25}$$

We also find it convenient to define the parameters

$$t = \frac{g'}{g} = \frac{s}{c} \tag{4.26}$$

where $s^2 + c^2 = 1$. In the continuum limit, $n \to \infty$, this model reduces to the one described in [51].

The horizontal bars in Figure 4.4 represent nonlinear sigma models Σ_j which break the gauge symmetry down to electromagnetism

$$G \longrightarrow U(1)_{EM} \tag{4.27}$$

giving mass to the other $3(n+1)$ gauge bosons. To leading order, the effective Lagrangian for these fields is

$$\mathcal{L}_{D\Sigma} = \frac{f^2}{4}\mathrm{Tr}\left[\sum_j \left(D_\mu \Sigma_j\right)^\dagger D^\mu \Sigma_j\right] \tag{4.28}$$

where

$$D_\mu \Sigma_j = \partial_\mu \Sigma_j + i g_j W_{j,\mu} \Sigma_j - i g_{j+1} \Sigma_j W_{j+1,\mu} \tag{4.29}$$

with $g_0 = g$, $g_j = \tilde{g}$ and $g_{n+1} = g'$. The nonlinear sigma model fields may be written

$$\Sigma_j = e^{i 2\pi_j / f} \ , \tag{4.30}$$

in terms of the Goldstone bosons (π_j) which become the longitudinal components of the massive gauge bosons. The π_j and W_j are written in matrix form and are

$$\pi_j = \begin{pmatrix} \frac{1}{2}\pi_j^0 & \frac{1}{\sqrt{2}}\pi_j^+ \\ \frac{1}{\sqrt{2}}\pi_j^- & -\frac{1}{2}\pi_j^0 \end{pmatrix} \ . \tag{4.31}$$

$$W_{j,\mu} = \begin{pmatrix} \frac{1}{2}W_{j,\mu}^0 & \frac{1}{\sqrt{2}}W_{j,\mu}^+ \\ \frac{1}{\sqrt{2}}W_{j,\mu}^- & -\frac{1}{2}W_{j,\mu}^0 \end{pmatrix} \tag{4.32}$$

$$W_{n+1,\mu} = \begin{pmatrix} \frac{1}{2}W_{n+1,\mu}^0 & 0 \\ 0 & -\frac{1}{2}W_{n+1,\mu}^0 \end{pmatrix} \tag{4.33}$$

The mass matrices of the gauge bosons can be obtained by going to unitary gauge ($\Sigma_j \to 1$). For the neutral gauge bosons, we find

$$M_n^2 = \frac{\tilde{g}^2 f^2}{4} \begin{pmatrix} x^2 & -x & 0 & 0 & \cdot & 0 & 0 \\ -x & 2 & -1 & 0 & \cdot & 0 & 0 \\ 0 & -1 & 2 & -1 & \cdot & 0 & 0 \\ \cdot & \cdot & \cdot & \cdot & \cdot & -1 & 0 \\ 0 & 0 & 0 & \cdot & -1 & 2 & -xt \\ 0 & 0 & 0 & \cdot & 0 & -xt & x^2 t^2 \end{pmatrix} \tag{4.34}$$

while the matrix $M_\pm^2$ for the charged gauge bosons is M_n^2 with the last row and

column removed.

The photon is massless and given by the wavefunction

$$v_\gamma = \frac{e}{\tilde{g}}\left(\frac{1}{x}, 1, \cdots, 1, \frac{1}{xt}\right) \tag{4.35}$$

where

$$\frac{1}{e^2} = \frac{1}{g^2} + \frac{n}{\tilde{g}^2} + \frac{1}{g'^2}. \tag{4.36}$$

After diagonalizing the gauge boson mass matrices, we find that the other masses and wavefunctions are given, at leading order in x, by the following expressions. The mass and wavefunction of the light W boson are

$$M_{W0} = \frac{\tilde{g} f x}{2\sqrt{(n+1)}} \tag{4.37}$$

$$v^0_{W0} = 1 \tag{4.38}$$

$$v^j_{W0} = \frac{n-j+1}{n+1}x \tag{4.39}$$

where the superscript 0 refers to the left-most $SU(2)$ group on the moose while the superscript $j = [1...n]$ refers to the $SU(2)$ gauge groups on the interior of the moose. The masses and wavefunctions of the charged KK modes are

$$M_{Wk} = \frac{\tilde{g} f}{\sqrt{2}}\sqrt{1 - \cos\left[\frac{k\pi}{n+1}\right]} \tag{4.40}$$

$$v^0_{Wk} = \frac{-x}{\sqrt{2(n+1)}}\cot\left[\frac{k\pi}{2(n+1)}\right] \tag{4.41}$$

$$v^j_{W_k} = \sqrt{\frac{2}{n+1}}\sin\left[\frac{jk\pi}{n+1}\right]. \tag{4.42}$$

Likewise, the mass and wavefunction of the light Z boson are

$$M_{Z0} = \frac{\tilde{g} f x}{2c\sqrt{(n+1)}} \tag{4.43}$$

$$v^0_{Z0} = c \tag{4.44}$$

$$v^j_{Z0} = \frac{c(n+1) - j/c}{n+1} x \tag{4.45}$$

$$v^{n+1}_{Z0} = -s, \tag{4.46}$$

where superscript $n+1$ refers to the $U(1)$ group. The masses and wavefunctions of the neutral KK modes are

$$M_{Zk} = \frac{\tilde{g} f}{\sqrt{2}} \sqrt{1 - \cos\left[\frac{k\pi}{n+1}\right]} = M_{Wk} \tag{4.47}$$

$$v^0_{Zk} = \frac{-x}{\sqrt{2(n+1)}} \cot\left[\frac{k\pi}{2(n+1)}\right] \tag{4.48}$$

$$v^j_{Zk} = \sqrt{\frac{2}{n+1}} \sin\left[\frac{jk\pi}{n+1}\right] \tag{4.49}$$

$$v^{n+1}_{Zk} = \sqrt{\frac{2}{n+1}} \frac{(-1)^k x}{t} \left[(n+1)a_1 + b_1\right] \tag{4.50}$$

$$a_1 = \frac{(-1)^k}{4(n+1)} \csc^2\left[\frac{k\pi}{2(n+1)}\right] \times \left[(-1)^k \sin\left(\frac{k\pi}{n+1}\right) - t^2 \sin\left(\frac{kn\pi}{n+1}\right)\right] \tag{4.51}$$

$$b_1 = \frac{-1}{2} \cot\left[\frac{k\pi}{2(n+1)}\right]. \tag{4.52}$$

We note that the W gauge boson mass is given by

$$M_W = M_{W0} \equiv \frac{gf}{2\sqrt{n+1}} = \frac{gv}{2}, \tag{4.53}$$

and, hence, we have the relation

$$f = \sqrt{n+1}\, v. \tag{4.54}$$

The ratio of the W and Z mass is

$$\frac{M_W}{M_Z} = \frac{M_{W0}}{M_{Z0}} = \frac{1}{c} \tag{4.55}$$

identifying c with $\cos\theta_W$ at leading order in x.

The ratio of M_W to the mass of the first KK mode M_{W_1} is

$$\frac{M_W}{M_{W_1}} = \frac{x}{\sqrt{2(n+1)\left(1-\cos\left[\frac{\pi}{n+1}\right]\right)}} \tag{4.56}$$

which relates x to the mass ratio M_W/M_{W_1} for a given n at leading order. From this we see that expansion in x is justified as long as $M_{W_1} \gg M_W$.

4.2.2 Fermion Sector

The vertical lines in Figure 4.4 represent the fermionic fields in the theory. The vertical lines below the circles represent the left chiral fermions while the vertical lines above the circles are the right chiral fermions. Each fermion is in a fundamental representation of the gauge group to which it is attached and a singlet under all the other gauge groups except $U(1)_{n+1}$. The charges under $U(1)_{n+1}$ are as follows: If the fermion is attached to an $SU(2)$ then its charge is 1/3 for quarks and -1 for leptons. If the fermion is attached to $U(1)_{n+1}$ its charge is twice its electromagnetic charge: 0 for neutrinos, -2 for charged leptons, 4/3 for up type quarks and $-2/3$ for down type quarks.

The fermion mass terms can be written down by extending the one for the three site model. Eqn. 2.2, to include n bulk terms.

$$\begin{aligned}\mathcal{L}_{\psi\Sigma} &= -M_F\Big[\varepsilon_L\bar{\psi}_{L0}\Sigma_0\psi_{R1} - \sum_j \bar{\psi}_{Lj}\psi_{Rj} \\ &+ \sum_j \bar{\psi}_{Lj}\Sigma_j\psi_{R,j+1} + \bar{\psi}_{Ln}\varepsilon_R\Sigma_n\psi_{R,n+1} + h.c.\Big]\end{aligned} \tag{4.57}$$

where the value of ε_L is the same for all fermions, while ε_R is a diagonal matrix which distinguishes flavors [30, 83]. For example for the top and bottom quark we have

$$\varepsilon_R = \begin{pmatrix} \varepsilon_{Rt} & 0 \\ 0 & \varepsilon_{Rb} \end{pmatrix} \tag{4.58}$$

The fermion mass matrix can be diagonalized by performing unitary transformations on the left- and right-handed fermions separately. To leading order in $\varepsilon_{L,R}$ we find the following masses and wavefunctions for the lightest fermion, F_0, in a given tower (which we associate with an ordinary standard model fermion)

$$M_{F_0} = M_F\varepsilon_L\varepsilon_{R_f} \tag{4.59}$$

$$v^0_{LF_0} = 1 \tag{4.60}$$

$$v^j_{LF_0} = \varepsilon_L \tag{4.61}$$

$$v^j_{RF_0} = \varepsilon_{R_f} \tag{4.62}$$

$$v^{n+1}_{RF_0} = 1 \tag{4.63}$$

while the expressions for the heavier states, F_k, are

$$M_{F_k} = 2M_F \cos\left[\frac{(n-k+1)\pi}{2n+1}\right] \tag{4.64}$$

$$v^0_{LF_k} = \frac{\varepsilon_L}{\sqrt{2n+1}} \tan\left[\frac{(n-k+1)\pi}{2n+1}\right] \tag{4.65}$$

$$v^j_{LF_k} = \frac{2(-1)^j}{\sqrt{2n+1}} \sin\left[\frac{2j(n-k+1)\pi}{2n+1}\right] \tag{4.66}$$

$$v^j_{RF_k} = \frac{(-1)^{n+k+j+1}2}{\sqrt{2n+1}} \sin\left[\frac{2(n-j+1)(n-k+1)\pi}{2n+1}\right] \tag{4.67}$$

$$v^{n+1}_{RF_k} = \frac{(-1)^k \varepsilon_{R_f}}{\sqrt{2n+1}} \tan\left[\frac{(n-k+1)\pi}{2n+1}\right] \tag{4.68}$$

For small ε_L, we see that the left-handed component of the lightest fermion in each tower is primarily located at site 0 – and the flavor-universal factor ε_L controls the amount of fermion "delocalization" along the moose. Likewise, the right-handed component is primarily located at site $n+1$, and the flavor-dependent quantities ε_{R_f} control the degree of delocalization. Since the amplitude for $t\bar{t} \to W^+W^-$ scattering will depend on the values of ε_L and ε_{R_t}, we need to evaluate these quantities; we will start with ε_L and then use it to constrain ε_{R_t}.

Precision electroweak corrections provide a useful source of constraints on the parameters of Higgsless models. While custodial symmetry generally keeps the tree-level value of $\Delta\rho = \alpha T$ sufficiently small, satisfying the bounds on S at tree level requires some degree of fermion delocalization [101, 102, 84, 50, 51, 26, 103, 49]. We will implement ideal fermion delocalization exactly as in chapter 2, i.e., by demanding that the tree-level value of $g_{We\nu}$ equal the SM value. An explicit calculation of $g_{We\nu}$ in this model, which requires expanding the wavefunctions, masses, and couplings to order ε_L^2 and order x^2, yields

$$g_{We\nu_n} = g_{We\nu_{SM}} \left(1 + \frac{n(n+2)}{6(n+1)} x^2 - \frac{n}{2}\varepsilon_L^2\right). \tag{4.69}$$

Therefore, the condition

$$\varepsilon_L^2 = \frac{n+2}{3(n+1)} x^2 \tag{4.70}$$

causes S to vanish at tree-level. Using Eqn. (4.56) this is equivalent to

$$\varepsilon_L^2 = \frac{2}{3}(n+2)\left(1 - \cos\left[\frac{\pi}{n+1}\right]\right)\frac{M_W^2}{M_{W_1}^2}, \tag{4.71}$$

in terms of physical masses. Here again, note that ε_L is small so long as $M_W \ll M_{W_1}$.

Finally, the parameter ε_{R_f} can be determined by taking the ratio of the masses of the light fermion and the first KK mode.

$$\frac{M_{F_0}}{M_{F_1}} = \frac{\varepsilon_L \varepsilon_{R_f}}{2\cos\left[\frac{n\pi}{2n+1}\right]} \tag{4.72}$$

Since we know ε_L, this gives a prediction for ε_{R_f} in terms of physical masses

$$\varepsilon_{R_f} = \frac{\sqrt{6}\cos\left[\frac{n\pi}{2n+1}\right]}{\sqrt{(n+2)\left(1 - \cos\left[\frac{\pi}{n+1}\right]\right)}} \frac{M_{F_0}}{M_{F_1}} \frac{M_{W_1}}{M_W}. \tag{4.73}$$

For all flavors except the top quark, this parameter is tiny; at leading order, we therefore set $\varepsilon_{R_f} = 0$ for all the light fermions. The size of ε_{R_t} affects $\Delta\rho$ at one loop; comparison of the experimental bounds on $\Delta\rho$ with the value calculated in Higgsless models [30, 83] shows that ε_{R_t} must also be relatively small. In what follows, we therefore keep only the leading terms in ε_{R_t}.

4.2.3 Goldstone Boson Sector

We will perform the computation of the process $t_+\bar{t}_+ \to W_L^+ W_L^-$ in the $n(+2)$ site model using the equivalence theorem. We must, therefore, determine the wavefunction of the Goldstone bosons associated with (eaten by) the massive gauge bosons. This is determined by the mixing between the two given in Eqn. (4.28). To find the mixing, we expand the nonlinear sigma-model field Σ_j and keep the terms linear in both the gauge bosons (W_j) and the Goldstone bosons (π_j). After these manipulations, Eqn. (4.28) becomes

$$\begin{aligned}\mathcal{L}_{\pi W} = -i\frac{\tilde{g}f}{2}\Bigg[& \left\{\partial_\mu \pi_0 \ , \ x\, W_0^\mu - W_1^\mu\right\} \\ & + \sum_{j=1}^{n-1}\left\{\partial_\mu \pi_j \ , \ W_j^\mu - W_{j+1}^\mu\right\} \\ & + \left\{\partial_\mu \pi_n \ , \ W_n^\mu - xt\, W_{n+1}^\mu\right\} \Bigg]\end{aligned} \tag{4.74}$$

from which we may read off the wavefunctions for the charged Goldstone bosons as

$$v_{\pi_k^\pm}^{[0]} = \frac{1}{N_{\pi_k^+}}\left(x\, v_{W_k}^0 - v_{W_k}^1\right) \tag{4.75}$$

$$v_{\pi_k^\pm}^{[j]} = \frac{1}{N_{\pi_k^\pm}}\left(v_{W_k}^j - v_{W_k}^{j+1}\right) \tag{4.76}$$

$$v_{\pi_k^\pm}^{[n]} = \frac{1}{N_{\pi_k^\pm}}\, v_{W_k}^n \tag{4.77}$$

where the N_{π_k} are normalization factors. Note that Nambu-Goldstone boson components are associated with the links rather than the gauge groups: the superscript [0] refers to the left-most link, the superscript [n] refers to the right-most link, and the superscripts [j] range from 1 through n-1 and denote the interior links of the Moose.

The wavefunctions for the neutral Goldstone bosons are similar

$$v^{[0]}_{\pi^0_k} = \frac{1}{N_{\pi^0_k}}\left(x\, v^0_{Z_k} - v^1_{Z_k}\right) \tag{4.78}$$

$$v^{[j]}_{\pi^0_k} = \frac{1}{N_{\pi^0_k}}\left(v^j_{Z_k} - v^{j+1}_{Z_k}\right) \tag{4.79}$$

$$v^{[n]}_{\pi^0_k} = \frac{1}{N_{\pi^0_k}}\left(v^n_{Z_k} - xt\, v^{n+1}_{Z_k}\right) \ . \tag{4.80}$$

but note that $v^{[n]}_{\pi^0_k}$ includes a contribution from the Z_k wavefunction on the $U(1)$ site.

These wavefunctions are particularly simple for the lightest modes, the W and Z: they are flat

$$v^{[l]}_{\pi^+_0} = \frac{1}{\sqrt{n+1}} = v^{[l]}_{\pi^0_0} \tag{4.81}$$

with the same value on all links $[l = 0...n]$ of the Moose.

4.2.4 Couplings

To obtain the couplings of the Goldstone bosons to the fermions, we start from Eqn. (4.58), expand the nonlinear sigma-model fields, and plug in the eigenmode wavefunctions we have just derived. Doing this, we find

$$\begin{aligned} g_{LtF_k\pi} &= -i\frac{\sqrt{2}M_F}{f}\left[\varepsilon_L v^0_{Lt} v^1_{RF_k} v^{[0]}_{\pi} + \sum_i v^i_{Lt} v^{i+1}_{RF_k} v^{[i]}_{\pi}\right. \\ &\qquad \left. + \varepsilon_R v^n_{Lt} v^{n+1}_{RF_k} v^{[n]}_{\pi}\right] \\ &= (-1)^k \frac{i\sqrt{2}M_F \varepsilon_L}{\sqrt{2n+1}(n+1)v} \tan\left[\frac{(n-k+1)\pi}{2n+1}\right] \end{aligned} \tag{4.82}$$

$$
\begin{aligned}
g_{RtF_k\pi} &= -i\frac{\sqrt{2}M_F}{f}\left[\varepsilon_L v^0_{LF_k} v^1_{Rt} v^{[0]}_\pi + \sum_i v^i_{LF_k} v^{i+1}_{Rt} v^{[i]}_\pi \right. \\
&\qquad \left. + \varepsilon_{Rt} v^n_{LF_k} v^{n+1}_{Rt} v^{[n]}_\pi \right] \\
&= \frac{i\sqrt{2}M_F \varepsilon_R}{\sqrt{2n+1}(n+1)v} \tan\left[\frac{(n-k+1)\pi}{2n+1}\right] \qquad (4.83)
\end{aligned}
$$

$$
\begin{aligned}
g_{tt\pi^+\pi^-} &= \frac{M_F}{f^2}\left[\varepsilon_L v^0_{Lt} v^1_{Rt} (v^{[0]}_\pi)^2 + \sum_i v^i_{Lt} v^{i+1}_{Rt} (v^{[i]}_\pi)^2 \right. \\
&\qquad \left. + \varepsilon_{Rt} v^n_{Lt} v^{n+1}_{Rt} (v^{[n]}_\pi)^2 \right] \\
&= \frac{m_t}{(n+1)v^2} \, . \qquad (4.84)
\end{aligned}
$$

Here we have denoted the lightest fermions (previously denoted F_0) by t and b, as appropriate, while leaving the corresponding KK modes as F_k (which, to leading order in $\varepsilon_{L,R}$, have the same properties for all quarks). Note that the four point vertex has an extremely simple form, and vanishes in the limit $n \to \infty$.

4.3 Unitarity Bounds on $t\bar{t} \to W_L W_L$

The diagrams that contribute at tree level to $t_+\bar{t}_+ \to W^+_L W^-_L$ are shown in Figure 4.5. We are again interested in the behavior at large energies, so we expand in the small parameters M^2_W/s and m^2_t/s; we also include all colors and both helicity polarizations in a coupled channel analysis (Eqn. (4.8)). The calculation is most easily performed using the equivalence theorem [3, 100]. Again, as in the SM (see Figure 4.3), the potential s-channel diagrams do not contribute to the $J = 0$ amplitude, and the only diagrams that contribute are shown in Figure 4.6.

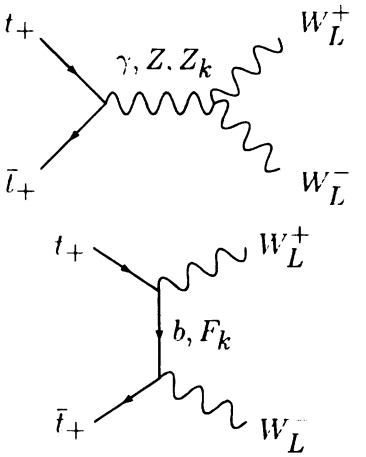

Figure 4.5: the process $t_+\bar{t}_+ \to W_L^+W_L^-$ in the $n(+2)$ site Higgsless model. There are analogous diagrams for the process $t_-\bar{t}_- \to W_L^+W_L^-$. As in the SM, most of the linear growth in $\sqrt{s}$ will cancel. All the persisting linear growth in $\sqrt{s}$ comes from the t channel diagrams.

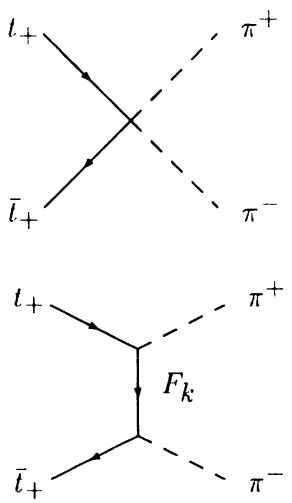

Figure 4.6: Diagrams contributing to unitarity violation at high energies in the process $t_+\bar{t}_+ \to \pi^+\pi^-$. There are analogous diagrams for the process $t_-\bar{t}_- \to \pi^+\pi^-$. The top diagram grows linearly with $\sqrt{s}$ for all energies, whereas the bottom diagrams only grow with $\sqrt{s}$ up to M_{F_k}, after which they fall off as $1/\sqrt{s}$.

The scattering amplitude arising from the diagrams in Figure 6 is

$$\mathcal{M} = \sqrt{6s}\left(g_{tt\pi^+\pi^-} - \sum_k \frac{M_{F_k} g_{LtF_k\pi}\, g_{RtF_k\pi}}{t - M_{F_k}^2}\right) \tag{4.85}$$

where the couplings are given in Eqns. (4.82) – (4.84).

The $J = 0$ partial wave can be extracted as

$$\begin{aligned} a_0 &= \frac{1}{32\pi}\int_{-1}^{1} d\cos\theta \mathcal{M} \\ &= \frac{\sqrt{6}}{16\pi}\left[g_{tt\pi^+\pi^-}\sqrt{s} + \sum_k g_{LtF_k\pi}\, g_{RtF_k\pi}\, g\left(\frac{\sqrt{s}}{M_{F_k}}\right)\right] \end{aligned} \tag{4.86}$$

where

$$g(x) = \frac{1}{x}\ln(1 + x^2) \tag{4.87}$$

This partial wave must be less than 1/2 to maintain unitarity, giving a bound on $\sqrt{s}$ and/or M_{F_1}. We have plotted this bound in Figures 4.7 and 4.8 for $n = 0, 1, 2, \cdots, 10, 20, 30$ and ∞. The $n = 0$ bound corresponds to the original AC bound of Eqn. (4.23).

We see from these figures that there are two important domains corresponding to different ranges of values for M_{F_1}. In the first domain, where $M_{F_1} \lesssim 4.5\,\text{TeV}$, we find that unitarity can be satisfied up to very large energies. In this limit, we find that the t channel diagram becomes irrelevant and the process is controlled by the four point vertex (Figure 4.6). For the lowest fermion masses, $M_{F_1} \ll 4.5\,\text{TeV}$, we find

$$a_0 \simeq \frac{\sqrt{6\,s}\, m_t}{16\pi v^2 (n+1)} \lesssim \frac{1}{2} \tag{4.88}$$

which gives the bound

$$\sqrt{s} \lesssim (n+1)\, 3.5\,\text{TeV} \tag{4.89}$$

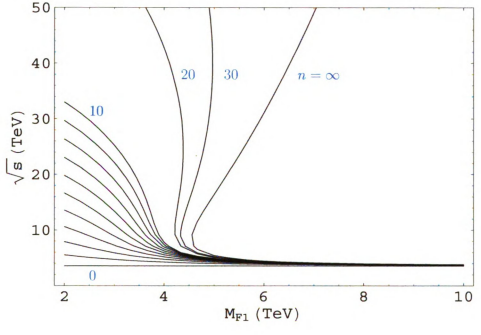

Figure 4.7: The scale where unitarity breaks down in the helicity nonconserving channel in the $n(+2)$ site model. Unitarity is valid in the region below and to the left of a given curve. The bottom-most curve is for $n = 0$ and is the AC bound. The line directly above the bottom one is for $n = 1$ and corresponds to the Three Site Model. The line directly above that is for $n = 2$ and so on until $n = 10$. The line above that is for $n = 20$, the line to the right of that is for $n = 30$ and the line to the right of that is the continuum limit ($n \to \infty$). We find that unitarity breaks down if either $\sqrt{s}$ is large or M_{F_1} is large. If M_{F_1} is large, then unitarity breaks down for $\sqrt{s}$ very close to the AC bound. On the other hand, if $M_{F_1} \lesssim 4.5\,\text{TeV}$, unitarity can be valid in this process to very high energies, with the precise value depending on the number of sites n.

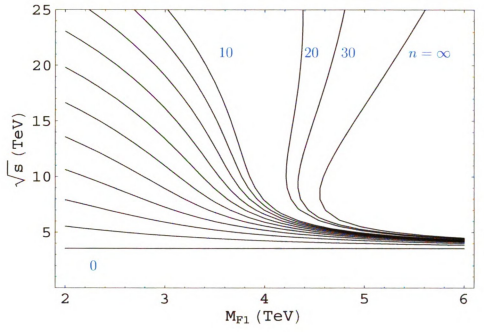

Figure 4.8: Expanded view of low $\sqrt{s}$ region of Figure 4.7.

In this "low" KK fermion-mass region, unitarity is valid to approximately $(n + 1)$ times the AC bound.

In the second domain, where $M_{F_1} > 4.5\,\text{TeV}$, we find that, for all n, unitarity breaks down at a value of $\sqrt{s}$ given approximately by the AC bound (Eqn. (4.23)) In Figures 4.7 and 4.8, we see that at $M_{F_1} \sim 4.5$ TeV, the curves corresponding to small n approach the $n = 0$ curve, while the curves for large n turn back on themselves, defining a wedge-shaped area in which unitarity is always violated starting at $\sqrt{s}$ of order a few TeV.

To understand why $M_{F_1} = 4.5$ TeV is the fermion mass value at which the theory crosses from the first to the second domain, we consider what happens as $n \to \infty$. In this limit, the four point vertex disappears and we are left with the partial wave

amplitude

$$\lim_{n\to\infty} a_0 = \frac{2\sqrt{6}M_{F_1}m_t}{\pi^4 v^2}\sum_k \frac{(-1)^{k+1}}{(2k-1)^2}\, g\left(\frac{\sqrt{s}}{(2k-1)M_{F_1}}\right) . \tag{4.90}$$

This sum is dominated by the first KK mode ($k = 1$). Thus, to locate the left most edge of the wedge-shaped in the $(\sqrt{s}, M_{F1})$ plane where unitarity is violated, we need only keep the first KK fermion mode

$$\lim_{n\to\infty} a_0(k=1) \approx \frac{2\sqrt{6}M_{F_1}m_t}{\pi^4 v^2} g\left(\frac{\sqrt{s}}{M_{F_1}}\right) . \tag{4.91}$$

The function $g(\sqrt{s}/M_{F_1})$ determines the shape of this bound. It is maximized for $\sqrt{s} = 2M_{F1}$ and gives the upper limit of M_{F_1},

$$M_{F_1} \lesssim \frac{\pi^4 v^2}{2\sqrt{6}m_t \ln(5)} \sim 4.25\,\text{TeV} , \tag{4.92}$$

if we want this amplitude to be unitary up to very high scales. Including the higher fermion KK modes changes this upper bound only slightly, to $\sim 4.5\,\text{TeV}$. Note that, in the continuum limit, the scattering amplitude does not grow at asymptotically high energies – a property ensured by various sum-rules satisfied by the couplings [104, 105]. Nonetheless, as illustrated in Figures 4.7 and 4.8, the properly normalized spin-0 coupled-channel amplitude exceeds the unitarity bound for various ranges of $\sqrt{s}$ and M_{F1}.

While this work demonstrates that the bound on the scale of fermion mass generation is independent of the bound on the scale of gauge-boson mass generation in these models, the physical significance of the fermion-mass-generation bound depends on the "high-energy" (UV) completion which underlies the $n(+2)$ site model. The simplest possible UV completion is one in which each of the nonlinear sigma-model

link theories is replaced by a linear Gell-mann Levy sigma model. In this case, the strength of the adjacent site couplings in Eqn. (4.57) is determined by a dimensionless Yukawa coupling of order M_F/f. The large-M_F limit, therefore, corresponds to large Yukawa coupling. In this case, the bound on M_F is expected to be related to the triviality bound on the corresponding Yukawa coupling [98, 99, 106].

4.4 Summary

In this chapter we have examined upper bounds on the scale of top-quark mass generation in viable deconstructed Higgsless models. These bounds are derived from the scale at which unitarity is violated in the helicity nonconserving amplitude for top-anti-top pairs to scatter into pairs of longitudinally polarized electroweak gauge bosons. We have shown that the scale of unitarity violation in this process depends on the mass of the additional vector-like fermion states that occur in these theories and, in this sense, the scale of fermion mass generation is *separate* from that of gauge-boson mass generation. For sufficiently light vector fermions, and for a deconstructed theory with sufficiently many lattice sites (that is, sufficiently close to the continuum limit), we have shown that the Appelquist-Chanowitz bound on the scale of top-quark mass generation is substantially weakened, while the bound is recovered as one increases the mass of the vector-like fermions. Our results are expected to apply to any model in which top-quark mass generation occurs, in part, through mixing between chiral and vector fermions.

BIBLIOGRAPHY

[1] S. Weinberg, Phys. Rev. Lett. **19**, 1264 (1967).

[2] P. W. Higgs, Phys. Rev. Lett. **13**, 508 (1964).

[3] J. M. Cornwall, D. N. Levin and G. Tiktopoulos, Phys. Rev. D **10**, 1145 (1974) [Erratum-ibid. D **11**, 972 (1975)].

[4] B. W. Lee, C. Quigg and H. B. Thacker, Phys. Rev. D **16**, 1519 (1977).

[5] S. Weinberg, Phys. Rev. D **13**, 974 (1976).

[6] E. Farhi and L. Susskind, Phys. Rept. **74**, 277 (1981).

[7] C. T. Hill and E. H. Simmons, Phys. Rept. **381**, 235 (2003) [Erratum-ibid. **390**, 553 (2004)] [arXiv:hep-ph/0203079].

[8] R. S. Chivukula, E. H. Simmons and J. Terning, Phys. Lett. B **331**, 383 (1994) [arXiv:hep-ph/9404209].

[9] R. S. Chivukula, S. B. Selipsky and E. H. Simmons Phys. Rev. Lett. **69**, 575 (1992) [arXiv:hep-ph/9204214].

[10] S. Dimopoulos and J. R. Ellis, Nucl. Phys. B **182**, 505 (1982).

[11] T. Appelquist, M. Piai and R. Shrock, Phys. Rev. D **69**, 015002 (2004) [arXiv:hep-ph/0308061].

[12] I. Antoniadis, Phys. Lett. B **246**, 377 (1990).

[13] I. Antoniadis, N. Arkani-Hamed, S. Dimopoulos and G. R. Dvali, Phys. Lett. B **436**, 257 (1998) [arXiv:hep-ph/9804398].

[14] I. Antoniadis and M. Quiros, Phys. Lett. B **392**, 61 (1997) [arXiv:hep-th/9609209].

[15] I. Antoniadis, C. Munoz and M. Quiros, Nucl. Phys. B **397**, 515 (1993) [arXiv:hep-ph/9211309].

[16] N. Arkani-Hamed, S. Dimopoulos and G. R. Dvali, Phys. Lett. B **429**, 263 (1998) [arXiv:hep-ph/9803315].

[17] L. Randall and R. Sundrum, Phys. Rev. Lett. **83**, 3370 (1999) [arXiv:hep-ph/9905221].

[18] L. Randall and R. Sundrum, Phys. Rev. Lett. **83**, 4690 (1999) [arXiv:hep-th/9906064].

[19] J. M. Maldacena, *The large n limit of superconformal field theories and supergravity*, *Adv. Theor. Math. Phys.* **2** (1998) 231–252, [hep-th/9711200].

[20] S. S. Gubser, I. R. Klebanov, and A. M. Polyakov, *Gauge theory correlators from non-critical string theory*, *Phys. Lett.* **B428** (1998) 105 114, [hep-th/9802109].

[21] E. Witten, *Anti-de sitter space and holography*, *Adv. Theor. Math. Phys.* **2** (1998) 253 291, [hep-th/9802150].

[22] O. Aharony, S. S. Gubser, J. M. Maldacena, H. Ooguri, and Y. Oz, *Large n field theories, string theory and gravity*, *Phys. Rept.* **323** (2000) 183 386, [hep-th/9905111].

[23] N. Arkani-Hamed, A. G. Cohen and H. Georgi, Phys. Rev. Lett. **86**, 4757 (2001) [arXiv:hep-th/0104005].

[24] C. T. Hill, S. Pokorski and J. Wang, Phys. Rev. D **64**, 105005 (2001) [arXiv:hep-th/0104035].

[25] H. Georgi, *A tool kit for builders of composite models*, *Nucl. Phys.* **B266** (1986) 274.

[26] R. S. Chivukula, E. H. Simmons, H. J. He, M. Kurachi and M. Tanabashi, Phys. Rev. D **71**, 115001 (2005) [arXiv:hep-ph/0502162].

[27] R. S. Chivukula, E. H. Simmons, H. J. He, M. Kurachi and M. Tanabashi, Phys. Rev. D **71**, 035007 (2005) [arXiv:hep-ph/0410154].

[28] R. S. Chivukula, E. H. Simmons, H. J. He, M. Kurachi and M. Tanabashi, Phys. Lett. B **603**, 210 (2004) [arXiv:hep-ph/0408262].

[29] R. S. Chivukula, E. H. Simmons, H. J. He, M. Kurachi and M. Tanabashi, Phys. Rev. D **70**, 075008 (2004) [arXiv:hep-ph/0406077].

[30] R. S. Chivukula, B. Coleppa, S. Di Chiara, E. H. Simmons, H. J. He, M. Kurachi and M. Tanabashi, Phys. Rev. D **74**, 075011 (2006) [arXiv:hep-ph/0607124].

[31] R. Casalbuoni, S. De Curtis, D. Dominici, and R. Gatto, *Effective weak interaction theory with possible new vector resonance from a strong higgs sector*, *Phys. Lett.* **B155** (1985) 95.

[32] R. Casalbuoni *et. al.*, *Degenerate bess model: The possibility of a low energy strong electroweak sector*, *Phys. Rev.* **D53** (1996) 5201–5221, [hep-ph/9510431].

[33] M. Bando, T. Kugo, S. Uehara, K. Yamawaki, and T. Yanagida, *Is rho meson a dynamical gauge boson of hidden local symmetry?*, *Phys. Rev. Lett.* **54** (1985) 1215.

[34] M. Bando, T. Kugo, and K. Yamawaki, *On the vector mesons as dynamical gauge bosons of hidden local symmetries*, *Nucl. Phys.* **B259** (1985) 493.

[35] M. Bando, T. Fujiwara, and K. Yamawaki, *Generalized hidden local symmetry and the a1 meson*, *Prog. Theor. Phys.* **79** (1988) 1140.

[36] M. Bando, T. Kugo, and K. Yamawaki, *Nonlinear realization and hidden local symmetries*, *Phys. Rept.* **164** (1988) 217-314.

[37] M. Harada and K. Yamawaki, *Hidden local symmetry at loop: A new perspective of composite gauge boson and chiral phase transition*, *Phys. Rept.* **381** (2003) 1–233, [hep-ph/0302103].

[38] C. T. Hill, Phys. Lett. **B 266** , 419-424 (1991); Phys. Lett. **B 345** , 483 (1995)

[39] C. T. Hill and S. Parke, Phys. Rev. **D49**, 4454 (1994).

[40] Christopher T. Hill, *Topcolor assisted technicolor*, Phys. Lett. **B 345**: 483-489 (1995) [hep-ph/9411426].

[41] K. Lane and E. Eichten, *Natural topcolor assisted technicolor*, Phys. Lett. **B 352**: 382-387 (1995).

[42] M. E. Peskin and T. Takeuchi, Phys. Rev. D **46**, 381 (1992).

[43] R. Foadi, S. Gopalakrishna, and C. Schmidt, *Higgsless electroweak symmetry breaking from theory space*, *JHEP* **03** (2004) 042, [arXiv: hep-ph/0312324].

[44] R. Sekhar Chivukula, D. A. Dicus, and H.-J. He, *Unitarity of compactified five dimensional yang-mills theory. Phys. Lett.* **B525** (2002) 175–182, [arXiv:hep-ph/0111016].

[45] R. S. Chivukula and H.-J. He, *Unitarity of deconstructed five-dimensional yang-mills theory*, *Phys. Lett.* **B532** (2002) 121–128, [arXiv:hep-ph/0201164].

[46] R. S. Chivukula, D. A. Dicus, H.-J. He, and S. Nandi, *Unitarity of the higher dimensional standard model*, *Phys. Lett.* **B562** (2003) 109–117, [arXiv:hep-ph/0302263].

[47] H.-J. He, *Higgsless deconstruction without boundary condition*, arXiv:hep-ph/0412113.

[48] R. Sekhar Chivukula, E. H. Simmons, H. J. He, M. Kurachi and M. Tanabashi, *Electroweak corrections and unitarity in linear moose models*, Phys. Rev. D **71** (2005) 035007 [arXiv:hep-ph/0410154].

[49] R. Sekhar Chivukula, E. H. Simmons, H. J. He, M. Kurachi and M. Tanabashi, *Ideal fermion delocalization in Higgsless models*, Phys. Rev. D **72**, 015008 (2005) [arXiv:hep-ph/0504114].

[50] R. Foadi, S. Gopalakrishna and C. Schmidt, Phys. Lett. B **606**, 157 (2005) [arXiv:hep-ph/0409266].

[51] R. Foadi and C. Schmidt, *An Effective Higgsless Theory: Satisfying Electroweak Constraints and a Heavy Top Quark*, Phys. Rev. D **73** (2006) 075011 [arXiv:hep-ph/0509071].

[52] The LEP Collaborations ALEPH, DELPHI, L3, OPAL and the LEP TGC Working Group. LEPEWWG/TC/2005-01; June 8, 2005.

[53] S. Willenbrock, arXiv:hep-ph/0410370.

[54] M. E. Peskin and D. V. Schroeder, "An Introduction To Quantum Field Theory"

[55] M. J. G. Veltman, *Diagrammatica: The path to Feynman rules* (Cambridge, 1994).

[56] S. Matsuzaki, R. S. Chivukula, E. H. Simmons and M. Tanabashi, Phys. Rev. D **75**, 073002 (2007) [arXiv:hep-ph/0607191].

[57] S. Eidelman *et al.* [Particle Data Group], Phys. Lett. B **592**, 1 (2004).

[58] K. Hagiwara, R. D. Peccei, D. Zeppenfeld and K. Hikasa, *Probing The Weak Boson Sector In E+ E- → W+ W-*, Nucl. Phys. B **282**, 253 (1987).

[59] R. S. Chivukula, E. H. Simmons, H. J. He, M. Kurachi and M. Tanabashi, *Multi-gauge-boson vertices and chiral Lagrangian parameters in higgsless models with ideal fermion delocalization*, Phys. Rev. D **72**, 075012 (2005) [arXiv:hep-ph/0508147].

[60] H. J. He *et al.*, Phys. Rev. D **78**, 031701 (2008) [arXiv:0708.2588 [hep-ph]].

[61] T. Aaltonen *et al.* [CDF Collaboration], Phys. Rev. Lett. **100**, 161803 (2008) [arXiv:0801.3877 [hep-ex]].

[62] A. Pukhov, arXiv:hep-ph/0412191.

[63] N. Arkani-Hamed, A. G. Cohen and H. Georgi, Phys. Lett. B **513**, 232 (2001) [arXiv:hep-ph/0105239]. For reviews, see, for example, M. Schmaltz and D. Tucker Smith, Ann. Rev. Nucl. Part. Sci. **55**, 229 (2005); M. Perelstein, Prog. Part. Nucl. Phys. **58**, 247 (2007) and references within.

[64] M. S. Carena, J. Hubisz, M. Perelstein and P. Verdier, Phys. Rev. D **75**, 091701 (2007) [arXiv:hep-ph/0610156].

[65] D. Choudhury and D. K. Ghosh, JHEP **0708**, 084 (2007) [arXiv:hep-ph/0612299].

[66] I. Low, JHEP **0410**, 067 (2004) [arXiv:hep-ph/0409025].

[67] J. Hubisz and P. Meade, Phys. Rev. D **71**, 035016 (2005) [arXiv:hep-ph/0411264].

[68] J. Hubisz, P. Meade, A. Noble and M. Perelstein, JHEP **0601**, 135 (2006) [arXiv:hep-ph/0506042].

[69] H. C. Cheng and I. Low, JHEP **0309**, 051 (2003) [arXiv:hep-ph/0308199].

[70] H. C. Cheng and I. Low, JHEP **0408**, 061 (2004) [arXiv:hep-ph/0405243].

[71] T. Han, H. E. Logan and L. T. Wang, JHEP **0601**, 099 (2006) [arXiv:hep-ph/0506313].

[72] C. X. Yue, L. H. Wang and J. Wen, Chin. Phys. Lett. **25**, 1613 (2008) [arXiv:0708.1225 [hep-ph]].

[73] A. Atre, M. Carena, T. Han and J. Santiago, arXiv:0806.3966 [hep-ph].

[74] R. S. Chivukula, N. D. Christensen, B. Coleppa and E. H. Simmons, Phys. Rev. D **75**, 073018 (2007) [arXiv:hep-ph/0702281].

[75] T. Appelquist and M. S. Chanowitz, *Unitarity Bound on the Scale of Fermion Mass Generation*, Phys. Rev. Lett. **59**, 2405 (1987) [Erratum-ibid. **60**, 1589 (1988)].

[76] W. J. Marciano, G. Valencia and S. Willenbrock, Phys. Rev. D **40**, 1725 (1989).

[77] M. Golden, Phys. Lett. B **338**, 295 (1994) [arXiv:hep-ph/9408272].

[78] F. Maltoni, J. M. Niczyporuk and S. Willenbrock, Phys. Rev. D **65**, 033004 (2002) [arXiv:hep-ph/0106281].

[79] D. A. Dicus and H. J. He, Phys. Rev. D **71**, 093009 (2005) [arXiv:hep-ph/0409131].

[80] C. H. Llewellyn Smith, Phys. Lett. B **46**, 233 (1973).

[81] D. A. Dicus and V. S. Mathur, Phys. Rev. D **7**, 3111 (1973).

[82] M. J. G. Veltman, Acta Phys. Polon. B **8**, 475 (1977).

[83] B. Coleppa, S. Di Chiara and R. Foadi, *One loop corrections to the rho parameter in Higgsless models*, arXiv:hep-ph/0612213.

[84] G. Cacciapaglia, C. Csaki, C. Grojean, M. Reece and J. Terning, *Top and bottom: A brane of their own*, *Phys. Rev. D* **72**, (2005) 095018 [arXiv:hep-ph/0505001].

[85] R. Sekhar Chivukula, E. H. Simmons, H. J. He, M. Kurachi and M. Tanabashi, Phys. Rev. D **75**, 035005 (2007) [arXiv:hep-ph/0612070].

[86] B. A. Dobrescu and C. T. Hill, *Electroweak symmetry breaking via top condensation seesaw*, Phys. Rev. Lett. **81**, 2634 (1998) [arXiv:hep-ph/9712319].

[87] R. S. Chivukula, B. A. Dobrescu, H. Georgi and C. T. Hill, *Top quark seesaw theory of electroweak symmetry breaking*, Phys. Rev. D **59**, 075003 (1999) [arXiv:hep-ph/9809470].

[88] H. J. He, C. T. Hill and T. M. P. Tait, *Top quark seesaw, vacuum structure and electroweak precision constraints*, Phys. Rev. D **65**, 055006 (2002) [arXiv:hep-ph/0108041].

[89] M. Suzuki, Phys. Rev. D **44**, 3628 (1991).

[90] R. F. Lebed and M. Suzuki, Phys. Rev. D **45**, 1744 (1992).

[91] D. B. Kaplan, Nucl. Phys. B **365**, 259 (1991).

[92] C. Csaki, J. Hubisz and P. Meade, arXiv:hep-ph/0510275.

[93] T. Appelquist and C. W. Bernard, *The Nonlinear Sigma Model In The Loop Expansion*, Phys. Rev. D **23**, 425 (1981).

[94] T. Appelquist and C. W. Bernard, *Strongly Interacting Higgs Bosons*, Phys. Rev. D **22**, 200 (1980).

[95] A. C. Longhitano, Phys. Rev. D **22**, 1166 (1980).

[96] A. C. Longhitano, *Low-Energy Impact Of A Heavy Higgs Boson Sector*, Nucl. Phys. B **188**, 118 (1981).

[97] T. Appelquist and G. H. Wu, *The Electroweak chiral Lagrangian and new precision measurements*, Phys. Rev. D **48**, 3235 (1993) [arXiv:hep-ph/9304240].

[98] M. S. Chanowitz, M. A. Furman and I. Hinchliffe, Phys. Lett. B **78**, 285 (1978).

[99] M. S. Chanowitz, M. A. Furman and I. Hinchliffe, Nucl. Phys. B **153**, 402 (1979).

[100] C. E. Vayonakis, Lett. Nuovo Cim. **17**, 383 (1976).

[101] L. Anichini, R. Casalbuoni and S. De Curtis, Phys. Lett. B **348**, 521 (1995) [arXiv:hep-ph/9410377].

[102] G. Cacciapaglia, C. Csaki, C. Grojean and J. Terning, *Curing the ills of Higgsless models: The S parameter and unitarity*, Phys. Rev. D **71** (2005) 035015 [arXiv:hep-ph/0409126].

[103] R. Casalbuoni, S. De Curtis, D. Dolce and D. Dominici, *Playing with fermion couplings in Higgsless models*, Phys. Rev. D **71**, 075015 (2005) [arXiv:hep-ph/0502209].

[104] C. Schwinn, Phys. Rev. D **69**, 116005 (2004) [arXiv:hep-ph/0402118].

[105] C. Schwinn, Phys. Rev. D **71**, 113005 (2005) [arXiv:hep-ph/0504240].

[106] M. B. Einhorn and G. J. Goldberg, Phys. Rev. Lett. **57**, 2115 (1986).